UTILIZATION OF A 3D SUSPENSION CULTURE SYSTEM AS A MODEL TO UNDERSTAND THE INTRINSIC EFFECT OF RADIATION TREATMENT ON SALIVARY GLANDS

by

Vicky Thao Nguyen

A Dissertation Submitted to the Faculty of the

DEPARTMENT OF NUTRITIONAL SCIENCES

In Partial Fulfillment of the

Requirements for the Degree of

DOCTOR OF PHILOSOPHY

In the Graduate College

THE UNIVERSITY OF ARIZONA

2018

THE UNIVERSITY OF ARIZONA
GRADUATE COLLEGE

As members of the Dissertation Committee, we certify that we have read the dissertation prepared by Vicky Thao Nguyen entitled, "Utilization of a 3D suspension culture system as a model to understand the intrinsic effect of radiation treatment on salivary glands" and recommend that it be accepted as fulfilling the dissertation requirement for the Degree of Doctor of Philosophy.

Dr. Kirsten Limesand — Date: 08/10/2018

Dr. Sean Limesand — Date: 08/10/2018

Dr. Lalitha Madhavan — Date: 08/10/2018

Dr. Ningning Zhao — Date: 08/10/2018

Final approval and acceptance of this dissertation is contingent upon the candidate's submission of the final copies of the dissertation to the Graduate College.

I hereby certify that I have read this dissertation prepared under my direction and recommend that it be accepted as fulfilling the dissertation requirement.

Dissertation Director: Dr. Kirsten Limesand — Date: 08/10/2018

STATEMENT BY AUTHOR

This dissertation has been submitted in partial fulfillment of requirements for an advanced degree at The University of Arizona and is deposited in the University Library to be made available to borrowers under rules of the Library.

Brief quotations from this dissertation are allowable without special permission, provided that an accurate acknowledgement of the source is made. Requests for permission for extended quotation from or reproduction of this manuscript in whole or in part may be granted by the head of the major department or the Dean of the Graduate College when in his or her judgment the proposed use of the material is in the interests of scholarship. In all other instances, however, permission must be obtained from the author.

SIGNED: Vicky Thao Nguyen

ACKNOWLEDGMENT

"You learn more in failure than you ever do in success"

My path to the PhD program in Nutritional Sciences was a bit unconventional. Unlike my peers in my cohort group, I came to the graduate program without any prior experience in clinical nor basic science research. My original plan when I first entered the program as a Master student was to obtain an advance degree to make myself more competitive for the dietetic internship. However, that all changed when I did my laboratory rotation in Kirsten's lab. Despite not having any background nor training in basic science research, Kirsten was very generous and willing to take me as a mentee. It was through her encouragement that I decided to switch to the PhD track at the conclusion of my second year in the program. To Kirsten, I am forever grateful not only because she saw a potential in me, but she has also provided a safe environment in which I can fail. It was only through those failures that I have grown at both a personal and professional level.

As a graduate student in the Nutritional Sciences graduate program, I was given the opportunity to be a teaching assistant. The enriching experience and the mentorship I have gained from my teaching mentors, principally Dr. Jennifer Ricketts, has made a lasting impact on my career.

And last but not least, to all the past and current members of the Kirsten Limesand lab, staff and faculty in the Nutritional Sciences department, friends, and my family for their constant support and encouragement throughout this journey.

Table of Contents

List of Figures

List of Tables

ABSTRACT

Over 50,000 patients are diagnosed with head and neck cancers (HNC) in the United States each year and about half a million worldwide. Current treatment of HNC utilizes a multidisciplinary approach, radiotherapy alone or in combination with chemotherapy and surgery. The major drawbacks of radiotherapy treatment of HNC is radiation exposure of non-malignant tissue (i.e. salivary glands). The majority of HNC patients undergoing radiotherapy treatment suffer from chronic salivary dysfunction. Loss of saliva is associated with a multitude of complications (i.e. dental decay, dysphagia, oral infections, etc.), all of which contribute to deteriorating quality of life in HNC populations. Currently, there is no definite treatment for radiation-induced salivary gland dysfunction and available palliative care therapies are short-term and fail to improve quality of life. Stem cell-based therapies are a promising avenue for the treatment of salivary gland hypofunction and existence of salivary stem cell populations has been reported following radiation treatment. However, the effect of radiation on these putative populations, and whether they can be stimulated to regenerate and restore saliva production in the damaged salivary glands is unknown. Thus, understanding the intracellular effect of radiation on the salivary stem cell populations and their response upon radiation injury will facilitate development of novel therapies for the treatment of radiation-induced salivary gland dysfunction. Using a 3-dimensional suspension cell culture, we show that stem/progenitor cells derived from irradiated salivary glands have a defect in cell self-renewal and differentiation capacity, and our data indicates the role of aPKCζ in mediating these molecular events. We propose that utilization of the suspension cell culture assay to elucidate the upstream and downstream effects of aPKCζ will

provide mechanistic insights that govern the non-responsive phenotype in the salivary stem/progenitor populations following radiation injury.

LITERATURE REVIEW

Head and Neck Cancers

Incidence and epidemiological risk factors

Head and neck cancer (HNC) encompasses a variety of tumors that originate in the hypopharynx, oropharynx, lip, oral cavity, nasopharynx, and larynx (Lo Nigro, Denaro et al. 2017). It is the sixth most common neoplasia and accounts for 6% cases of cancer worldwide. In the United States, more than 50,000 patients are diagnosed with HNC annually. The main risk factors associated with HNC include tobacco use, alcohol consumption, and human papillomavirus (HPV) infection (Vigneswaran and Williams 2014). Diagnosis of HNC is often more prevalent in an older male population, between the fiftieth and sixtieth year of life, with a male to female ratio of 2:1 (Mountzios 2015). However, in recent years, there has been an increased incidence of HPV-related head and neck cancers and this epidemic rise is often observed in a younger population who present no modifiable risk factors such as tobacco and alcohol use (Young, Xiao et al. 2015).

Treatment of head and neck cancers

Due to the localization and tumor stage at the time of diagnosis, treatment of HNC solely on a surgical approach limits the ability to maximize survival outcomes. Thus, treatment of HNC utilizes a multimodality approach, which includes a regimen of surgery followed by radiotherapy (RT), with or without chemotherapy (CT) or concurrent chemoradiotherapy (CRT) (Lo Nigro, Denaro et al. 2017). Surgery remains the initial treatment of choice for HNC patients if there is a possibility of complete removal of the tumor with maximal preservation of non-malignant tissues and minimal aesthetic impact

(Cognetti, Weber et al. 2008, Belcher, Hayes et al. 2014). However, due to the complexities of the oral cavity, it is a challenge to eliminate tumors solely on a surgical approach. Thus, the current standard of care for head and neck cancer involves a combination of therapies, usually surgical resection followed by adjuvant radiation with or without chemotherapy (Belcher, Hayes et al. 2014, Lo Nigro, Denaro et al. 2017). Studies have shown that there is improved locoregional control and overall survival rate in HNC patients who received the addition of cisplatin-based chemotherapy to radiation postoperatively compared to adjuvant radiation treatment alone (Inohara, Takenaka et al. 2015, Lee, Schoder et al. 2016)

In cases of human papillomavirus (HPV)-associated HNC, current treatment therapies are modified due to the demographic and favorable prognosis in this patient population to reduce the treatment-related complications (Denaro, Merlano et al. 2016, Lo Nigro, Denaro et al. 2017). Patients with HPV-associated oropharyngeal cancer are often younger, with less comorbidities and the disease is more chemo and radiosensitive. Treatment guidelines currently include reduced radiotherapy doses, replacement of cisplatin with cetuximab for chemotherapy, and use of immunotherapy to reduce acute and chronic toxicities (Specenier and Vermorken 2013, Bauman, Cohen et al. 2017, Schuler, Laban et al. 2017).

Radiation-induced salivary hypofunction and xerostomia

One of the drawbacks of radiotherapy treatment of head and neck cancer is that surrounding non-malignant tissues, such as the salivary glands, are injured and this can lead to long lasting side effects (Vissink, Jansma et al. 2003, Grundmann, Mitchell et al. 2009). The major complaint by HNC patients who underwent radiotherapy treatment is

xerostomia, a sensation of severe dry mouth. Xerostomia is often associated with reduced production of saliva and salivary gland hypofunction (Dirix, Nuyts et al. 2006, Plemons, Al-Hashimi et al. 2014). It has been reported that approximately 64% of HNC long-term survivors who underwent RT treatment experience moderate to severe xerostomia (Guggenheimer and Moore 2003, Dirix, Nuyts et al. 2006). Radiation-induced damage to the salivary glands alters the volume, consistency, and pH of the secreted saliva. The change in the quantity and composition of saliva produced leads to changes in the oral environment. As a result, HNC patients are at an increased risk of dental caries and oral infections, leading to oral discomfort and pain (Trotti 2000, Brosky 2007, Pinna, Campus et al. 2015). Despite being potentially cured from their cancer, the quality of life of HNC patients is reduced due to the malnutrition and psychosocial problems associated with xerostomia (Jabbari, Kim et al. 2005, Braam, Roesink et al. 2007)

Radiation-induced salivary damage is directly related to radiation dosimetry, which includes total dose, fraction size, and duration of treatment (Deasy, Moiseenko et al. 2010). Improved radiation modalities, such as intensity-modulated radiotherapy (IMRT) and intensity modulated proton therapy (IMPT) have been developed over the years to optimize delivery of radiation to the targeted tumor sites and sparing the non-malignant surrounding tissues. It is well established that IMRT allows for significant sparring of the parotid glands and this is associated with improved salivary rates in HNC patients posttreatment (Eisbruch, Ship et al. 2003, Lee, Kang et al. 2016). Despite the clinical efficacy of IMRT, sparring of the salivary glands is often not possible due to the localization and stage of the tumors, and even with this modality of radiation therapy,

xerostomia and salivary hypofunction may still develop in HNC patients (Collan, Kapanen et al. 2012).

Anatomy and function of the salivary glands

The salivary glands are groups of exocrine organs that function in saliva production, a watery substance that is excreted in the mouth. In humans, 90% of the total saliva is produced by the major salivary glands, which comprise of the parotid, submandibular, and sublingual glands. Adult salivary glands consist of the glandular secretory tissue (parenchyma) and the supporting connective tissue (stroma). The parenchyma comprises the secretory endpieces known as the acini, which are connected to the oral cavity through a system of ducts (Johns 1977, Holmberg and Hoffman 2014). Saliva production is a two-step process: 1) initial production of isotonic plasma-like fluid by acinar serious and mucous cells and 2) modification of the ionic content of saliva by ductal cells. Salivary secretion is directly under neural control and is innervated by the parasympathetic (PANS) and sympathetic (SANS) arms of the autonomic nervous system. PANS and SANS can directly affect salivary secretion by innervating the acinar cells that supply the glands (Proctor and Carpenter 2007, Proctor and Carpenter 2014). From both an anatomic and physiological standpoint, direct damage to the salivary epithelium or indirect damage to the surrounding nerves, vasculature, and stoma can affect salivary gland function.

Direct radiation damage to the salivary glandular tissue

Studies performed in different animal models, ranging from rodents to non-human primates, have consistently shown that radiation causes histological changes to the architecture of the salivary gland tissues. This is evident by atrophy in the acinar cell

compartment, development of interstitial fibrosis, and loss of glandular weight (Stephens, King et al. 1986, Vissink, s-Gravenmade et al. 1990, Li, Shan et al. 2005). Besides the reduction in the volume of saliva secreted, the composition of saliva in post-irradiated salivary glands is also altered. Analysis of saliva collected from HNC patients who suffered from radiation-induced salivary gland hypofunction show that the remaining saliva is high in electrolytes and low in amylase content. Additionally, the profile of other secretory elements, such as immunoglobulins A and G, lysozyme, and lactoferrin is also altered (Makkonen, Tenovuo et al. 1986, Laheij, Rasch et al. 2015).

Indirect radiation damage to the associated nerves, vasculature, and stroma

Peripheral innervation plays a crucial role in the stimulation of saliva secretion by the salivary glands. Parasympathetic denervation of parotid glands in developmental models of sheep show that loss of parasympathetic innervation not only led to decreases in saliva secretion, but also atrophy of the acinar cells (Patterson, Lloyd et al. 1975). Histological evaluation of submandibular gland biopsies from HNC patients undergoing radiotherapy treatment showed that parasympathetic nerves, as indicated by GFRa2 immunostaining, were reduced by ~60% when compared to non-irradiated controls (Knox, Lombaert et al. 2013) . Using an *ex vivo* explant culture, recent work from the same group further showed that innervation of the irradiated salivary glands by cholinergic mimetics led to replenishment of SOX2+ cells, a progenitor cell population that is essential for the maintenance of secretory acinar cells (Emmerson et al., 2018).

In vivo and *in vitro* studies in animal models have shown that radiation can directly cause damage to the vasculature by upregulating pro-inflammatory cytokines and

adhesion molecules, which are involved in the recruitment of inflammatory cells to the site of injury (Weintraub, Jones et al. 2010). Radiation-induced vessel lesions are reminiscent of atherosclerosis lesions, which exhibit histological features like lipid accumulation, inflammation, thrombosis, and increased intima thickness (Basavaraju and Easterly 2002). Decreased microvascular density and blood flow, and apoptosis of microvascular endothelial cells were reported in salivary glands of mice and minipigs at a very early time point (24 hours) following radiation treatment (Cotrim, Sowers et al. 2007, Mizrachi, Cotrim et al. 2016). It is hypothesized that radiation-induced vascular damage may contribute to the development of fibrosis in the irradiated glands.

Collectively, all the aforementioned studies suggest that radiation damage to the peripheral nerves and vasculature system might also contribute to salivary gland hypofunction due to the loss of molecular communications between the supporting structures and the parenchyma.

Potential mechanisms of radiation-induced salivary gland dysfunction

DNA damage and acinar cell death

Ionizing radiation can cause DNA damage by 1) directly causing breakage of the phosphodiester bond or 2) indirectly through the production of reactive oxygen species (ROS) due to the radiolysis of water molecules, which result in the production of hydrogen peroxide, superoxide, and hydroxyl radicals (Azzam, Jay-Gerin et al. 2012, Lomax, Folkes et al. 2013). In response to DNA damage, several cellular pathways are upregulated, which all lead to the activation of the tumor suppressor p53. p53 is a transcription factor that is involved in regulation of DNA repair, cell cycle arrest, senescence, and apoptotic genes (Fei and El-Deiry 2003, Helton and Chen 2007). In the event of DNA damage, the conventional first line of defense is transient cell cycle arrest and activation of DNA repair pathways. If DNA repair fails, the cell would undergo programmed cell death to avoid accumulating mutations and preserve genetic fidelity (Latif, Harvey et al. 2001, Branzei and Foiani 2008).

In a rodent model, radiation doses ranging from 2.5-10 Gy cause extensive DNA damage, initiating an apoptotic program, characterized by an upregulation of p53-dependent apoptotic genes (Avila, Grundmann et al. 2009). These acute responses were also observed in a radiation model of miniature pigs and rhesus monkeys (Stephens, King et al. 1986, Li, Shan et al. 2005). Modulation of the apoptosis pathways, either by knocking out p53 or constitutively activating AKT by genetic models, show that p53 is essential in eliciting an apoptotic response in the irradiated salivary glands (Avila, Grundmann et al. 2009, Limesand, Said et al. 2009). Pharmacological modulation of cell cycle arrest by administration of a cyclin-dependent kinase inhibitor, Roscovitine, prior

to radiation treatment was able to preserve salivary function in irradiated mice (Martin, Hill et al. 2012). Together, these studies show that the acute response to radiation-induced DNA damage is mediated through activation of p53-dependent apoptosis and cell cycle arrest pathways and correlates with chronic salivary gland dysfunction.

Damage to secretory pathways

Besides causing DNA damage, ROS generation by ionizing radiation can have a biological effect on other cellular components. In salivary glands, it has been demonstrated that radiation has disruptive effects on associated-membrane ion channels, cellular receptors, and calcium signaling, which all play an important role in saliva production and secretion (Coppes, Roffel et al. 2000, Coppes, Meter et al. 2005, Liu, Cotrim et al. 2013).

As discussed previously, salivary secretion is mediated by parasympathetic innervation and release of cholinergic factors (i.e. acetylcholine). Stimulation of the muscarinic receptors by cholinergic agonists results in an influx of Ca^{2+} into the cytoplasm and the increase in intracellular Ca^{2+} concentration activates basolateral K^+ channels and apical Cl^- channels, leading to an osmotic gradient and saliva secretion (Ambudkar 2012). Alterations in Ca^{2+} mobilization have been shown to correlate with radiation-induced hyposalivation (Coppes, Roffel et al. 2000, Coppes, Meter et al. 2005, Liu, Cotrim et al. 2013). Coppes et al. have shown that radiation treatment impairs the ability of parotid glands to mobilize calcium from intracellular stores to the cytoplasm via disruption of protein kinase C alpha (PKCα) association with the plasma membrane (Coppes, Meter et al. 2005). In a similar fashion, radiation was shown to activate the transient potential melastatin-like 2 (TRPM2), a Ca^{2+} permeable non-selective cation

channel, in both cultured human submandibular cells and murine submandibular glands *in vivo*. Genetic ablation of TRPM2 was able to preserve salivary gland function 30 days post-irradiation (Liu, Cotrim et al. 2013).

Aquaporins are water permeable transmembrane proteins that regulate fluid mobility from the interstitium to the lumen. In the salivary glands, aquaporin-1 (AQP1) is expressed on the endothelial cells while aquaporin-5 (AQP5) is found on the apical side of acinar cells (Delporte and Steinfeld 2006). Radiation can cause deregulation of aquaporin channels, preventing proper water movement resulting in salivary hyposalivation. For example, the expression and localization of AQP5 was significantly reduced at the apical and lateral plasma membrane of acinar cells of rats treated with radiation. Attempts to restore AQP5 expression following radiation, either by pretreatment with pharmacologic agonists targeting the muscarinic receptor or α_1-adrenoreceptor, have been shown to restore salivary flow rates to pre-irradiated level (Takakura, Takaki et al. 2007, Han, Wang et al. 2015). These studies demonstrate the importance of aquaporin channels in facilitating salivary gland function at homeostasis and its potential role following radiation treatment.

Disruption of salivary stem and progenitor cells

Following an injury event, many tissues have the capacity to repair and replenish the damaged areas through the utilization of stem cells (Poss 2010). The exact identity of salivary stem/progenitor cells is currently unknown; however, a ductal ligation model has demonstrated that submandibular salivary glands are capable of regenerating following damage. In this induced injury model, a metal clip is surgically placed on the main duct of the submandibular glands. Five days following ductal ligation, cellular atrophy

followed by near complete loss of differentiated acinar cells can be observed. Following ligation and subsequent de-ligation, the glands are able to fully regenerate (Tamarin 1971, Walker and Gobe 1987, Scott, Liu et al. 1999). In a series of pulse-chase experiments, Takahashi and colleagues demonstrated that the acinar cell precursors first arose from the ductal compartment and subsequent regeneration of the glands was dependent on the proliferation and differentiation of these newly formed acinar cells (Takahashi, Schoch et al. 1998). This suggested that regeneration and maintenance of the obstructed salivary glands involved the participation of both ductal- and acinar-derived cells.

The ability of the ligated glands to fully regenerate demonstrates that salivary glands possess some regenerative potential. However, the regulatory mechanisms governing the homeostasis and regenerative processes of the salivary glands are not fully known. Compared to the de-ligated glands, irradiated glands do not fully regenerate. The reason for the lack of regeneration in the irradiated glands could be attributed to the direct effect of radiation on the endogenous stem and progenitor populations or the disruption of the microenvironment in which the stem cells reside, or both (Konings, Coppes et al. 2005, Tatsuishi, Hirota et al. 2009).

Ionizing radiation can cause DNA damage within stem cells and the repair mechanism is tissue-specific and dependent on the pluripotent state of the stem cells. For example, embryonic stem cells have been shown to predominantly use the high fidelity homologous recombination (HR) repair pathway to repair double-strand DNA breaks (Mandal, Blanpain et al. 2011). Adult stem cells, such as hematopoietic stem cells and bulge stem cells of the skin epidermis, rely primarily on the efficient, but often error

prone non-homologous end joining (NHEJ) repair pathway (Mohrin, Bourke et al. 2010, Mandal, Blanpain et al. 2011).

Little is known about the direct effect of radiation on resident salivary stem/progenitor cells. It has been hypothesized that salivary stem cells may be killed or sterilized in the course of radiation, thus preventing glandular regeneration (Konings, Coppes et al. 2005). In agreement with this hypothesis, it was demonstrated that by sparing the excretory duct from radiation exposure during treatment, there was marked improvement in salivary function (van Luijk, Pringle et al. 2015). Historically, the ductal region of the salivary glands has been hypothesized to be the location where salivary stem cells reside (Takahashi, Schoch et al. 1998). Thus, this led the authors to conclude that damage to the resident salivary stem cells may be the contributing factor causing radiation-induced salivary gland dysfunction. Utilizing a pulse-chase assay, Chibly and colleagues showed that label retaining cells, which resembled salivary stem/progenitor cells in terms of their stem cell marker profiles and *in vivo* self-renewal capacity, are found at similar levels in both the ductal and acinar compartments of the salivary glands following radiation (Chibly, Querin et al. 2014). Additionally, recent work by Aure et al. and Emmerson et al. demonstrate that besides the major ductal structures, the acinar compartment of the salivary glands also contains a putative population of cells that is capable of regeneration (Aure, Konieczny et al. 2015, Emmerson, May et al. 2018). This suggests the regenerative process in the salivary glands involves multiple populations of stem cells and they reside in different compartments of the glands.

The stem cell niche is the *in vivo* microenvironment where stem cells reside. The microenvironment plays a crucial role in the maintenance and regulation of stem cell

function (Jones and Wagers 2008). For example, in the perivascular niche where haemopoietic stem cells (HSC) reside, endothelial and CXC-chemokine ligand 12 (CXCL12) stromal cells are responsible for the production of stem cell factor (SCF), which is required for the maintenance of HSC (Nagasawa, Hirota et al. 1996, Sugiyama, Kohara et al. 2006, Wang and Wagers 2011). Ablation of CXCL12 stromal cells impairs the synthesis of SCF and leads to a reduction in cycling lymphoid and erythroid progenitor cells, the progeny of hematopoietic stem cells (Omatsu et al., 2010). It was shown in an embryonic explant culture of submandibular glands that removal of parasympathetic ganglion decreased the number and morphogenesis of Keratin 5 (K5) progenitor cells, indicating that the parasympathetic innervation is important in maintaining a salivary progenitor population (Knox, Lombaert et al. 2010). Using the same explant culture system, Knox et al. have shown that radiation treatment caused a reduction in the parasympathetic nerves, but not the resident K5 progenitor cells. Treatment of the irradiated submandibular explant tissue with neurturin, a neurotrophic growth factor that regulates neuron survival and function, reduced neuronal apoptosis and increased expression of genes that are involved in parasympathetic innervation (Knox, Lombaert et al. 2013). This implies that radiation caused a decrease in innervation of the salivary progenitor cells due to neuronal apoptosis, leading to the lack of activation and subsequent regeneration of the glands by salivary stem cells.

Clinical management of xerostomia

Pharmacological agents

Stimulation of salivary output can be achieved using pharmacological agents, known as "sialogogues." Pilocarpine and cevimeline are the only two sialogogues currently approved by the U.S. Food and Drug Administration for the treatment of xerostomia primarily due to radiotherapy treatment (Vivino, Al-Hashimi et al. 1999). Pilocarpine and cevimeline are cholinergic, parasympathetic agonists and act to stimulate any residual function of the salivary glands post radiation treatment. Effectiveness of these sialogogues is short term and the beneficial effect ceases as soon as administration of the stimulant stops (Johnson, Ferretti et al. 1993, LeVeque, Montgomery et al. 1993). Pre-clinical studies in rats show that pretreatment with pilocarpine significantly prevents the loss of salivary gland function, and this physiological effect is due in part to compensatory proliferation of the undamaged cells (Burlage, Roesink et al. 2008, Burlage, Faber et al. 2009). However, the effectiveness of pilocarpine in humans is more variable and beneficial effect is dependent on the dose distribution in the parotid glands (Burlage et al., 2008; Haddad and Karimi, 2002). A recent Cochrane review concluded that there is insufficient data to determine the benefit of pilocapine with regard to xerostomia, salivary flow rate, and overall quality of life (Riley, Glenny et al. 2017).

Radioprotective agents, such as amifostine act as free radical scavengers and have shown to be moderately effective in the amelioration of radiation-induced salivary gland dysfunction and xerostomia (Wasserman, Brizel et al. 2005, Hensley, Hagerty et al. 2009). Phase III clinical trials demonstrated that administration of amifostine before and during radiotherapy treatment had the potential to reduce symptoms of dry mouth (Brizel,

Wasserman et al. 2000, Jellema, Slotman et al. 2006). However, due to the lack of consensus guidelines and the radioprotective effect amifostine might have on tumors, it is a controversial issue whether amisfostine is safe for use in patients (Koukourakis 2003, Oronsky, Goyal et al. 2018).

Non-pharmacological methods

Non-pharmacological approaches that aim to stimulate residual function or promote wound healing in irradiated salivary glands include acupuncture, electrical stimulation, and hyperbaric oxygen treatment (HBOT). The mode of action for these therapies (i.e. electrical stimulation and acupuncture) is the communication between the peripheral nerves and the salivary glands (Furness, Bryan et al. 2013). The effects of acupuncture on saliva secretion and management of xerostomia-related symptoms has been reported in HNC patients and can be sustained for at least 6 months and up to 3 years (Blom and Lundeberg 2000). While there is evidence that the aforementioned therapies may be a viable therapeutic option for the management of salivary gland dysfunction and xerostomia, there is insufficient evidence that these therapies significantly improved salivary gland function due to diverse causes of xerostomia in these patients and the lack of control placebo group in the reported studies (Bakarman and Keenan 2014, Assy and Brand 2018).

Additionally, hyperbaric oxygen treatment (HBOT) has also been proposed as a therapeutic option to promote wound healing in irradiated salivary glands (Cankar, Finderle et al. 2011). A systematic review evaluating the efficacy of HBOT reported that HBOT improved salivary gland function and reduced the perception of xerostomia in HNC patients who suffered from radiation-induced salivary gland hypofunction.

However, the majority of the studies included in the systematic review lack a control group, suggesting that more studies are needed to evaluate whether HBOT is a viable option for patients with chronic loss of salivary function (Fox, Xiao et al. 2015). In the event of severe hyposalivation when stimulation of residual salivary secretion is insufficient, saliva lubricants are recommended to patients. These saliva lubricants have gel-like properties to resemble the viscoelasticity of natural saliva (Regelink, Vissink et al. 1998).

Therapies under development

Protective therapies

Pre-clinical studies in rodent models have demonstrated that pre-administration with selective growth factors prevents radiation-induced hyposalivation. Pretreatment of mice with recombinant insulin-like growth factor-1 (IGF-1) leads to activation of the Akt pathway, suppression of acute apoptosis, and preservation of salivary function. In a similar fashion, pre-administration of Keratinocyte growth factor (KGF) to mice induces the proliferation of ductal cells, the region of the salivary glands where stem/progenitor cells are believed to reside (Lombaert, Brunsting et al. 2008). This increase in the ductal cell pool is correlated with the preservation of glandular function following radiation. Glial cell line-derived neurotropic factor (GDNF) has also been shown to ameliorate radiation-induced salivary dysfunction and it is hypothesized that it might be modulated through the enrichment of the Lin-CD24+c-Kit+Sca1+ cells, a population of putative salivary stem/progenitor cells that have high capacity for proliferation, self-renewal, and differentiation *in vitro* (Xiao, Lin et al. 2014).

Restorative therapies

Gene therapy

Gene therapy has been investigated as a therapeutic option for radiation-induced salivary gland dysfunction. The use of adenoviral-mediated aquaporin-1 cDNA (AdhAQP1) transfer to drive the expression of Aquaporin-1, a water channel, in the remaining ductal cells has shown promising results in ameliorating radiation-induced salivary gland dysfunction in studies with mice, rats, miniature pigs, and macaques (Delporte, O'Connell et al. 1997, Shan, Li et al. 2005). An open label clinical trial was

initiated by Baum and colleagues to use the AdhAQP1 vector in irradiated parotid glands of subjects previously treated for head and neck cancer with radiotherapy. In five out of the eleven subjects enrolled in the study trial, the gene therapy was found to increase salivary flow rate from the parotid glands by 50%, as well as reduce symptoms related to radiation-induced salivary gland dysfunction (Baum, Alevizos et al. 2012). While gene therapy is a promising therapeutic option, the delivery of viral vector raises various concerns, including the risk of insertional mutagenesis and adverse immune responses. Currently, a clinical trial is under review to use a less immunogenic viral vector, serotype 2 adeno-associated viral (AAV2) vector for AdhAQP1-mediated gene therapy (Momot, Zheng et al. 2014).

Tissue engineering

Transplantation of bioengineered salivary gland (SG) tissue using cells cultured with biomaterial and growth factors has been proposed as a therapeutic option in patients suffering from salivary gland hypofunction. This application requires the proper maintenance of salivary cells in a biocompatible and biodegradable 3D scaffold to promote tissue organogenesis (Pradhan and Farach-Carson 2010, Peters, Naim et al. 2014). *In vitro* studies have demonstrated that biological and biocompatible materials like collagen and Matrigel are capable of promoting the expansion of acinar-like cells; however, these biomaterials are deemed not suitable for clinical translation and no studies have been conducted to examine the viability, maintenance, and secretory function of SG engineered tissue *in vivo* (Maria, Zeitouni et al. 2011, Pradhan-Bhatt, Harrington et al. 2013).

Regenerative therapies

Salivary gland stem cell: current knowledge & future prospects

Currently, a comprehensive profile of salivary gland stem cells is not known. It is still an area of active research to characterize the identity of these putative populations and understand their fate following radiation. Work in both developmental and radiation models have identified multiple populations of cells that exhibit stem-like features.

Lineage tracing studies by Bullard et al. reported Ascl3+ cells to be a precursor of both ductal and acinar cell types in the parotid, submandibular, and sublingual glands. Interestingly, Ascl3+ cells were not a precursor to Keratin 5+ cells, which have been shown to be important during development of murine submandibular glands (Bullard, Koek et al. 2008, Arany, Catalan et al. 2011, Rugel-Stahl, Elliott et al. 2012). In a series of pulse-chase experiments, Kwak et al. identified a population of Keratin 14+ cells, basal progenitor cell marker, in the intercalated and excretory ducts of submandibular glands.

In a radiation model, studies by Lombaert et al. showed that by transplanting as little as two hundred c-Kit+ cells into irradiated recipient mice, the function of radiation-impaired submandibular glands was partially restored (Lombaert, Brunsting et al. 2008). In these studies, c-Kit+ cells were found to possess the capacity for self-renewal and differentiate into both acinar and ductal cells *in vivo* and *in vitro*. It remains elusive whether the transplanted c-Kit+ cells directly participated in the regeneration of the glands and if the endogenous c-Kit+ cells aid in the regenerative process. Utilizing the hematopoietic stem cell surface marker system, Xiao et al. isolated a more pure population of salivary stem/progenitor cells. Transplantation of this target population,

Lin-CD24+cKit+Sca-1, into irradiated recipient mice partially restored saliva production and number of functional acini (Xiao, Lin et al. 2014).

Utilizing a pulse-chase assay and current profile of putative salivary stem/progenitor markers, Chibly et al. found that label retaining cells, which exhibited characteristics of salivary stem/progenitor cells, are maintained following radiation (Chibly, Querin et al. 2014). Similarly, recent work by Emmerson et al. shows that SOX2+ cells, a progenitor population that gives rise to the acinar compartment of the salivary glands during development, is present following radiation. Furthermore, it was demonstrated in an *ex vivo* explant culture that stimulation of the nerves by cholinergic mimetics led to proliferation of resident SOX2+ cells in the irradiated salivary glands (Emmerson, May et al. 2018). Taken together, these studies raise future research questions that it may be the intracellular effect of radiation damage on the endogenous stem and progenitor cell pool, rather than the loss of this population, that contributes to radiation-induced glandular dysfunction.

Paradigm of regenerative process in adult tissue

Natural regeneration

As previously discussed, the regenerative process is driven by stem cells, a potent population of cells that have the capability to give rise to lineage-committed cells to replenish the damaged tissue. Thus, it is thought that loss of this putative population following an injury event would prevent the tissue from self-repair. However, work in other tissue models (i.e. intestine, pancreas, and liver) have demonstrated that other resident cell populations besides stem cells can participate in the regenerative process given the right stimuli (Thorel, Nepote et al. 2010, Tian, Biehs et al. 2011, Miyajima, Tanaka et al. 2014, Kopp, Grompe et al. 2016). A well-studied example of this is adult intestinal cells. During homeostasis, LGR5+ (Leu-rich repeat-repeating G protein-coupled receptor 5-expression) crypt base columnar (CBC) stem cells drive epithelial renewal by giving rise to progenitor cells (i.e. DLL1+ secretory, LGR5+ LRC Paneth, and +4 stem cells), which differentiate into lineage-specific goblet, tuft, and paneth cells. Ionizing radiation results in the loss of actively proliferating LGR5+ CBC stem cells, but leaves the +4 stem cells and the intestinal niche intact. The surviving +4 stem cell population, in this case, acts as the "reserve" stem cell pool by replenishing the LGR5+ CBC pool to drive the regeneration of the injured intestinal epithelium (Tian, Biehs et al. 2011, Buczacki, Zecchini et al. 2013). *Ex vivo* organoid culture studies show that LGR5- cells can be converted to LGR5+ stem cells when exposed to WNT3A, ligand of the Wnt signaling pathway, and the driving force behind intestinal epithelium renewal during homeostasis (Sato, van Es et al. 2011).

Induced regeneration

The intestinal-tissue regeneration model provides evidence that the capacity of a tissue to repair and regenerate is linked to the microenvironment of the healing wound, and not necessarily to the inability of the cells to participate in the regenerative process (Dolan, Dawson et al. 2018). Regenerative failure might be caused by a toxic wound environment where the lack of secreting factors by the microenvironment leads to inactivation of signaling pathways that are necessary to drive regeneration. Thus, induced regeneration can be achieved by identifying targets that are involved in the regenerative process and how their deficiency causes a non-regenerative response in a wound environment. For example, amputation of the chick limb during the embryonic stage leads to a non-regenerative response. Application of Fibroblast growth factor-2 (FGF2) to the amputation site stimulates reprogramming of the mesodermal cells and induces limb regeneration (Taylor, Anderson et al. 1994, Kostakopoulou, Vargesson et al. 1997). Radiation-induced salivary dysfunction could be an example of a regeneration-incompetent injury where the regeneration response must be induced. Preclinical studies in rodent models have demonstrated that irradiated salivary glands are responsive post-treatment to a selection of growth factors (i.e. IGF1, KGF, and GDNF), which translated to restoration of physiologic function (Lombaert, Brunsting et al. 2008, Grundmann, Fillinger et al. 2010, Xiao, Lin et al. 2014). Additionally, activation of the ectodysplasin/ectodysplasin receptor (EDA/EDAR), a signaling pathway that is critical in the growth of salivary glands during embryonic development, was able to restore saliva output to pre-irradiated levels (Hill, Headon et al. 2014). In summary, the aforementioned studies suggested that given the right stimuli, the irradiated salivary glands can be

stimulated and saliva production can be restored at a chronic time point following radiation damage.

Statement of the problem

Approximately over 50,000 patients are diagnosed with head and neck cancers (HNC) in the United States each year and about half a million worldwide. Current treatment of HNC utilizes a multidisciplinary approach, radiotherapy alone or in combination with chemotherapy and surgery. The major drawbacks of radiotherapy for head and neck cancers is radiation exposure of non-malignant tissue (i.e. salivary glands). The majority of HNC patients undergoing radiotherapy suffer from chronic salivary dysfunction. Loss of saliva is associated with a multitude of complications (i.e. dental decay, dysphagia, oral infections, etc.), all of which contribute to deteriorating quality of life in the HNC population. Currently, there is no definitive treatment for radiation-induced salivary gland dysfunction and available palliative cares are short-term and fail to improve quality of life. Stem cell-based therapies are a promising avenue for the treatment of salivary gland hypofunction and continued existence of salivary stem cell populations have been reported following radiation treatment. However, the effect of radiation on these putative populations, and whether they can be stimulated to regenerate and restore saliva production in the damaged salivary glands is unknown. Thus, understanding the intracellular effect of radiation on salivary stem cell populations and their response upon radiation injury will facilitate development of novel therapies for the treatment of radiation-induced salivary gland dysfunction.

CHAPTER 1

INTRODUCTION

Annually, head and neck cancer (HNC) has more than 500,000 new cases worldwide (Parkin, Bray et al. 2005). The current treatment for HNC utilizes a multimodality approach, which includes surgery in combination with radiotherapy (RT) and chemotherapy (Cmelak 2012). Despite the application of intensity-modulated radiation therapy (IMRT) to spare the salivary glands during HNC treatment, the parotid glands are frequently still damaged due to close proximity to the tumor sites (Lin, Kim et al. 2003, Schmitt 2011). Consequently, HNC patients often suffer from permanent xerostomia following radiotherapy treatment (Devi and Singh 2014). Current preventive and palliative care for the management of RT-related xerostomia are limited and largely ineffective (Lopez-Jornet, Camacho-Alonso et al. 2012, Furness, Bryan et al. 2013, Fox, Xiao et al. 2015). This poses a health concern because reductions in the quantity of saliva can greatly affect the quality of life of HNC patients. Such patients suffer from increased oral infection rates, difficulty chewing and swallowing food, malnutrition, and difficulty in speaking (Spielman, Ben-Aryeh et al. 1981, Pedersen, Bardow et al. 2002).

Adult stem and progenitor cells (SSCs) have been identified in many tissues (e.g. skin, gut, bone marrow) and are known to play an important role in the continuous repair and regeneration of tissues following damage (Wilson, Laurenti et al. 2008, Snippert, Haegebarth et al. 2010, Tian, Biehs et al. 2011). In many tissues, stem cells are activated to initiate the repair process when there is an excessive loss of differentiated cells or by environmental cues. This is followed by the proliferation and differentiation of progenitor cells to replenish the existing cell pool (Biteau, Hochmuth et al. 2011, Hsu and Drummond-Barbosa 2011, Mascre, Dekoninck et al. 2012). In accordance with this

paradigm of stem cell-based regeneration, it is thought that putative salivary stem/progenitor cells (SSCs) have the potential to regenerate salivary glands following radiation damage (Okumura, Nakamura et al. 2003, Coppes and Stokman 2011). However, it has been demonstrated both clinically and in mouse models of radiation-induced salivary gland damage that there is a lack of regeneration following radiation treatment (Grundmann, Mitchell et al. 2009, Vissink, Mitchell et al. 2010). Ionizing radiation exposure can disrupt tissue homeostasis and regeneration by either 1) directly damaging the SSC pool or 2) indirectly disturb the *in vivo* environment that is necessary to maintain the stem/progenitor pools (Chibly, Nguyen et al. 2014, Mendelson and Frenette 2014). It remains elusive whether the lack of regeneration by salivary glands following radiation treatment is due to direct damage to the SSC pool or disruption of the SSC niche environment.

Previous studies have shown that transplantation of putative salivary stem/progenitor cells, based on identification of cell surface markers c-Kit^{+}, CD24^{+}, Lineage^{-}, Sca-1^{+}, one day following radiation treatment can partially restore salivary gland function (Lombaert, Brunsting et al. 2008, Nanduri, Maimets et al. 2011, Xiao, Lin et al. 2014). Additionally, administration of growth factors (e.g. Insulin-like growth factor 1 (IGF1), Keratinocyte growth factor (KGF), Glial cell line-derived neutrophic factor (GDNF)) at an early critical time point (1-4 days) following radiation treatment have also been effective in restoring salivary gland function (Lombaert, Brunsting et al. 2008, Grundmann, Fillinger et al. 2010, Xiao, Lin et al. 2014). Taken together, these findings suggest that at an early time point following radiation treatment, the putative SSC pools are not lost in the course of radiation and are still responsive to external

stimuli. However, it remains unclear whether salivary stem/progenitor cells retain their regenerative capacity when stimulated by an external cue at chronic time points post radiation damage. It would provide great therapeutic insight to understand the "window of opportunity" where these cellular populations could be stimulated to regenerate during chronic time points of radiation-induced salivary gland dysfunction.

Sphere-forming assays have been widely used in other systems, including the brain, lung, pancreas, and breast to retrospectively characterize a heterogeneous population of cells that exhibit stem cell-like behavior based on the capacity to self-renew and differentiate *in vitro* (Pastrana, Silva-Vargas et al. 2011). In this study, we utilized an ex vivo sphere formation cell culture to assess the self-renewal capacity of cells derived from parotid glands at a chronic time point following radiation treatment. There was a significant reduction in sphere formation from irradiated parotid glands and supplementation with growth factors restored self-renewal properties to levels similar to unirradiated controls. Defining the self-renewal and differentiation potential of irradiated salivary cells may provide therapeutic value for the development of regenerative therapies for damaged salivary glands.

MATERIALS AND METHODS

Mice and sphere forming assay

All experiments were conducted in 4-6 week old or 8 week old female FVB mice. All mice were maintained and treated in accordance with protocols approved by the University of Arizona Institutional Animal Care and Use Committee (IACUC). A total of 44 mice were used for sphere culture across 22 individual experiments. For each experiment, parotid glands from 2 mice were collected and salisphere formation was propagated using a sphere culture technique as previously described (Lombaert, Brunsting et al. 2008, Chibly, Querin et al. 2014). Cells were suspended in serum free medium supplemented with or without 2.5%, 5%, or 10% fetal bovine serum (FBS) (Hyclone, Logan, UT) and plated at a density of 200,00 cells in ultra-low attachment plates (Corning, Corning, NY). Culture condition and numbers of primary cell preparations for each experiment are indicated in each figure legend.

Radiation treatment

Mice were anesthetized with Ketamine/Xylazine (50mg/kg (K)+10 mg/kg (X)) followed by exposure to a single dose of 5 Gy targeted to the head and neck region using a ^{60}Cobalt Teletherapy unit (Theratron-80, Atomic Energy of Canada Ltd), with the rest of the body protected by a lead shield. The 5 Gy dose was chosen based on previous work demonstrating significant reductions in salivary function and differentiation status (as determined by amylase expression) of parotid salivary glands (Grundmann, Fillinger et al. 2010). Thirty days after irradiation, a sub-group of irradiated mice were injected intravenously through the tail vein with 5µg recombinant IGF-1 (GroPrep, Adelaide, Australia) for three consecutive days (days 31-33, approximately 24 hours apart; Fig 6A).

This dose of IGF-1 was chosen because it was previously shown to restore salivary gland function post-radiation treatment (Grundmann, Fillinger et al. 2010).

Saliva Collection

Eight week old female FVB mice were treated with targeted head and neck radiation with and without post-therapy IGF1 as described in Figure 1.10. On day 60 after radiation treatment, mice were injected i.p. with carbachol (0.25 mg/kg body weight) and saliva was collected for 5 minutes. Total saliva was collected by vacuum aspiration from 6 mice per treatment group: untreated FVB, irradiated, and IGF1 treated group on ice following carbachol injection into pre-weighted tubes and stored at -80˚C as previously described (Lin, Johnson et al. 2001, Limesand, Schwertfeger et al. 2006).

Cell viability assay

Cell viability was assessed using the thiazolyl blue tetrazolum bromide (MTT; Thermo Scientific, Waltham, MA) assay. At pre-determined time points, the MTT solution (5mg/mL) was added to each well for 4 hours at 37˚C. Formazan crystals formed in salisphere cells were solubilized with DMSO (Fisher Scientific, Waltham, MA). Lysates were transferred to 96-well plates (Corning) and absorbance was measured at 540 nm using the Ultramark Microplate Reader (Biorad, CA, USA).

EdU incorporation and Immunofluorescence staining

At pre-determined time points, salispheres were fixed directly in culture by adding 1 volume of 10% buffered formalin for 20 minutes at room temperature. After fixation, salispheres were permeabilized with 0.2% Triton X in PBS for 20 minutes at room temperature. Target-specific staining of salispheres was performed in suspension by incubating in primary antibody diluted 1:100 in 1% BSA overnight at 4°C: anti-Ki-67

(12201, Cell Signaling, Danvers, MA), anti-Keratin 5 (PRB-160P, Covance, Princeton, NJ), anti-Keratin 14 (PRB-155P, Covance), anti-Aquaporin 5 (AB3559, Labome, Princeton, NJ), and anti-NKCC1 (a59791, Abcam, Cambridge, UK); followed by incubation in secondary anti-rabbit Alexa 594 (A-11307, Invitrogen, Carlsbad, CA) at 1:500 dilution. For EdU incorporation, primary salispheres were incubated in culture medium containing 10μM EdU (5-ethynyl-2′-deoxyuridine, Invitrogen) for one hour prior to fixation. The EdU staining protocol was adapted from manufacturer's instructions (Click-It Plus EdU Alexa Fluor 488 Imaging Kit, Life Technologies, Grand Island, NY) to stain salispheres directly in suspension. Salispheres were pelleted by centrifugation at 4000 rpm for 5 minutes and resuspended in EdU click-it cocktail for 30 minutes at room temperature. Images were acquired with an Intelligent Imaging Innovations (Danvers, Colorado) configured instrument including a Zeiss Marianas 100 Microscopy Workstation (Oberkochen, Germany), Yokogawa CSU-X1 M1 Spinning Disk (Musashino, Tokyo, Japan) and Photometrics Evolve 512 EMCCD (Tucson, Arizona) using a Zeiss EC Plan-Neifluar 40X/1.3 NA oil objective and a .5μm z-separation between the slices in the stack. The Spinning Disk includes a Semrock Di01-T488/568 dichroic beam splitter and a Em01-R488/568 dual bandpass emission filter for 488 nm ex- BP 525/43 em and 561 nm ex- BP 642/117 em imaging.

Western blot analysis

Salispheres were collected, rinsed with phosphate-buffered saline (PBS), and lysed in RIPA buffer that contained 5 mM sodium orthovanadate (Fisher Scientific) and protease inhibitor cocktail (Sigma-Aldrich, St. Louis, MO) on ice for 30 minutes. Supernatants were harvested after centrifugation at 12,000 rpm for 15 minutes (4°C).

Five micrograms of protein sample was loaded onto 10% polyacrylamide gels and then transferred to 0.45 µm Immobolin-P membranes (Millipore, Billerica, MA). The membranes were blocked with 5% BSA and then immunoblotted overnight at 4°C with one of the following antibodies: anti-Keratin 5, anti-Keratin 14, and anti-ERK 1/2 (1:2000, Cell Signaling). For detection, SuperSignal substrate was used as instructed by the manufacturer (Thermo Scientific).

Determination of Size and Total Number of Salispheres

Salisphere number and size were assessed on Days 4-14 in culture. To do this, 25 bright field images were randomly captured from each well using Optixcam Summit OSC-3.0x TMS-DK3-5 camera (Microscope Store, Roanoke, VA, USA). The diameter of individual salispheres was measured using 1.46 ImageJ software. For each experiment, the number of salispheres was manually counted from a minimum of 15 images per well from 3 to 10 wells. The number of wells analyzed for salisphere count for each experiment is indicated in each figure legend. Only salispheres with a diameter of >50µm were counted due to the utilization of a 40 µm diameter filter to obtain a single cell suspension prior to plating.

Proliferation Analysis

Proliferation of salispheres was assessed through Ki-67 immunostaining on different days of culture. To do this, between 10-20 confocal 3D stack images per treatment condition were randomly selected for analysis. The number of 3D stack images used for the proliferation analysis in each experiment is indicated in each figure legend. Cells were manually counted from every fifth slice in the z-stack image using the Cell Counter program from ImageJ. Proliferation of an individual salisphere was determined

by the sum of the number of positive cells/total number of cells from the accumulated slices in a single z-stack image. Analysis of EdU, Keratin 14, and Keratin 5 levels were carried out using a similar manual counting technique.

Statistical analyses

Statistical analyses were performed using SPSS (version 24.0, SPSS Inc., Chicago, IL, USA). Two-sided independent sample t-tests were performed to compare the number of salispheres between treatment groups at different days in culture. One-way ANOVA was performed on the log transformed data of Ki-67 proliferation index of an individual salisphere to satisfy the normality assumption. Tukey post hoc multiple comparisons were conducted to compare the differences in salisphere proliferation between groups of different salisphere sizes, days in culture, and treatment conditions. One-way ANOVA was performed on dual expression of EdU/Keratin 14 and EdU/Keratin 5 by salisphere cells. No transformation was needed to satisfy the assumptions of normality and homogeneity of variances. Tukey post hoc multiple comparisons were conducted to compare differences in EdU/Keratin 14 and EdU/Keratin 5 dual expression between groups of culture conditions and treatment conditions. Similarly, one-way ANOVA with Tukey post hoc comparisons were run to compare mean salivary flow rates across untreated control, irradiated, and IGF1 treated groups. Graphical generation was done using Graph-Pad (version 5.0, San Diego, CA).

RESULTS

Sphere-forming efficiency decreases following radiation

To evaluate the sphere-forming efficiency of irradiated parotid glands, the number and size of salispheres were quantified over time in culture. FVB mice (4-6 week old) were subjected to a single 5 Gy dose of targeted head and neck radiation and parotid glands were harvested 30 days post treatment for sphere-forming assay. On each cell isolation day, spheres were grown from unirradiated mice for comparison. By day 7, the presence of salispheres can be detected and the number and size of salispheres increased with longer time in culture (Figure 1.1A). Assessment of salisphere formation reveals a significant decrease in the number of salispheres formed in the irradiated glands compared to untreated controls (Figure 1.1B). MTT (3-(4,5-dimethylthiazol-2-yl)-2,5-diphenyltetrazolium bromide) assay did not detect a difference in cell viability between cells derived from untreated and irradiated glands under serum-free medium condition (Figure 1.2). The proliferation capacity of untreated and radiation-derived salispheres was also assessed through Ki-67 immunostaining. At early time points (days 4-7), the culture consists mostly of free-floating clusters of cells that are less than 50μm in diameter, which will be referred to as small salispheres (Figure 1.1C, 1.3A and 1.3B). The proliferation percentage of small salispheres ranges from 10-50% in the untreated group and 0-60% in the irradiated group (Figure 1.3C). Interestingly ~35% of the spheres in the irradiated group exhibit no proliferation at day 7. Due to the different responses to growth in the irradiated spheres, there is no significant difference in proliferation compared to unirradiated controls (P= 0.078). Following a longer period of time in culture (day 14), the proliferation capacity of salispheres derived from untreated and irradiated cells

significantly decreases, regardless of salisphere size (Figure 1.3C). These results suggest that decreased salisphere formation from irradiated glands may not be due to a decrease in cell viability, rather a subset population that is less responsive to proliferate in serum-free medium condition at early time points in culture.

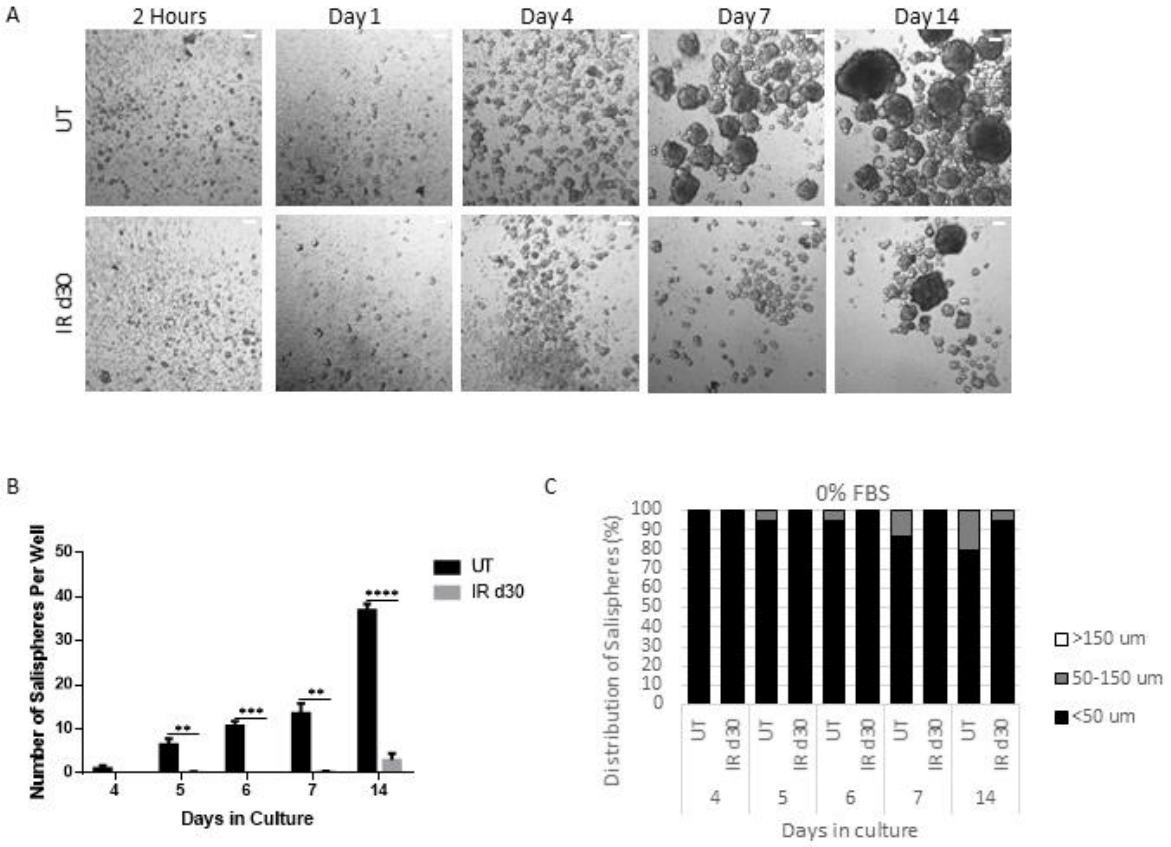

Figure 1. 1: Sphere-forming efficiency decreases following radiation.
A single 5 Gy dose of radiation (IR d30) was given to 4-6 week old female FVB mice and parotid glands were collected 30 days following radiation for sphere formation assay. Representative bright field images of salispheres grown from untreated control (UT) and irradiated (IR d30) glands in serum-free media at different time points in culture (A). Number of salispheres was quantified per 6 wells from 3 primary cell preparations per treatment group at days 4, 5, 6, 7, and 14 in culture and expressed as average ± SEM (B). Representative graphs showing the distribution of salisphere sizes among all the salispheres counted from one UT and IR d30 primary sphere preparation (C). P values were obtained with 2-sided unpaired t-test (n=3), **p<.01, ***p<.001, ****p<.0001. Scale bar= 50μm.

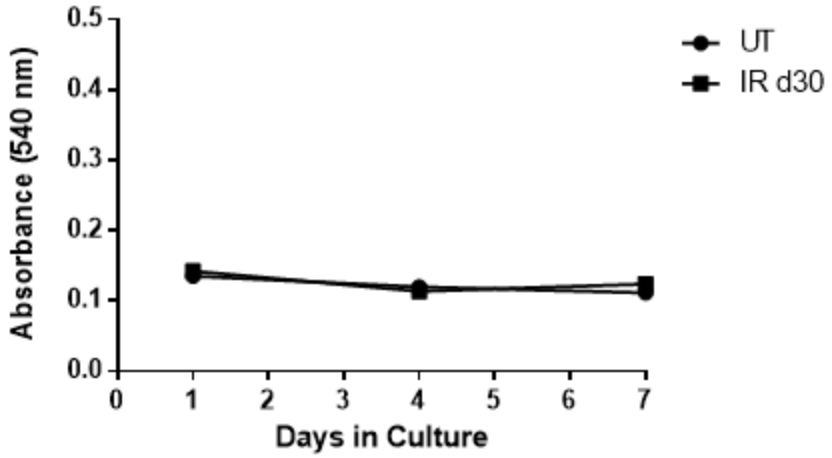

Figure 1.2: Cell viability assay of salispheres derived from untreated and irradiated mice. Viability of salisphere cells derived from untreated (UT) and irradiated (IR d30) parotid glands was assessed at different time points in serum-free culture using MTT assay. Absorbance measurement was obtained from one UT and IR d30 primary sphere preparation (A).

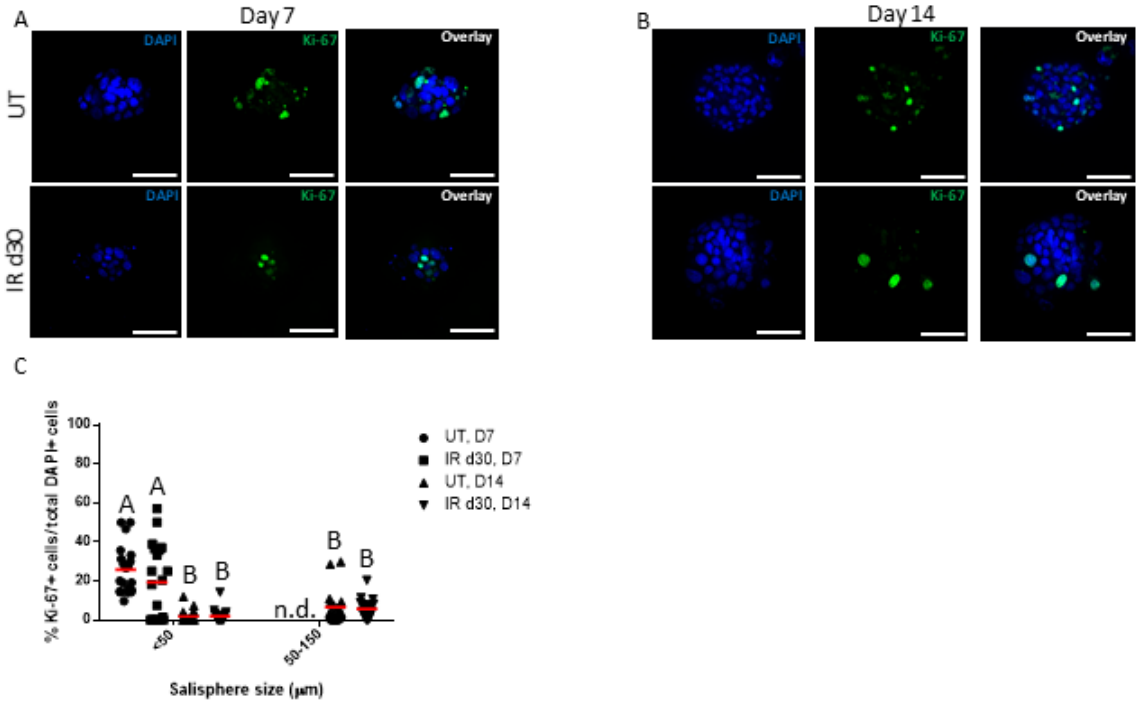

Figure 1.3: Similar proliferation rates are observed in untreated and irradiated salispheres cultured in serum-free conditions.

Untreated and irradiated parotid-derived salispheres were fixed after 7 and 14 days in culture and stained for Ki-67 (green). Representative confocal immunofluorescence images are shown. Ki-67 was expressed in salisphere-derived cells at both early (day 7) and later (day 14) time points in culture (A-B). Percentage of Ki-67+ proliferating cells was quantified from 20 salispheres, of different sizes (<50µm, 50-150µm), at day 7 and 14 for both treatment groups and expressed as percent of proliferation by individual salisphere (red bar= mean percent of proliferation by group). At day 7 in culture, medium-sized salispheres (50-150µm) were rarely detected, thus this analysis was not determined (n.d.). Significant differences ($p < 0.05$) were determined using a one-way ANOVA with post-hoc Tukey multiple-comparison tests on the log transformed data of Figure 2C. Groups with the same letter are not significant different from each other (C). Scale bar= 50µm.

FBS increases sphere-forming efficiency of irradiated parotid-derived cells

To determine whether sphere-forming cells from irradiated mice can be stimulated to respond and form salispheres, fetal bovine serum (FBS) was supplemented into the culture medium and the number and size of salispheres were determined at 4, 5, 6, and 7 days after the start of culture (Figure 1.4). By day 4, the presence of salispheres can be detected in both untreated and irradiated groups. Increasing FBS concentration and longer time in culture results in the formation of larger salispheres (Figure 1.4A and 1.4B). For the untreated group, the total number of salispheres in 2.5%, 5%, and 10% FBS with a diameter (D_s) >50 μm gradually decreases with longer time in culture. By 7 days in culture, the number of salispheres falls to a level of approximately one-half of the initial value (2.5% FBS: 221 at day 4 vs. 102 at day 7; 5% FBS: 169 at day 4 vs. 73 at day 7; 10%: 80 at day 4 vs. 33 at day 7). In contrast, the total number of salispheres from irradiated mice gradually increases with 2.5% and 5% FBS culture conditions (2.5% FBS: 10 at day 4 vs. 73 at day 7; 5% FBS: 44 at day 4 vs. 75 at day 7). At days 4, 5, and 6 in culture, the total number of 2.5% FBS-treated salispheres derived from irradiated glands is significantly lower than the number of salispheres from unirradiated mice. In addition, at day 4 in culture, the total number of irradiated 5% FBS-treated salispheres is also significantly lower compared to untreated group. In contrast, there is no difference in the number of salispheres formed between untreated and irradiated groups when supplemented with a higher concentration of FBS (10%) (Figure 1.4C).

In parallel, as the total number of salispheres fell, both the maximal diameter ($D_{s\text{-}max}$) and the proportion of larger salispheres increases (Figure 1.4D). At day 7 in culture, almost all the 2.5% FBS-treated salispheres from the untreated group have a diameter

value between 50 and 150 µm. In the untreated group, large spheres (D_S >150µm) emerge at an earlier time in culture (day 5) with supplementation of higher FBS concentration (5% and 10%), and their proportion increases until the end of the culture period (day 7). Compared to the untreated group, the D_s^{max} of FBS-treated salispheres derived from irradiated glands is smaller and within a size range between 50 and 150 µm. Even with longer time in culture and the addition of higher FBS concentrations, the proportion of large-size salispheres (D_S >150µm) is less than untreated group (Figure 1.4D).

It was previously reported that there is nearly a 2-fold decrease in the number of salispheres formed from the submandibular glands harvested from old mice compared to young mice (Maimets, Bron et al. 2015). Since the majority of HNC patients are adults and 4-6 week old mice could be defined as juveniles, we evaluated whether mice that were 8 weeks old at the time of radiation exhibited a similar phenotype when salisphere cultures were evaluated 30 days after radiation treatment. Similar to what was previously observed in Figure 1.4, FBS supplementation of irradiated cells derived from mice that were 8 weeks old at the time of treatment, increases the number of salispheres along with the formation of larger salispheres upon longer culture periods (Figure 1.5). These results suggest that the addition of FBS improves salisphere formation from irradiated parotid glands, albeit the rate at which salispheres are formed and enlarged is lower compared to untreated controls.

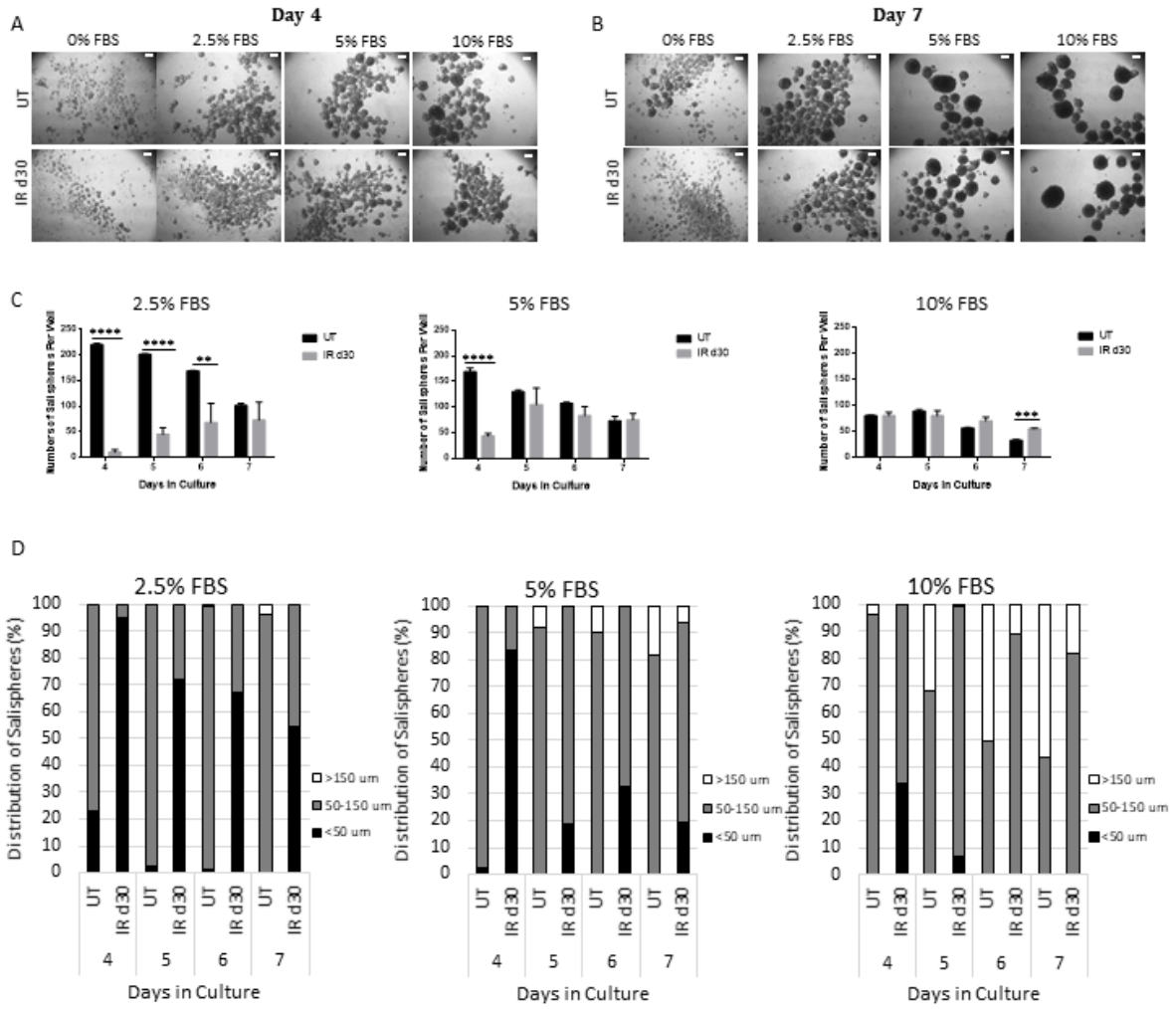

Figure 1.4: FBS increases sphere-forming efficiency of irradiated parotid-derived cells.
Representative bright field images of salispheres grown from UT (untreated) and IR d30 (irradiated) glands in serum-free media, supplemented with different concentrations of fetal bovine serum (FBS), taken at day 4 (A) and 7 (B) in culture. Number of salispheres was quantified per 6 wells from 3 primary cell preparations per treatment group at days 4-7 in culture and expressed as average ± SEM. P values were obtained with a 2-sided unpaired t-test (n=3), **p<.01, ***p<.001, ****p<.0001 (C). Representative graphs showing the distribution of salisphere sizes among all the salispheres counted from one UT and IR d30 primary sphere preparation (D). Scale bar= 100µm.

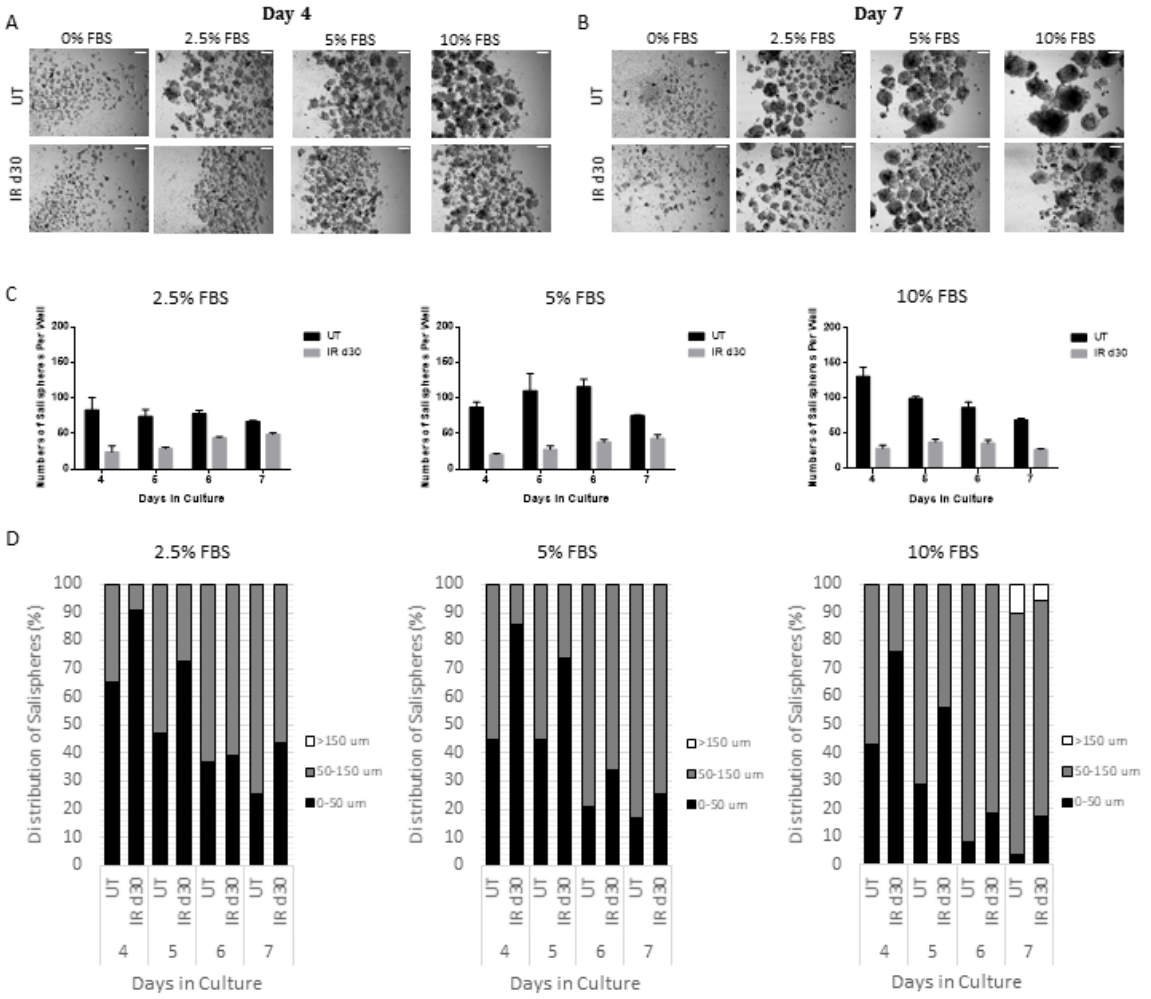

Figure 1.5: FBS increases sphere-forming efficiency of irradiated parotid derived cells from adult salivary glands.

A single 5 Gy dose of radiation (IR d30) was given to 8 week old female FVB mice and parotid glands were collected 30 days following irradiation for sphere formation assay. Representative bright field images of salispheres grown from UT (untreated) and IR d30 (irradiated) glands in serum-free media, supplemented with different concentration of fetal bovine serum (FBS), taken at day 4 (A) and 7 (B) in culture. Representative graph of the average number (± SEM) of salispheres from 3 wells per treatment group days 4-7 in culture from one UT and IR d30 primary sphere preparation. Representative graphs showing the distribution of salisphere sizes among all the salispheres counted from one UT and IR d30 primary sphere preparation (D). Scale bar= 100µm.

Proliferation rates are similar in salispheres supplemented with FBS from untreated and irradiated mice

To investigate whether the increase in sphere-forming efficiency of irradiated parotid-derived cells is due to an increase in the proliferative capacity in the presence of FBS, salispheres supplemented with 2.5% or 10% FBS were fixed after 4 and 7 days in culture and immunostained for Ki-67 (Figure 1.6A and 1.6B). There is an increase in the mean proliferation percentage of 2.5% FBS-treated salispheres (Figure 1.6C and 1.6D) derived from untreated glands compared to salispheres maintained in serum-free culture (0-50µm: 44.95% at day 4 in 2.5% FBS vs. 27.27% at day 7 in 0% FBS). Regardless of salisphere size, there is no significant difference in proliferative capacity of salispheres derived from untreated glands maintained in 2.5% FBS (Day 4: 44.58% in small salispheres (D_S <50µm) vs. 43.87% in medium sized salispheres (D_S: 50-150µm)). However, the rate of proliferation of 2.5% FBS-treated salispheres derived from untreated glands significantly decreases with longer time in culture (small salisphere (D_S <50µm): 44.58% at day 4 vs. 18.46% at day 7; medium salispheres (D_S: 50-150µm): 40.63% at day 4 vs. 15.97% at day 7). Overall, it appears that the proliferation rate of salispheres from untreated and irradiated mice is similar when considering salisphere size, different FBS concentrations (2.5% vs. 10%) or days in culture (Figure 1.6C and 1.6D). Salispheres derived from mice that were 8 weeks old at the time of treatment, proliferate in culture with a similar pattern with regards to salisphere size, FBS supplementation and time in culture (Figure 1.7). These results indicate that FBS supplementation stimulates proliferation rates of salispheres to a similar extent in

untreated and irradiated salivary glands and increasing time in culture decreases total proliferation rates.

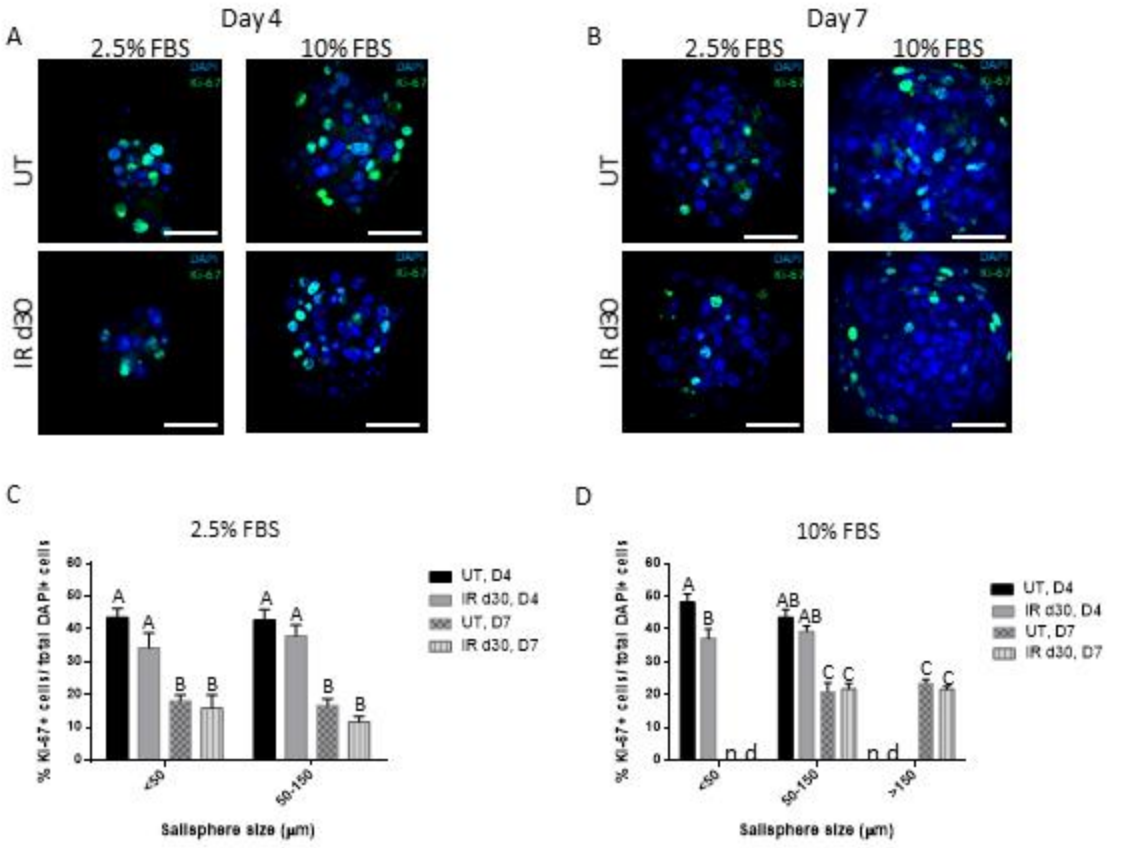

Figure 1.6: Similar proliferation rates are observed in untreated and irradiated salisphere cultures supplemented with FBS.

Untreated and irradiated parotid-derived salispheres, maintained under different FBS concentrations, were fixed after 4 and 7 days in culture and stained for Ki-67 (green). Representative confocal immunofluorescence images are shown (A-B). Percentage of Ki-67+ proliferating cells was quantified from 20 salispheres, of different sizes (<50µm, 50-150µm, >150µm) and maintained under different FBS concentration (2.5% and 10%), at days 4 and 7 for both treatment groups and expressed as average ± SEM. At day 4 in 10% FBS culture condition, large-sized salispheres (>150µm) were rarely detected. Likewise, small-sized salispheres (<50µm) were rarely observed at day 7 in culture. Thus, these analyses were not determined (n.d.). Significant differences ($p < 0.05$) were determined using a one-way ANOVA followed by post-hoc Tukey multiple-comparison tests on the log transformed data of Figure 4C and 4D. Groups with the same letter are not significant different from each other. (C-D). Scale bar= 50µm.

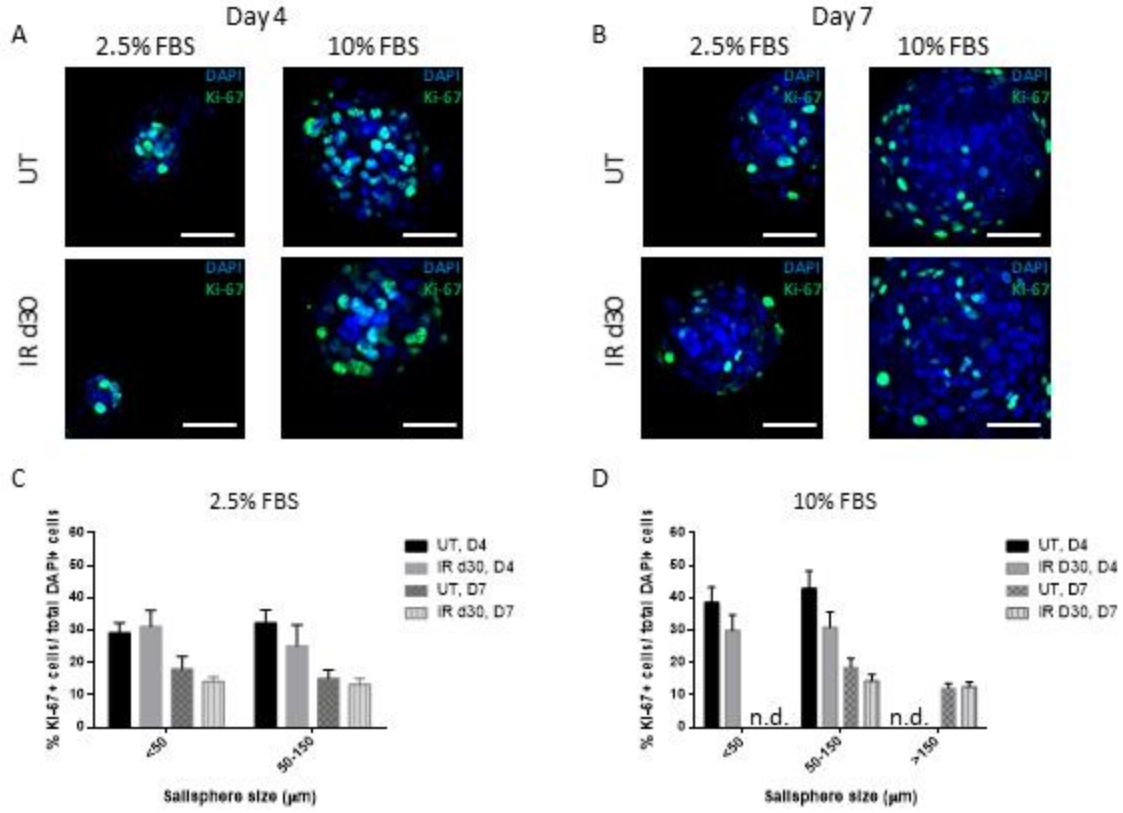

Figure 1.7: Similar proliferation rates are observed in untreated and irradiated salisphere cultures from adult salivary glands.

Untreated (UT) and irradiated (IR d30) parotid-derived salispheres from 8 week old female FVB mice, maintained under different FBS concentrations, were fixed after 4 and 7 days in culture and stained for Ki-67 (green). Representative confocal immunofluorescence images are shown (A-B). Percentage of Ki-67+ proliferating cells was quantified from 10 salispheres, of different sizes (<50µm, 50-150µm, >150µm) and maintained under different FBS concentration (2.5% and 10%), at day 4 and 7 for both treatment groups and expressed as average ± SEM (C-D). At day 4 in 10% FBS culture condition, large-sized salispheres (>150µm) were rarely detected. Likewise, small-sized salispheres (<50µm) were rarely observed at day 7 in culture. Thus these analyses were not determined (n.d.). Scale bar= 50µm.

Expression of salivary stem/progenitor and acinar cell markers in salispheres

Previous studies have reported that salispheres are highly enriched in Keratin 5 (K5)- and Keratin 14 (K14)-positive cells, two progenitor markers that are known to be important during embryonic development of submandibular glands (SMG) (Knox, Lombaert et al. 2010, Lombaert, Abrams et al. 2013, Xiao, Lin et al. 2014). To determine if salispheres derived from untreated and irradiated parotid glands maintained under different FBS concentrations express the aforementioned markers, we performed immunofluorescence staining following 7 days in culture (Figure 1.8A and 1.8B). Keratin 5 and 14 positive cells are observed in salispheres derived from both untreated and irradiated parotid glands grown in each FBS culture condition. The presence of K5 and K14 in FBS-treated salispheres was confirmed with immunoblots (Figure 1.8C and 1.8D). The highest total levels of K14 or K5 are detected in 0% FBS conditions for salispheres from untreated mice versus 2.5% FBS conditions for salispheres from irradiated mice. To investigate the contribution of Keratin 5- and Keratin 14-positive cells to the increased proliferation observed with FBS supplementation, salispheres were incubated with EdU one hour prior to collection and dual immunostained for EdU and K14 or K5. Quantification of EdU/K14 dual positive cells reveals that 24% and 18% of the proliferating population of cells expressed the progenitor marker K14 from untreated and irradiated salispheres maintained in 2.5% FBS respectively (Figure 1.8E). With regard to the expression profile of Keratin 5 under 2.5% FBS medium condition, 19.6% and 21.7% of the total EdU+ cells in salispheres derived from untreated and irradiated parotid glands express Keratin 5 (Figure 1.8F). A slightly higher contribution of K14 and K5 cells to the total proliferative population is observed in salispheres maintained in 10%

FBS and this is statistically significant for EdU/K14 dual positive cells derived from untreated mice and EdU/K5 dual positive cells derived from irradiated mice. When directly comparing salisphere cells derived from untreated and irradiated glands, no significant differences are observed in the percentage of EdU/K14+ and EdU/K5+ cells.

Additionally, it was recently shown that salispheres contained cells with acinar cell characteristics, as indicated by the increase in expression of acinar cell markers aquaporin-5 (Aqp5) and NKCC1 (Shubin, Felong et al. 2017). To assess the acinar cell phenotype in sphere culture, salispheres derived from both untreated and irradiated parotid glands, grown in serum-free (0% FBS) and FBS supplemented (2.5% FBS) culture conditions, were stained with Aqp5 and NKCC1. Aqp5- and NKCC1-expressing cells are observed in both FBS treated and non-FBS treated salispheres (Figure 1.9). Taken together, these data suggest that K14, K5, Aqp5, and NKCC1 continue to be expressed in salisphere cultures supplemented with FBS and contribute to the overall proliferative rate of salispheres.

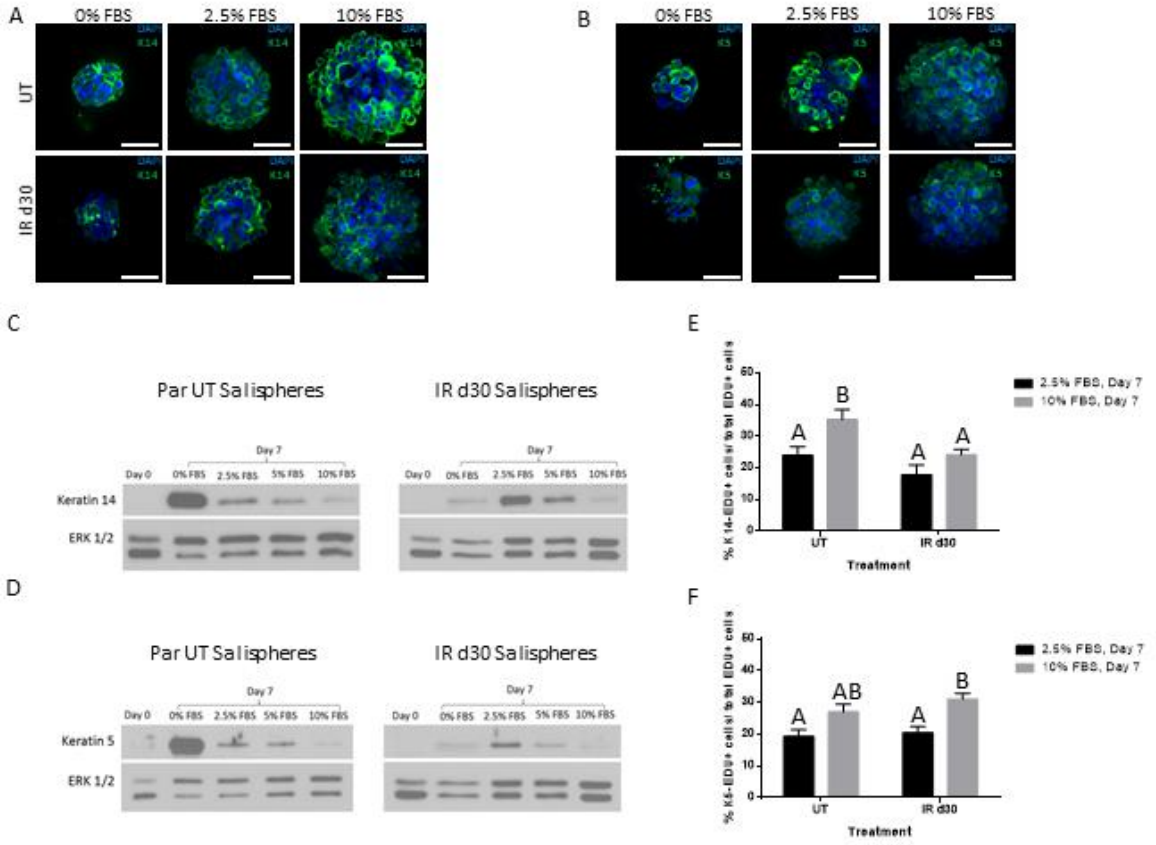

Figure 1.8: Expression of salivary stem/progenitor markers by salisphere cells.
Untreated and irradiated parotid-derived salispheres, maintained under different FBS concentrations, were fixed after 7 days in culture and stained for Keratin 5 (K5) or Keratin 14 (K14) (green). Representative confocal immunofluorescence images are shown (A-B). Representative immunoblot of protein extracts from untreated and irradiated salispheres grown under different FBS concentration medium, collected at day 7 in culture, and probed for Keratin 5 and Keratin 14 (C-D). On day 7 of culture, salispheres were labelled with EdU for 1 hour *in vitro,* fixed, and dual stained for EdU and Keratin 5 or Keratin 14. Percentage of dual EdU-K14+ or Edu-K5+ cells was quantified from 20 salispheres, maintained under different FBS concentrations, for both treatment groups and expressed as mean percent of K14+ or K5+ proliferating cells (± SEM) within an individual salisphere. Significant differences ($p < 0.05$) were determined using a one-way ANOVA followed by post-hoc Tukey multiple-comparison tests. Groups with the same letter are not significant different from each other (E-F). Scale bar= 50µm.

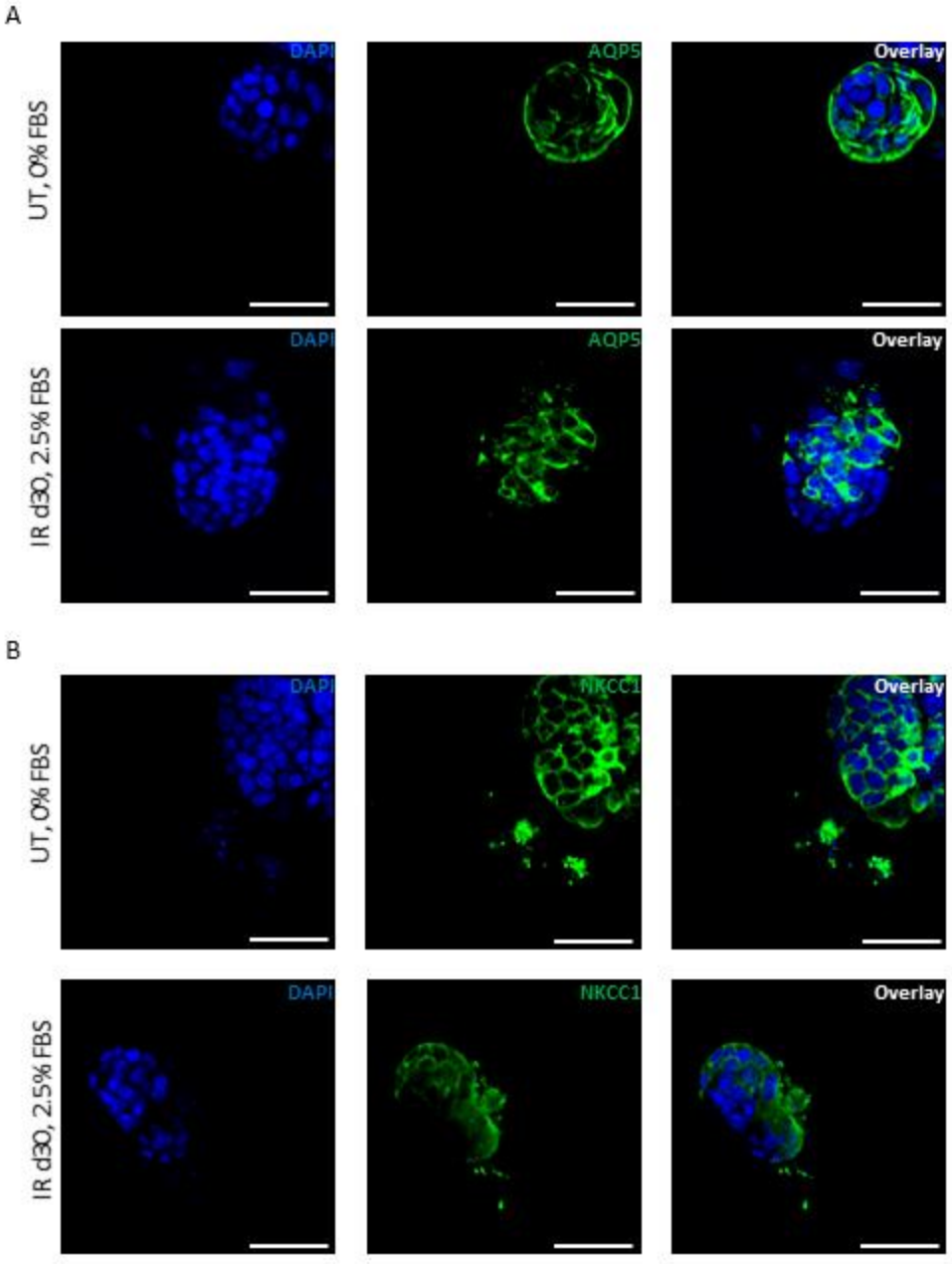

Figure 1.9: Expression of acinar cell markers by salisphere cells derived from untreated and irradiated mice.
Untreated (UT) and irradiated (IR d30) parotid-derived salispheres, maintained under different FBS concentrations, were fixed after 7 days in culture and stained for Aquaporin 5 (AQP5) and NKCC1 (green). Representative confocal immunofluorescence images are shown (A-B). Scale bar= 50µm.

In vivo post-radiation administration of IGF1 increases sphere-forming efficiency of irradiated parotid-derived cells.

Previous work from our lab has demonstrated that administration of IGF1 four days after radiation leads to full restoration of salivary function (Grundmann, Fillinger et al. 2010). The post-therapeutic effect of IGF1 on salivary function following radiation treatment led us to hypothesize that IGF1, like FBS, may increase the sphere-forming efficiency of irradiated parotid-derived cells. To this end, 4-6 week old FVB mice were subjected to a single dose of 5 Gy radiation and thirty days following radiation treatment, IGF1 was administered (Figure 1.10A). At day 60, salivary flow rates are restored in IGF1 treated mice (Figure 1.10B) and parotid glands were collected for sphere-forming assay. There is an increased number of salispheres formed in the IGF1-treated glands when compared to irradiated glands (Figure 1.10C). Ki-67, Aqp5, and NKCC1 immunofluorescent staining of salispheres shows that IGF1 salisphere-derived cells are proliferating and exhibit acinar cell markers under serum-free culture conditions (Figure 1.10D, Figure 1.11). Similar effects on salisphere generation were observed when 8 week old mice were subjected to the same experimental design (Figure 1.12). These data suggest that following radiation treatment, a cellular population remains that can be stimulated *in vivo* with IGF1 to restore sphere-forming capacity thirty days later.

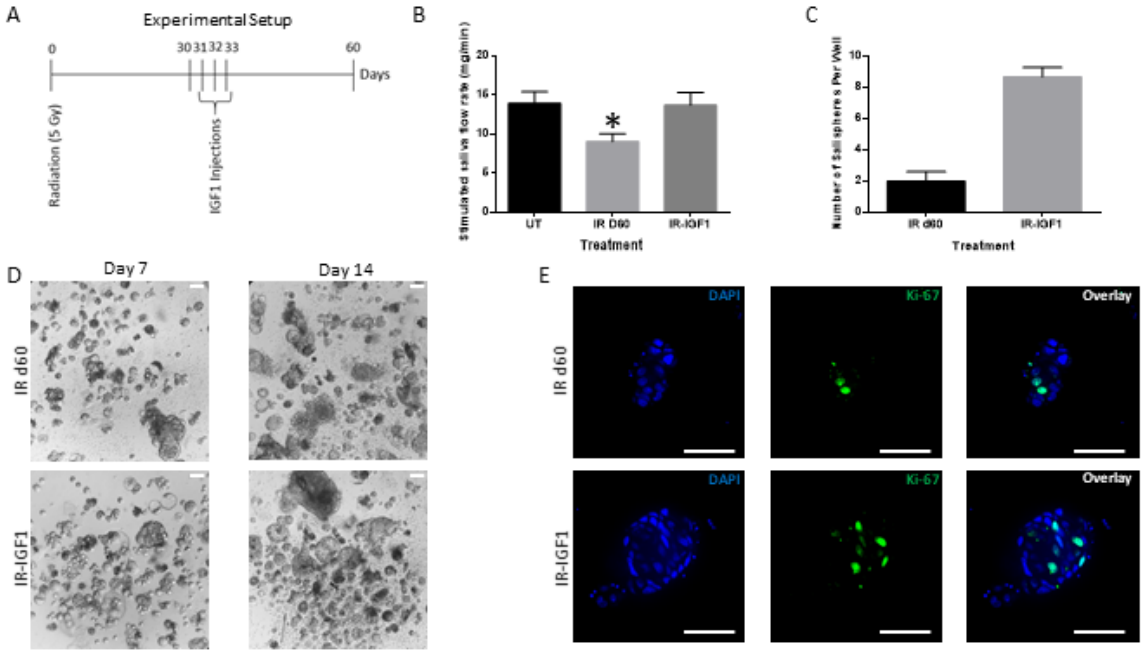

Figure 1.10: Post-radiation treatment with IGF1 increases sphere-forming efficiency of irradiated parotid-derived cells.

A single 5 Gy dose of radiation was given to 4-6 week old or 8 week female FVB mice followed by injections of insulin growth factor 1 (IGF1) on days 31-33 as depicted (A). Stimulated salivary flow rates were determined as described in the materials and methods section on day 60. The graph represents the mean saliva flow rate from 6 mice (8 week old) per treatment group: untreated control (UT), irradiated (IR d60), and IGF1 treated (IR-IGF1). Significant differences (*$p<0.05$) were determined using a one-way ANOVA followed by a post-hoc Tukey multiple comparison test (B). Thirty days following IGF1 treatment, parotid glands were collected for sphere formation assay. Representative graph of the average number (± SEM) of salispheres from 10 wells per treatment group on day 7 in culture from one IR d60 and IR+IGF primary sphere preparation (C). Representative bright field images of salispheres grown from irradiated (IR d60) and IGF1 treated (IR-IGF1) glands in serum-free media at different time points in culture (D). Irradiated (IR d60) and IGF1 (IR-IGF1) treated parotid-derived salispheres were fixed after 7 days in culture and stained for Ki-67 (green). Representative confocal immunofluorescence images are shown (E). Scale bar= 50µm.

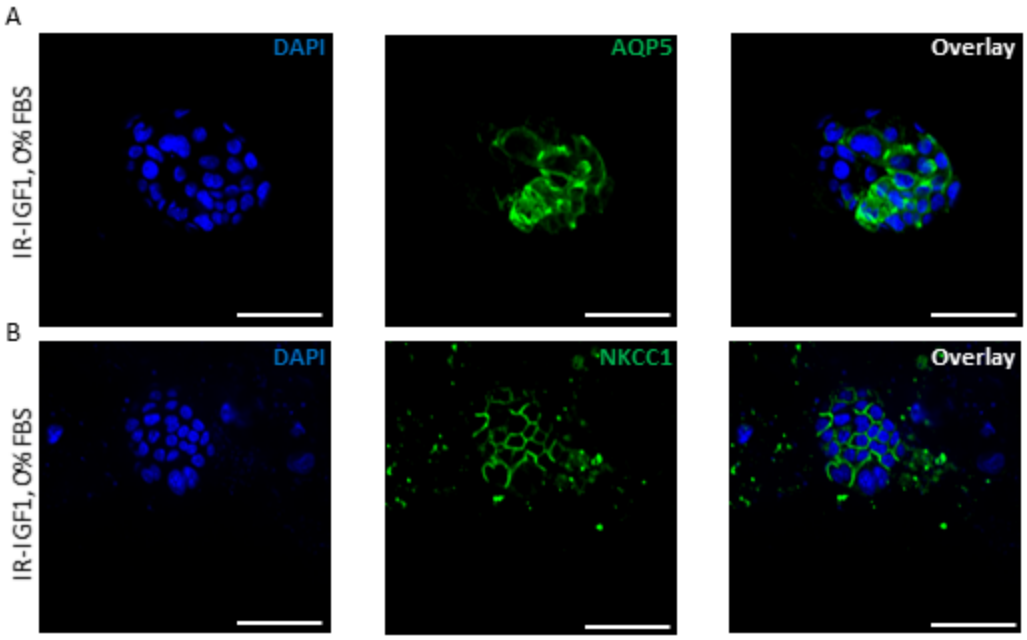

Figure 1.11: Expression of acinar cell markers by salisphere cells derived from irradiated mice receiving post therapy IGF1.
Salispheres grown from IGF1 treated parotid glands, maintained in serum free media, were fixed after 14 days in culture and stained for Aquaporin 5 (AQP5) and NKCC1 (green). Representative confocal immunofluorescence images are shown (A-B). Scale bar= 50µm.

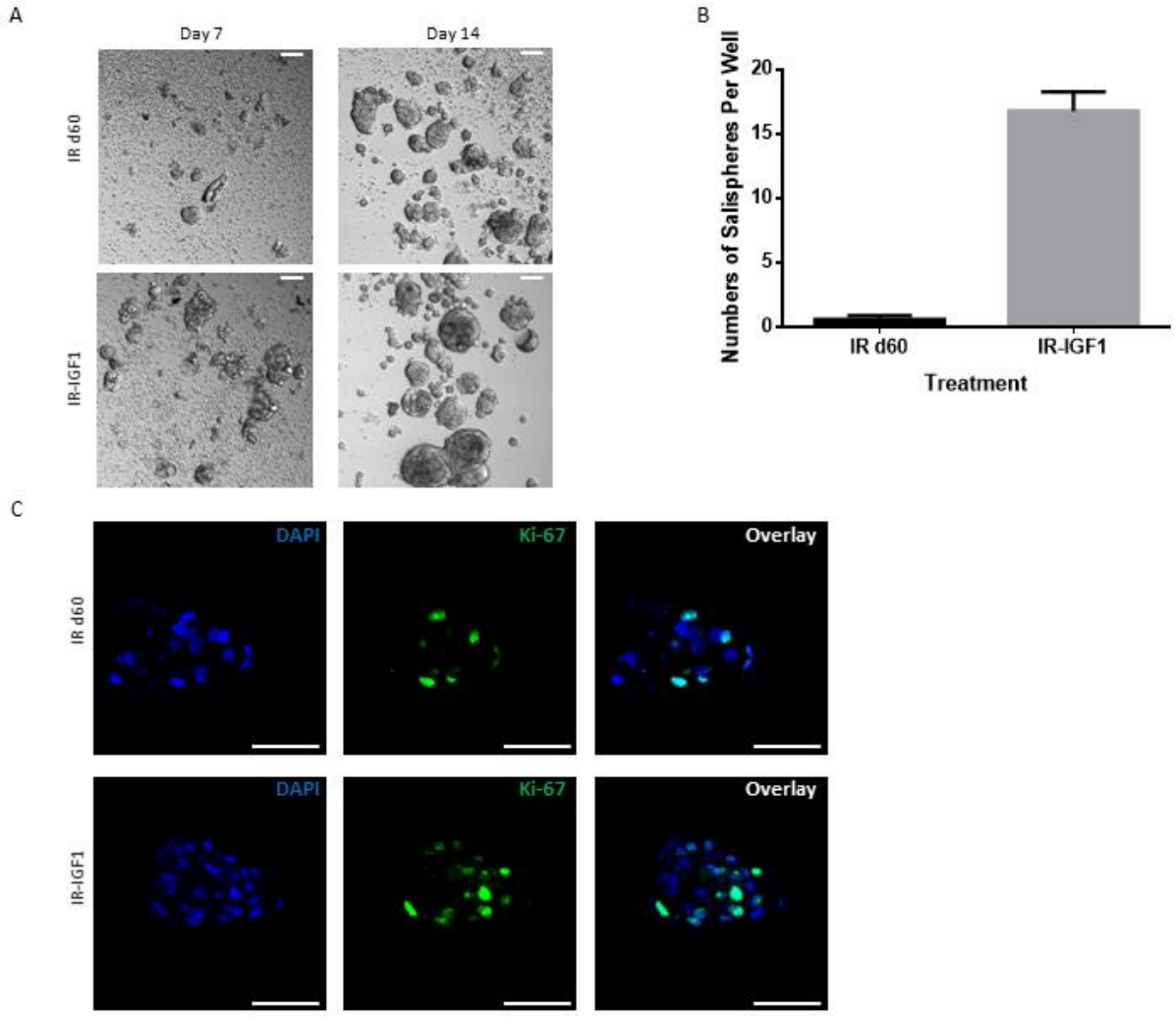

Figure 1.12: Post-treatment of IGF1 increases sphere-forming efficiency of irradiated parotid-derived cells from adult salivary glands.
A single 5 Gy dose of radiation was given to 8 week old FVB mice followed by injections of insulin growth factor 1 (IGF1) on days 31-33 as depicted in Figure 6A. Thirty days following IGF1 treatment, parotid glands were collected for sphere formation assay. Representative bright field images of salispheres grown from irradiated (IR d60) and IGF1 treated (IR-IGF1) glands in serum-free media at different time points in culture (A). Representative graph of the average number (± SEM) of salispheres from 10 wells per treatment group on day 7 in culture from one IR d60 and IR+IGF primary sphere preparation (B). Irradiated (IR d60) and IGF1 treated (IR-IGF1) parotid-derived salispheres were fixed after 7 days in culture and stained for Ki-67 (green). Representative confocal immunofluorescence images are shown (C). Scale bar= 50µm.

DISCUSSION

Stem cell therapy holds great promise for the treatment of salivary gland dysfunction, the most common post-therapy complication for head and neck cancer patients (Lombaert, Brunsting et al. 2008, Nanduri, Maimets et al. 2011, Xiao, Lin et al. 2014, Pringle, Maimets et al. 2016). Previous studies have shown that expansion of the SSC pool either prior to radiation treatment or one day following radiation exposure through administration of growth factors (e.g. KGF, GDNF) partially restored salivary gland function (Lombaert, Brunsting et al. 2008, Xiao, Lin et al. 2014). This suggested that at an early acute phase (one day post radiation), the SSC pool is not depleted and can be triggered to respond given the right stimuli. Recently, it was shown that the percentage of salivary gland label-retaining cells, which resembled SSCs in terms of *in vitro* self-renewal capacity and expression of stem/progenitor markers, is maintained as late as 30 days following radiation treatment (Chibly, Querin et al. 2014). However, it is not completely understood whether at chronic time points following radiation damage, putative SSCs can still be stimulated and involved in repair and regeneration of salivary glands. The current study demonstrates that a subset population of parotid-derived cells capable of self-renewal in ex vivo sphere-forming assay are still present 30 days after radiation and respond to administration of extracellular growth factors.

In accordance with previous findings in the submandibular gland (Lombaert, Brunsting et al. 2008, Nagle, Hosper et al. 2016), our data demonstrates that a single dose (5 Gy) of radiation results in a significant reduction in the number of salispheres formed in culture from parotid glands. Interestingly, the decrease in sphere formation does not appear to be due to a loss in cell viability. Quantification of Ki-67 levels shows that 35%

of salispheres derived from irradiated glands exhibit zero Ki-67 positive cells after seven days in serum-free medium culture. In contrast, all salispheres from untreated glands contained Ki-67 positive cells. This suggests that radiation could induce a non-responsive state in SSC; however due to the considerable variability in proliferation levels there were no significant differences between treatment groups. After 14 days in culture, the proliferative capacity is significantly reduced when compared to day 7 irrespective of radiation treatment. Previous work from other sphere culture systems (e.g. neurosphere, mammosphere) have demonstrated that prolonging the time period of primary culture significantly reduced the proliferation of sphere-forming cells (Xiong, Gao et al. 2011, Manuel Iglesias, Beloqui et al. 2013). This may suggest that the unresponsive phenotype observed in the irradiated parotid derived cells at an early time in culture (day 7) may not be due to the duration of the culture condition, but due to the inherent dormant state of the cells following radiation treatment.

It was previously reported by Tatsuishi et al. that salivary stem/progenitor cells were still present in submandibular glands surgically resected from patients who underwent radiotherapy, but the cells are in a dormant, quiescent state (Tatsuishi, Hirota et al. 2009). Findings from this study lead us to hypothesize that the decrease in salisphere formation may be a feature of quiescent irradiated SSCs. To determine whether supplementation with growth factors would stimulate cells derived from the irradiated parotid glands to proliferate and form salispheres in culture, we supplemented the serum-free media with FBS. Regardless of treatment, the addition of FBS to the medium stimulated the formation of large salispheres. Interestingly, compared to untreated controls, the size of salispheres derived from irradiated cells is smaller when

cultured in a low concentration of FBS, suggesting a dose-response effect. However, while the rates at which salispheres are formed and enlarged are lower compared to untreated controls, there is no significant difference in proliferation rates of salispheres derived from untreated glands compared to irradiated glands, regardless of FBS concentration, salisphere size, or days in culture. Similar effects were observed when radiation was conducted on 8 week old mice. Our results demonstrate that the addition of FBS, which contains a cocktail of growth factors, promotes the expansion of salispheres from irradiated parotid glands. More importantly, we show that 30 days post treatment, a time point that continues to exhibit a significant loss of salivary function, the irradiated cells can be stimulated by growth factors *in vitro* and form spheres in culture. This suggests that even at a later time point following radiation, there is a subset population of cells that retain the capacity for self-renewal.

Genetic lineage tracing experiments in a SMG development model showed that Keratin 5+ (K5) and Keratin 14+ (K14) cells are multipotent progenitor cells that give rise to various cell types in the epithelial compartment of the submandibular glands (Knox, Lombaert et al. 2010, Lombaert, Abrams et al. 2013, Kwak and Ghazizadeh 2015). In the current study, immunohistochemical (IHC) staining and immunoblotting data demonstrate that salispheres derived from irradiated glands continue to express Keratin 5 and Keratin 14. Additionally, approximately 20-30% of proliferating cells are K5 or K14 positive within salispheres derived from irradiated glands. At day 7, both FBS and non- FBS treated salispheres contained Aqp5+ and NKCC1+ cells. This suggests that FBS supplementation did not seem to alter the cellular composition (SSC or acinar) within salispheres derived from untreated or irradiated mice.

We have previously shown that stimulation with IGF1 after radiation-induced salivary gland dysfunction has been initiated leads to a restoration of stimulated salivary flow rates (Grundmann, Fillinger et al. 2010). The current study extended this model by delaying the IGF1 injections to day 30 instead of day 4 and determined salisphere formation thirty days later (radiation day 60). We observe that IGF1 stimulation *in vivo* can promote self-renewal capacity of the irradiated cells remaining at radiation day 30 when evaluated by an ex vivo sphere assay at radiation day 60. A recent study by Marmary et al. demonstrated that 60 days following radiation, there is a prominent increase in senescence-associated β galactosidase activity within the ductal cell compartment of irradiated SMG glands (Marmary, Adar et al. 2016). The authors postulated that senescence-mediated events contribute to the chronic loss of salivary gland function post irradiation. Our study suggests that 30 days post-radiation may be within a window of opportunity where the parotid salivary cells can still be stimulated and restoration of function is obtainable.

In summary, our study demonstrates that cells derived from irradiated parotid glands require an external stimulus to maximize ex vivo expansion. Characterization and stimulation of this salivary stem/progenitor cell sub-population may provide a promising avenue for cell-based therapy for radiation-induced salivary damage in a clinical setting.

CHAPTER 2

INTRODUCTION

More than 50,000 cases of head and neck cancers (HNC) are reported each year in the United States (Siegel, Miller et al. 2017). Despite the utilization of radioprotection strategies (i.e., Intensity-modulation radiation therapy (IMRT)) to spare the salivary glands during HNC treatment, current γ-radiation therapy treatment for head and neck cancers leads to chronic salivary gland dysfunction (Collan, Kapanen et al. 2012, Lee, Kang et al. 2016). Subsequently, chronic dry mouth syndrome (i.e., "xerostomia"), which is often associated with salivary gland dysfunction, severely undermines the oral health of HNC patients. Such patients suffer from increased oral infection rates, difficulty chewing and swallowing food, malnutrition, and difficulty speaking (Trotti 2000, Brosky 2007, Pinna, Campus et al. 2015).

Proper salivary gland function and saliva secretion requires proper apical and basolateral polarization of acinar and ductal cells within the glands. Structurally, salivary glands comprise of multiple secretory acinar units that are connected to the oral cavity via the salivary ducts. Saliva production and secretion occurs in two stages: 1) saliva production and secretion by the acinar compartment and 2) saliva modification by the salivary ducts (Proctor and Carpenter 2007, Proctor and Carpenter 2014). Proper apical and basal polarization of acinar and ductal cells ensures that the structural integrity of the glands is maintained and that there is unidirectional movement of saliva into the oral cavity. Due to significant acinar cell loss following ionizing radiation exposure, disruption of cell-cell adhesion and rearrangement of cytoskeleton results in disruption of apical and basal polarity of the remaining acinar and ductal cells (Vissink, s-Gravenmade et al. 1990, Li, Shan et al. 2005, Wong, Pier et al. 2018). In the ischemic kidney injury

model, damage to the proximal tubule cells results in disruption of epithelial polarity and redistribution of Na^+,K^+,-ATPase from the basolateral to apical membrane, leading to reduced Na^+ reabsorption (Molitoris and Nelson 1990, Kwon, Corrigan et al. 1999). This shows that proper establishment of the epithelial polarity following injury damage is important for maintenance of normal cellular structure and function.

Chibly et al. have shown that salivary gland dysfunction correlated with compensatory proliferation of label retaining cells, a subset of population of salivary cells that exhibited stem-like features, at an early time point (day 5) following radiation injury (Chibly, Wong et al. 2018). It was demonstrated that this early compensatory proliferation program is mediated through the inactivation of atypical protein kinase C zeta (aPKCζ), an isoform of protein kinase C, a family of serine/threonine kinases that play key roles in many cellular signaling processes. While the proliferation of label retaining cells from irradiated mice returned to untreated control level, protein level of aPKCζ was not restored. Beside its role in regulating cellular proliferation, aPKCζ has been shown to play a role in establishment and maintenance of cellular polarity in epithelial tissues (Vasavada, Wang et al. 2007, Whyte, Thornton et al. 2010, Llado, Nakanishi et al. 2015). In an epithelial disease model, such as Polycystic Kidney Disease (PKD), defects in polarity complexes have been shown to disrupt normal renal structure and function (Charron, Nakamura et al. 2000, Roitbak, Ward et al. 2004)..

In this study we test the hypothesis that chronic salivary gland hypofunction following radiation treatment is due to loss of intrinsic polarity cues in salivary cells and mediated through the kinase activity of aPKCζ. *Ex vivo* suspension cell culture system propagates the formation of a heterogenous population of salispheres, free-floating

spherical three-dimensional (3D) structures, from salivary-derived cells that differ in structural organization (Pradhan, Liu et al. 2010, Pradhan-Bhatt, Harrington et al. 2013, Shubin, Felong et al. 2017, Nguyen, Dawson et al. 2018). One of the subtypes of salisphere, termed acini, is characterized by spherical 3D layers of cells surrounding a hollow central lumen. The second subtype of salisphere, termed sphere, is defined as 3D spherical layers of cells that lack a lumen. We utilized the suspension cell culture to assess the acini formation capacity, an indirect assessment of cellular polarity, of cells derived from irradiated parotid glands. There is a significant reduction in acini formation from irradiated parotid glands and a similar defect in acini formation is observed in salivary cells treated with PKCζ pseudosubstrate inhibitor. Understanding the regulatory role of aPKCζ in cell polarization of salivary glands would provide mechanistic insights for development of novel therapies for radiation-induced salivary gland dysfunction and xerostomia.

MATERIALS AND METHODS

Mice and sphere forming assay

All experiments were conducted in 4-6 week old FVB mice. All mice were maintained and treated in accordance with protocols approved by the University of Arizona Institutional Animal Care and Use Committee (IACUC). A total of 24 mice were used for suspension cell culture across 12 individual experiments. For each experiment, parotid glands from two mice were collected and salisphere formation was propagated using a sphere culture technique as previously described (Lombaert, Brunsting et al. 2008, Chibly, Querin et al. 2014). Cells were suspended in serum free medium and plated at a density of 200,000 cells in ultra-low attachment plates (Corning, Corning, NY). The myristoylated PKCζ pseudosubstrate inhibitor (5μM) (Thermo Scientific, Waltham, MA) was added to primary cells at the time of plating, unless otherwise stated.

Radiation treatment

Mice were anesthetized with Ketamine/Xylazine (50mg/kg (K)+10 mg/kg (X)) followed by exposure to a single dose of 5 Gy targeted to the head and neck region using a ^{60}Cobalt Teletherapy unit (Theratron-80, Atomic Energy of Canada Ltd), with the rest of the body protected by a lead shield. The 5 Gy dose was chosen based on previous work demonstrating significant reductions in salivary function and differentiation status (as determined by amylase expression) of parotid salivary glands (Grundmann, Fillinger et al. 2010).

Immunofluorescence staining

At pre-determined time points, salispheres were fixed directly in culture by adding one volume of 10% buffered formalin for 20 minutes at room temperature. After

fixation, salispheres were permeabilized with 0.2% Triton X in PBS for 20 minutes at room temperature. Target-specific staining of salispheres was performed in suspension by incubating in primary antibody diluted 1:100 in 1% BSA overnight at 4°C: anti-ZO-1 (61-7300, Invitrogen, Carlsbad, CA), anti-β-catenin (8480, Cell Signaling, Danvers, MA), anti-NKCC1 (a59791, Abcam, Cambridge, UK), and anti-phospho-PKCζ^{T560} (ab62372, Abcam, Cambridge, UK); followed by incubation in secondary anti-rabbit Alexa 594 (A-11307, Invitrogen, Carlsbad, CA) at 1:500 dilution. Salispheres were pelleted by centrifugation at 4000 rpm for 5 minutes and resuspended in DAPI (4',6-diamidino-2-phenylindole) for 5 minutes at room temperature. Images were acquired with an Intelligent Imaging Innovations (Danvers, Colorado) configured instrument including a Zeiss Marianas 100 Microscopy Workstation (Oberkochen, Germany), Yokogawa CSU-X1 M1 Spinning Disk (Musashino, Tokyo, Japan) and Photometrics Evolve 512 EMCCD (Tucson, Arizona) using a Zeiss EC Plan-Neifluar 40X/1.3 NA oil objective and a .5µm z-separation between the slices in the stack. The Spinning Disk includes a Semrock Di01-T488/568 dichroic beam splitter and a Em01-R488/568 dual bandpass emission filter for 488 nm ex- BP 525/43 em and 561 nm ex- BP 642/117 em imaging.

Determination of Size and Total Number of Salispheres

Salisphere number and size were assessed on day 7 in culture. To do this, 25 bright field images were randomly captured from each well using Excelis AU-300-HD camera (Accu-Scope, Commack, NY, USA). The diameter of individual salisphere was measured using 1.46 ImageJ software. For each experiment, the number of salispheres was manually counted from a minimum of 15 images per well from 3 to 10 wells. The

number of wells analyzed for salisphere count for each experiment is indicated in each figure legend. Only salispheres with a diameter of >50μm were counted due to the utilization of a 40 μm diameter filter to obtain a single cell suspension prior to plating.

Assessment of Lumen Formation in Salispheres

Lumen formation of salispheres was assessed through DAPI immunostaining on day 7 in culture. To do this, 20 confocal 3D stack images per treatment were randomly selected for analysis. The number of 3D stack images used for lumen formation analysis in each experiment is indicated in each figure legend. The top, middle, and bottom slice in the z-stack image of each salisphere were carefully examined for the presence of hollow lumen.

Analysis of distribution of polarity and differentiation markers in salispheres

Distribution of polarity markers in salisphere cells was assessed through ZO-1, β-catenin, and aPKCζ^{T560} immunostaining on day 7 in culture. To do this, between 10-20 confocal 3D stack images per treatment condition were randomly selected for analysis. The number of 3D stack images used for the polarity analysis in each experiment is indicated in each figure legend. Cells were manually counted from the top, middle, and bottom slice in the z-stack image using the Cell Counter program from ImageJ. Distribution of polarity markers of an individual salisphere was determined by the sum of the number of positive cells/total number of cells from the accumulated slices in a single z-stack image. Analysis of distribution of differentiation markers (i.e. NKCC1) by salisphere cells was carried out using a similar manual counting technique.

Statistical analyses

A calculation of sample size by power analysis was conducted to determine the number of salisphere images needed in each statistical analysis and is indicated in each figure legend. Statistical analyses were performed using SPSS (version 24.0, SPSS Inc., Chicago, IL, USA). Two-sided independent sample t-tests were performed to compare the percentage of acini formed between treatment groups at day 7 in culture. Non-parametric Mann-Whitney test was conducted to compare differences in the distribution of polarity markers (i.e. ZO-1, β-catenin, and aPKCζ^{T560}) and differentiation markers (i.e. NKCC1) between groups of salisphere and treatment conditions. Graphical generation was done using Graph-Pad (version 5.0, San Diego, CA).

RESULTS

Decreased formation of acini in irradiated parotid glands

To evaluate the acini formation capacity of irradiated parotid-derived cells, the number of spheres and acini was quantified at day 7 in culture, the earliest time point in which acini formation is observed (Figure 2.1). Analysis of confocal cross-section images of untreated and radiation derived-salispheres show that there is a significant decrease in the number of acini formed in the irradiated glands compared to untreated controls (Figure 2.2). This suggests that radiation treatment may disrupt the ability of parotid salivary cells to form acini in culture.

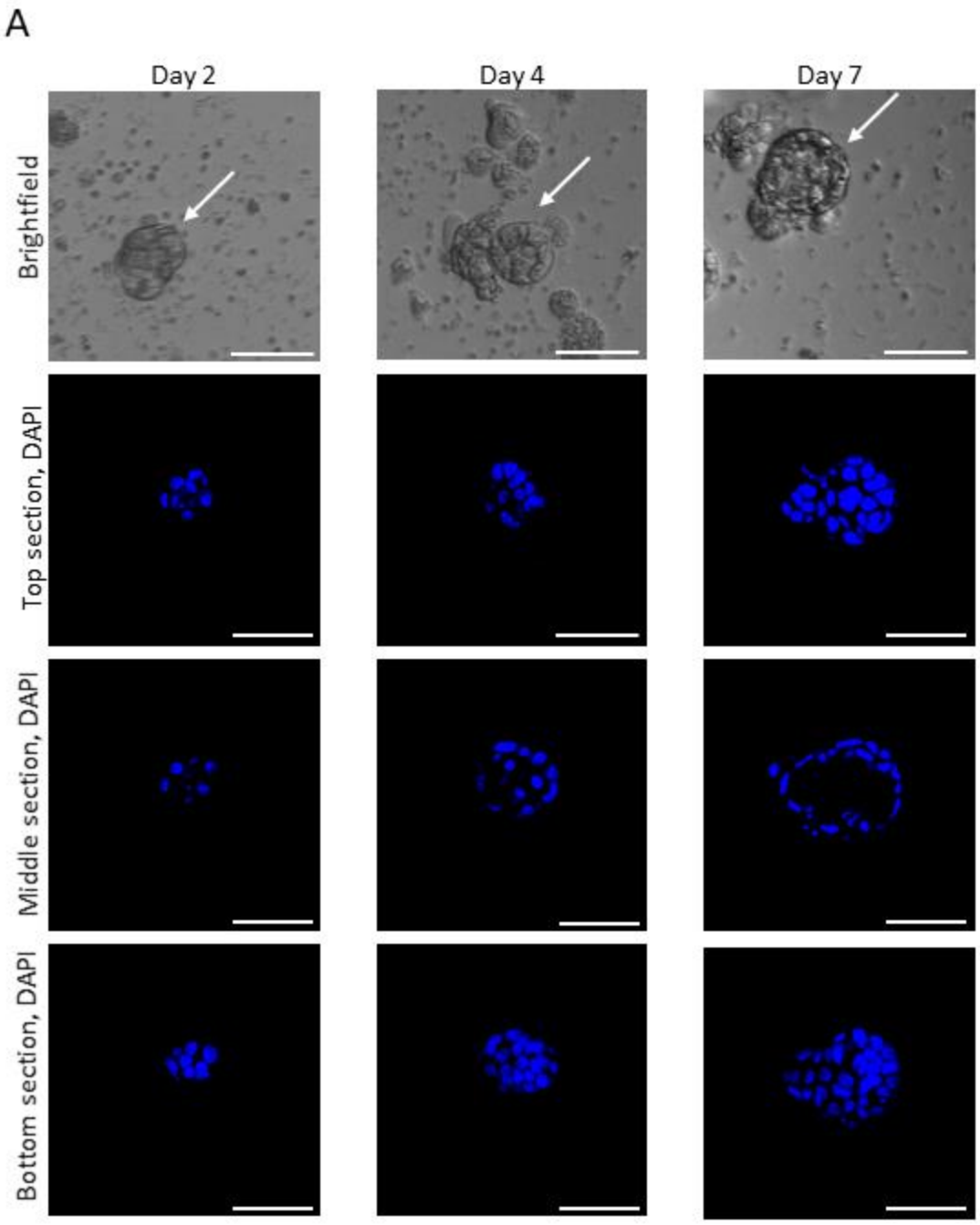

Figure 2.1: Formation of primary salivary acini.
Sphere formation was propagated from murine parotid glands and parotid-derived salispheres were fixed after 2, 4, and 7 days in culture and stained for nuclear DAPI (blue). Representative brightfield images and confocal cross-section images through the top, middle, and bottom section of day 2, 4, and 7 salispheres are shown (A). Scale bar= 50µm.

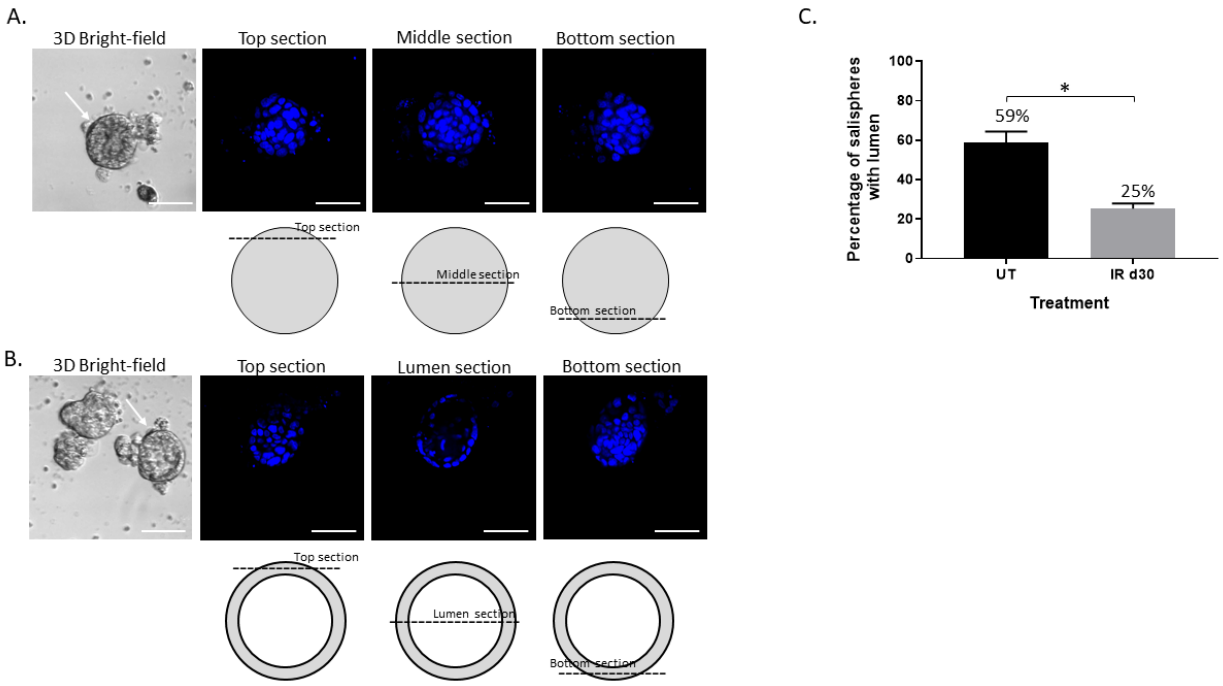

Figure 2.2: Decreased formation of acini in irradiated parotid glands.
A single 5 Gy dose of radiation (IR d30) was given to 4-6 week old female FVB mice and parotid glands were collected 30 days following radiation for sphere formation assay. Untreated control (UT) and irradiated (IR d30) parotid-derived salispheres were fixed after 7 days in culture and stained for nuclear DAPI (blue). Representative bright field images and confocal cross-section images through the top, middle, and bottom section of day 7 sphere (A) and acini (B) are shown. The schematic diagrams overlaying each section illustrate lumen formation in acini structure. Quantification of the percentage of acini formation over time in culture (day 7) from untreated and irradiated glands (C). For statistical analysis, 20 salispheres were examined in each experiment at day 7 after plating, and the results represent the means ± SEM of three independent experiments. P-values were obtained with 2-sided unpaired t-test (n=3), *p<.05. Scale bar= 50μm.

Distribution of polarity markers by salisphere cells

Previous work in epithelial cell models, such as mammary, kidney, and bronchial epithelial cells, have shown that acini formation required expression and appropriate localization of proteins that are involved in the establishment of polarity (Whyte, Thornton et al. 2010, Fessart, Begueret et al. 2013, Gao, Yang et al. 2017). To determine if spheres and acini derived from untreated and irradiated parotid glands show differential localization and level of polarity proteins, we performed ZO-1 and β-catenin immunofluorescence staining of untreated and radiation-derived salispheres following 7 days in culture. ZO-1, an apical tight junction protein, stains on the peripheral surface of the acini. β-Catenin, a cell-cell adhesion protein, stains on the lateral-apical cell border of acini (Figure 2.3Ai-ii). Quantification of ZO-1 and β-catenin levels from the top, middle, and bottom slice of the z-stacks reveal that 72% and 89% of the cells within acini derived from untreated parotid glands are positive for the polarity markers respectively. On the contrary, the polarity markers are unevenly distributed throughout spheres from untreated glands and only 40% and 39% of the cells are marked positive for ZO-1 and β-catenin, which is significantly lower compared to the levels of these polarity mediators within acini (Figure 2.3Aiv-v and 2.3Ci-ii). Similar spatial distribution and quantification differences of ZO-1 and β-catenin are observed between acini and spheres that are derived from irradiated glands (ZO-1: 75% in acini vs. 31% in sphere; β-catenin: 84% in acini vs. 65% in sphere) (Figure 2.3Bi-ii, 2.3Bvi-v, and 2.3Di-ii). aPKCζ an isoform of protein kinase C, a family of serine/threonine kinases, has been shown to be a key polarity regulator in the polarization of mammary acini (Whyte, Thornton et al. 2010). To investigate whether aPKCζ plays a role in the polarization of acini in these parotid gland

cultures, we performed aPKCζ^{T560} immunofluoresence staining. aPKCζ^{T560}, an active form of aPKCζ that distributes to the apical side of the plasma membrane, is found to localize on the periphery of both untreated and radiated-derived acini (Figure 2.3Aiii and 2.3Biii). Like ZO-1 and β-catenin, aPKCζ^{T560} is unevenly distributed on the peripheral surface of untreated and irradiated spheres (Figure 2.3Avi and 2.3Bvi). Quantification of aPKCζ^{T560} levels indicates significantly higher levels in acini when compared to spheres regardless of treatment (Figure 2.3Ciii and 2.3Diii). Interestingly, analysis of the percentage of aPKCζ^{T560}+ cells show that acini derived from the irradiated parotid glands have a significant lower percentage of aPKCζ^{T560}+ cells compared to acini from untreated control (acini: 66% in untreated control vs. 48% in irradiated). These results show that parotid gland derived-acini have higher levels of polarity proteins when compared to spheres.

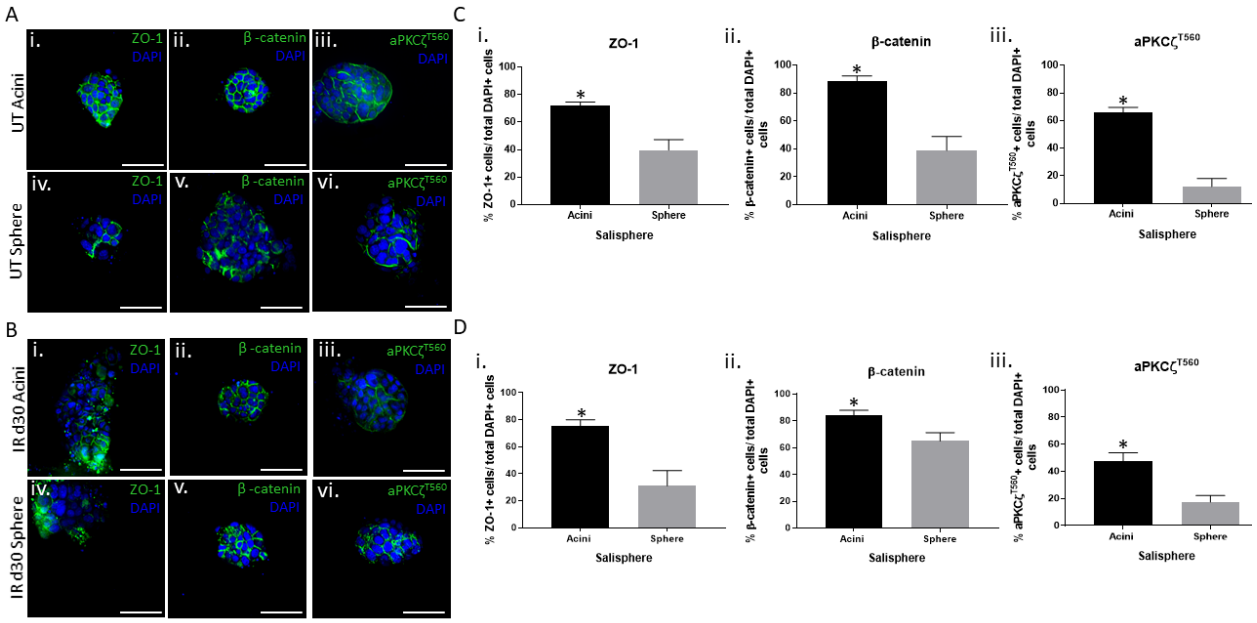

Figure 2.3: Distribution of polarity markers by salisphere cells.
Untreated control (UT) and irradiated (IR d30) parotid-derived salispheres were fixed after 7 days in culture and stained for ZO-1, β-catenin, and aPKCζ^{T560}. Representative confocal images through the top section of untreated (A) and irradiated (B) day 7 acini and sphere-like structure are shown. Percentage of ZO-1+, β-catenin+, and aPKCζ^{T560}+ cells were quantified from 10 acini and 10 spheres across three independent experiments of untreated (C) and irradiated (D) salispheres and expressed as mean percent of ZO-1+, β-catenin+, or aPKCζ^{T560}+ cells (± SEM) within an individual salisphere. Significant differences ($p < 0.05$) were determined using the non-parametric Mann-Whitney test. Scale bar= 50μm.

Distribution of acinar cell markers by salisphere cells

It has been shown in mammary epithelial cells (MEC) that acini formation correlated with MEC differentiation *in vitro*. Expression of the mammary differentiation factor STAT5B was found to be highly up-regulated in mammary acini compared to sphere (Furuta, Jiang et al. 2005). Shubin et al. demonstrated that primary salivary cells encapsulated in poly(ethylene glycol) (PEG) hygrogels formed multi-lumen 3D acini structures and are enriched with acinar cell differentiation markers (i.e. Aquaporin 5 (Aqp5) and NKCC1) (Shubin, Felong et al. 2017). To evaluate the spatial distribution of differentiation markers in spheres and acini derived from untreated and irradiated parotid glands, we performed NKCC1 immunofluorescence staining of untreated and radiation-derived salispheres following 7 days in culture (Figure 2.4A and 2.4B). NKCC1, a sodium-potassium-chloride co-transporter that localizes to the basolateral membrane of acinar cells in the salivary glands, is uniformly distributed throughout acini. In contrast, NKCC1 is unevenly concentrated throughout spheres, regardless of treatment. Quantification of NKCC1 levels shows that 62% of the cells from the untreated-derived acini are positive for the acinar cell marker. On the contrary, only 26% of the cells from the untreated-derived spheres are positive for NKCC1, which is significantly lower when compared to the acini (Figure 2.4C). Similar distribution and quantification of NKCC1 are observed between acini and spheres that are derived from irradiated glands (NKCC1: 49% in acini vs. 8% in sphere) (Figure 2.4B and 2.4D). To summarize, these data show that parotid gland derived-acini are comprised mostly of NKCC1+ cells and salivary acini formation is correlated with salivary cells differentiation *in vitro*.

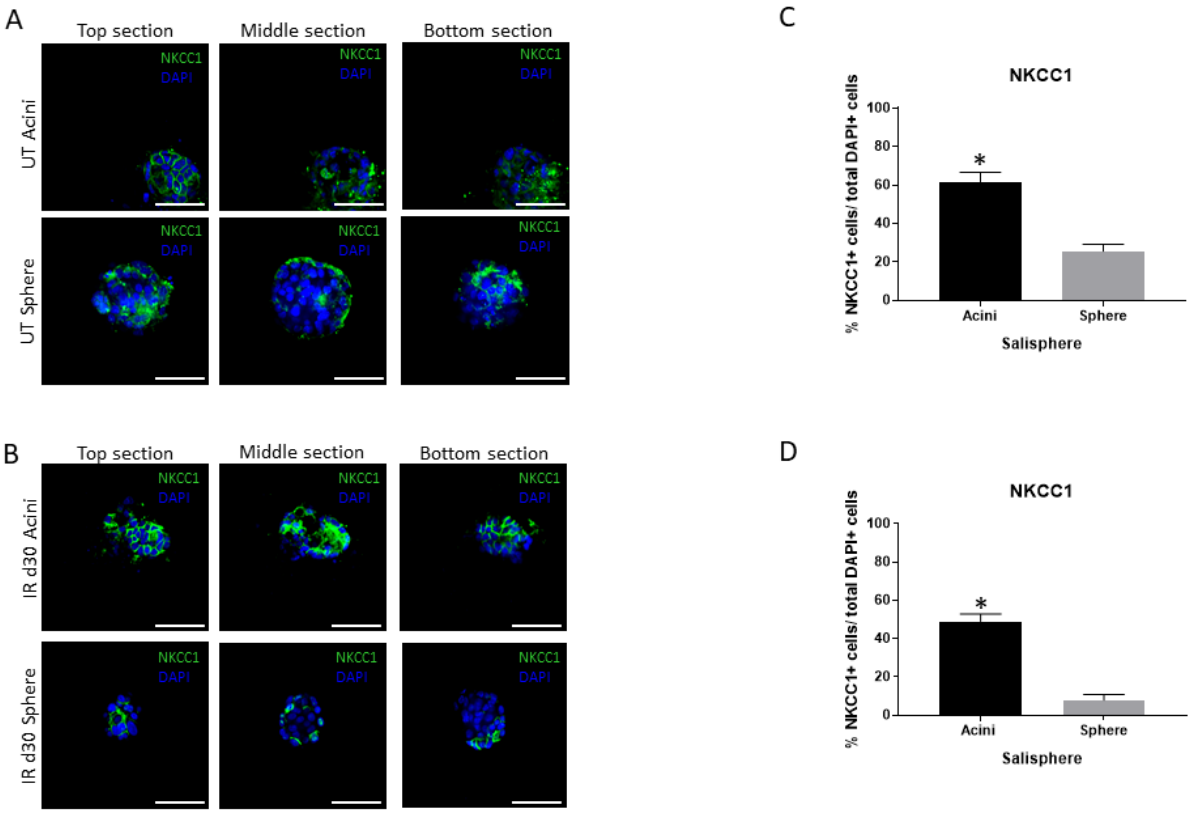

Figure 2.4: Distribution of differentiation marker by salisphere cells.
Untreated control (UT) and irradiated (IR d30) parotid-derived salispheres were fixed after 7 days in culture and stained for NKCC1. Representative confocal cross-section images through the top, middle, and bottom section of untreated (A) and irradiated (B) day 7 acini and sphere-like structure are shown. Percentage of NKCC1+ cells were quantified from 10 acini and 10 spheres across three independent experiments of untreated (C) and irradiated (D) salispheres and expressed as mean percent of NKCC1+ cells (± SEM). Significant differences ($p<0.05$) were determined using the non-parametric Mann-Whitney test. Scale bar= 50µm.

Inhibition of PKCζ activity decreases acini-forming efficiency of parotid-derived cells

To investigate whether the polarity regulator aPKCζ plays a role in the formation of parotid gland-derived acini, we inhibited the kinase activity of aPKCζ by treating the cells with a myristoylated PKCζ pseudosubtrate inhibitor, which confers auto-inhibition by binding to the substrate-binding site and masks the phosphorylation sites (Whyte, Thornton et al. 2010, Xiong, Li et al. 2016). To evaluate the salisphere-forming efficiency of parotid glands in the presence of PKCζ inhibitor, the number and size of salispheres were quantified over time in culture. Assessment of salisphere formation shows that there is no significant difference in the total number of salispheres formed by the parotid-derived cells treated with the PKCζ inhibitor compared to untreated controls (Figure 2.5A and 2.4B). Next, we evaluated acini formation in the parotid-derived cells treated with the inhibitor by quantifying the number of spheres and acini at day 7 in culture. Analysis of confocal cross-section images of untreated control and PKCζ inhibitor derived-salispheres show that there is a significant decrease in the number of acini formed in cultures treated with the inhibitor (Figure 2.5C). Immunofluorescence staining of spheres formed in the presence of the PKCζ inhibitor shows that ZO-1 and β-catenin are randomly distributed in spheres. In contrast, the majority of cells in acini are positive for the polarity markers. (Figure 2.5D). Despite less acini formed in the inhibitor culture, quantification of ZO-1 and β-catenin levels in acini that were generated show that 70% and 79% of the cells are positive for ZO-1 and β-catenin respectively. In contrast, 33% and 54% of the cells from the inhibitor-treated spheres are marked positive for ZO-1 and β-catenin, which is significantly lower when compared to acini (Figure 2.5Ei-ii).

Analysis of the percentage of ZO-1+ and β-catenin+ cells show that the polarity profile of acini and spheres from the inhibitor culture does not significantly differ from that of the untreated controls (ZO-1, acini: 72% in untreated vs. 70% in inhibitor culture; ZO-1, sphere: 40% in untreated vs. 33% in inhibitor culture; β-catenin, acini: 89% in untreated vs. 80% in inhibitor culture; β-catenin, sphere: 39% in untreated vs. 54% in inhibitor culture). Taken together, these results show that inhibition of PKCζ activity decreases the acini-forming efficiency of parotid-derived cells but not the levels of polarity proteins in the forming acini.

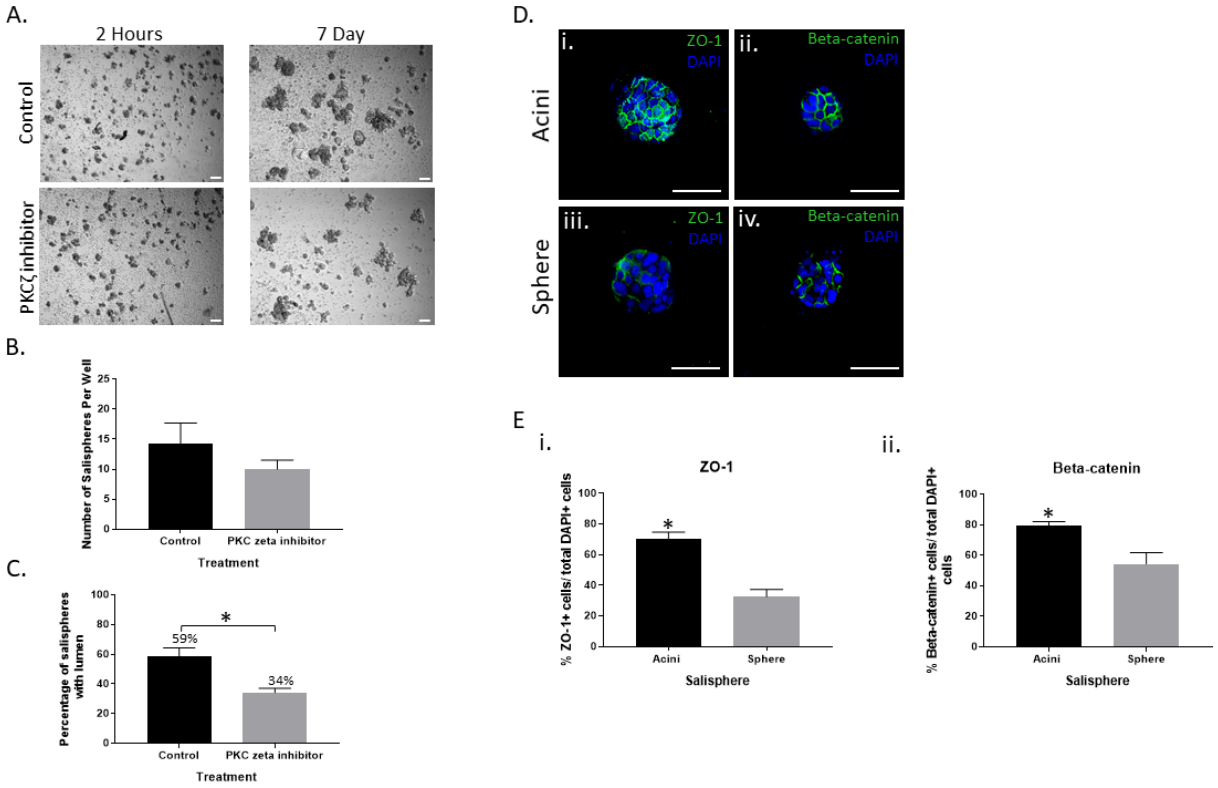

Figure 2.5: Inhibition of PKCζ activity decreases acini-forming efficiency of parotid-derived cells. Representative bright field images of salispheres grown from parotid glands in serum free-media, treated with PKCζ pseudosubstrate inhibitor, taken at day 7 (A) in culture. Number of salispheres was quantified per 6 wells from 3 primary cell preparations per treatment group at day 7 in culture and expressed as average ± SEM. P-values were obtained with a 2-sided unpaired t-test (n=3), *p<.05 (B). Quantification of the percentage of acini formation over time in culture (day 7) from untreated control and PKCζ inhibitor-treated glands. For statistical analysis, 20 salispheres were examined in each experiment at day 7 after plating, and the results represent the mean ± SEM of three independent experiments. P-values were obtained with 2-sided unpaired t-test (n=3), *p<.05 (C). Untreated control and PKCζ pseudosubtrate inhibitor treated-salispheres were fixed after 7 days in culture and stained for ZO-1 and β-catenin. Representative confocal immunofluorescence images are shown (D). Percentage of ZO-1+ and β-catenin+ cells were quantified from 10 acini and 10 spheres across three independent experiments of PKCζ inhibitor treated- salispheres and expressed as mean percent of ZO-1+ or β-catenin+ cells (± SEM) within an individual salisphere (Ei-ii). Significant differences ($p < 0.05$) were determined using the non-parametric Mann-Whitney test. Scale bar= 50µm.

DISCUSSION

Stem cell-based therapy is a promising avenue for the treatment of salivary gland dysfunction, the most common post-therapy complication associated with the treatment of head and neck cancers (Aure, Arany et al. 2015, Lombaert, Movahednia et al. 2017). The main delivery platform for stem cell-based therapeutics is either through cell transplantation or stimulation of endogenous stem cell populations by pharmacological agents (Romagnani, Lasagni et al. 2007, Lombaert, Brunsting et al. 2008, Fischbach, Bluestone et al. 2013, Xiao, Lin et al. 2014). While preclinical studies in rodent models have shown stem cell transplantation as a promising option for the treatment of radiation-induced salivary gland hypofunction, the lack of a comprehensive profile of salivary gland stem cells make this treatment plan currently not applicable in the clinical setting (Lombaert, Brunsting et al. 2008, Nanduri, Maimets et al. 2011, Xiao, Lin et al. 2014, Pringle, Maimets et al. 2016). It was previously hypothesized that the endogenous salivary stem/progenitor cell pool is sterilized in the course of radiation (Vissink, Jansma et al. 2003); however, a number of studies have identified the continued presence of salivary stem/progenitor populations following radiation injury ((Tatsuishi, Hirota et al. 2009, Chibly, Querin et al. 2014, Chibly, Wong et al. 2018, Emmerson, May et al. 2018, Nguyen, Dawson et al. 2018). Chibly et al. demonstrated that label-retaining cells, a subpopulation of salivary cells that exhibited stem-like features both *in vivo* and *in vitro*, is maintained following radiation treatment (Chibly, Querin et al. 2014). In addition, a subset population of parotid-derived cells present at a chronic time point following radiation are capable of self-renewal and respond to administration of extracellular

growth factors (Nguyen, Dawson et al. 2018). Similarly, Emmerson et al. have also shown that SOX2+ cells, a progenitor population that give rise to the acinar compartment of the salivary glands during development, is present following radiation and could be stimulated by cholinergic mimetics (Emmerson, May et al. 2018). Thus, understanding the intracellular effect of radiation damage on the endogenous salivary stem/progenitor population may provide insight in identifying targets that are involved in the wound healing process for the treatment of salivary gland dysfunction. Chibly and colleagues have shown in rodent model of radiation-induced salivary gland injury that salivary gland hypofunction coincided with global inactivation of aPKCζ nd that aPKCζ is required to restore salivary gland function in irradiated glands (Chibly, Wong et al. 2018). However, the intrinsic effect of aPKCζ inactivation on irradiated salivary glands is not completely understood. In the current study, we show that radiation disrupts acini formation, which involves the polarization of acinar-like salivary cells, and demonstrate the important role of aPKCζ in salivary acini formation.

In accordance with previous findings that use 3D biomaterial-based scaffold systems to propagate acini formation, this study demonstrates that acini formed in a suspension culture system consisted of a single layer of epithelial cells surrounding a hollow lumen (Pradhan, Liu et al. 2010, Pradhan-Bhatt, Harrington et al. 2013, Shubin, Felong et al. 2017). Acini formation coincides with establishment of cell polarity, as indicated by the distribution and localization of tight junction proteins ZO-1 and β-catenin. Quantification of ZO-1, β-catenin, and NKCC1 levels show that the polarity and differentiation protein profile between acini and spheres is starkly different. Additionally, our study is the first to report that cells derived from irradiated parotid glands form more

spheres and less acini in culture, suggesting that radiation causes a loss of intrinsic polarity cues.

A previous study in a mammary epithelial model demonstrated the role of aPKCζ as a polarity regulator that is necessary for acini formation (Whyte, Thornton et al. 2010). Utilizing the same kinase inhibitor strategy, we observed partial disruption of salivary acini formation but the efficiency rate of salisphere formation was not affected. Established models of epithelial acini formation have shown that acini morphogenesis is a step-wise process that involved proliferation, establishment of apicobasal polarity, cellular differentiation, and lumen clearance (Debnath, Muthuswamy et al. 2003, Furuta, Jiang et al. 2005). Polarity and differentiation protein profile of salivary acini suggests that like the mammary acini formation model, establishment of polarity and cellular differentiation program are key molecular events in salivary acini formation. Particularly, findings from the inhibitor experiment indicate that aPKCζ play an important role in regulating those events. A previous study has demonstrated the role of aPKCζ in regulating the initiation of proliferation in a subset population of salivary gland cells (i.e. label retaining cells) at homeostasis and upon radiation injury. Based on the analysis of the rate of acini formation of cells derived from irradiated parotid glands and those from inhibitor culture (acini: 25% from irradiated vs. 34% from inhibitor culture), suggests that inactivation of aPKCζ as a result of radiation damage alters the intricate balance between proliferation and differentiation of salivary cells.

In summary, our study demonstrates that cells derived from irradiated parotid glands fail to form polarized acini structures in culture and the regulatory role of aPKCζ

in salivary acini formation. Future studies will be necessary to determine whether upstream regulators or downstream effectors of aPKCζ could be use as therapeutic targets to promote restorative responsive in the irradiated salivary glands.

CHAPTER 3

INTRODUCTION

Accurate detection of single cell nuclei from microscopy images is essential for extracting biological information to understand important biological processes, such as disease progression and diagnosis, cellular morphogenesis, and signaling events (Nandy, Chellappa et al. 2016, Xing and Yang 2016). In the cytology field, the manual cell counting method remains the gold standard (Louis and Siegel 2011, Cadena-Herrera, Esparza-De Lara et al. 2015). However, this method is time consuming, labor intensive, and is subjected to user's bias (Maruhashi, Murakami et al. 1994, Louis and Siegel 2011). Development of an automated cell counting method is an area of active research in both the biological and computer science fields as it could address the issues of manual cell counting method. However, robust and reliable cell detection and segmentation algorithms are still lacking despite significant progress that has been made in the field of automated image processing (Xing and Yang 2016). Using 2-dimensional (2D) histopathological images of human breast tissue, Kofahi et al. developed a cell detection and segmentation algorithm that uses an adaptive multiscale Laplacian-of-Gaussian (LoG) filtering to detect cells (Al-Kofahi, Lassoued et al. 2010). This filtering operation method locates the cell of interest by "smoothing" the image through a series of filters to detect any discontinuities in intensity from one pixel to another in an image. Ram et al. proposed a cell detection and segmentation algorithm using the Fast radial symmetry transform (FRST) method to detect cell nuclei in 3-dimensional (3D) images of Drosophila ovarian germline (Ram and Rodríguez 2013, Ram and Rodriguez 2016). Each detected cell is then segmented, a computerized process that contours the outer edge of the nuclei, using a combination of the Random walker and watershed algorithms. The

drawbacks of the aforementioned proposed algorithms are that it makes strong assumptions on the homogenous intensity profile, shape, and size of the cells, thereby limiting the algorithm's generalizability. Lastly, Nandy and colleagues proposed a 3D cell detection and segmentation algorithm by segmenting cell nuclei in a 2D slice-by-slice image, followed by graph-cut optimization to detect the 3D cell nuclei (Nandy, Chellappa et al. 2016). While this proposed algorithm may be reliable in detecting cell nuclei in 3D confocal images, the high computation time it takes to process, segment, and detect the cell nuclei make it a less feasible method. As previously discussed, the major drawback of the existing 3D cell detection and segmentation algorithms is that it limits generalizability and the segmentation and detection tasks often fail when processing images from tissues of higher organisms (i.e. mice and humans) due to the image's heterogenous intensity profile, low signal-to-noise ratio, and partial overlapping of cells of varying sizes and shapes. 3D confocal images of salispheres, a three-dimensional cluster of cells derived from mouse parotid glands, present with the aforementioned characteristics of higher organism tissues, thus making it a difficult task to segment and detect cell nuclei when applying the existing algorithms (Lombaert, Brunsting et al. 2008, Chibly, Querin et al. 2014, Nguyen, Dawson et al. 2018). However, these 3D confocal images of salispheres serve as a great training dataset for development of a more robust and reliable 3D cell segmentation and detection algorithm because it has the potential to address the fundamental challenges in 3D automated image processing and analysis. Thus, motivated by the advanced performance of convolutional neural networks (CNN) in the application of computer vision and medical image analysis, we utilized the machine learning approaches and proposed a 3D convolutional network for jointly

segmenting and detecting cell nuclei in 3D microscopy images of salispheres. We empirically validated the performance task of the proposed algorithm and demonstrated that our algorithm outperformed other benchmark methods using conventional cell segmentation and detection evaluations metrics.

MATERIALS AND METHODS

Mice and sphere forming assay

All experiments were conducted in 4-8 week old female FVB mice. All mice were maintained and treated in accordance with protocols approved by the University of Arizona Institutional Animal Care and Use Committee (IACUC). For each experiment, parotid glands from 2 mice were collected and salisphere formation was propagated using a sphere culture technique as previously described (Lombaert, Brunsting et al. 2008, Chibly, Querin et al. 2014). Cells were suspended in serum free medium supplemented with or without 2.5%, 5%, or 10% fetal bovine serum (FBS) (Hyclone, Logan, UT) and plated at a density of 200,00 cells in ultra-low attachment plates (Corning, Corning, NY).

Immunofluorescence staining

At pre-determined time points, salispheres were fixed directly in culture by adding one volume of 10% buffered formalin for 20 minutes at room temperature. After fixation, salispheres were permeabilized with 0.2% Triton-X in PBS for 20 minutes at room temperature. Target-specific staining of salispheres was performed in suspension by incubating in primary antibody diluted 1:100 in 1% BSA overnight at 4°C: anti-Ki-67 (12201, Cell Signaling, Danvers, MA), followed by incubation in secondary anti-rabbit Alexa 594 (A-11307, Invitrogen, Carlsbad, CA) at 1:500 dilution. Salispheres were pelleted by centrifugation at 4000 rpm for 5 minutes and counterstained with DAPI (4’,6-diamidino-2-phenylindole) for 5 minutes at room temperature. Images were acquired with an Intelligent Imaging Innovations (Danvers, Colorado) configured instrument including a Zeiss Marianas 100 Microscopy Workstation (Oberkochen, Germany), Yokogawa CSU-X1 M1 Spinning Disk (Musashino, Tokyo, Japan) and Photometrics

Evolve 512 EMCCD (Tucson, Arizona) using a Zeiss EC Plan-Neifluar 40X/1.3 NA oil objective and a .5µm z-separation between the slices in the stack. The Spinning Disk includes a Semrock Di01-T488/568 dichroic beam splitter and a Em01-R488/568 dual bandpass emission filter for 488 nm ex- BP 525/43 em and 561 nm ex- BP 642/117 em imaging.

Three-dimensional (3D) confocal images of salispheres will be referred to as Dataset 1 in future analysis. Dataset 2 consisted of 120 3D images from the Broad Bioimage Benchmark Collection (BBBC) dataset BBBC024 (Svoboda, Kozubek et al. 2009). This dataset is a synthetic creation of 3D HL60 cell line.

Proliferation analysis

Proliferation levels within 3D salisphere images from Dataset 1 was assessed through Ki-67 immunostaining on different days of culture. To do this, between 10-20 confocal 3D stack images per treatment condition were randomly selected for analysis. Cells were manually counted from every fifth slice in the z-stack image using the Cell Counter program from Fiji ImageJ. Proliferation of an individual salisphere was determined by the sum of the number of positive cells/total number of cells from the accumulated slices in a single z-stack image.

3D image processing by Fiji ImageJ

Adjustment of pixel intensity of 3D confocal images of salispheres was carried out by manually adjusting the brightness and contrast setting of the display images using Fiji ImageJ software. To obtain uniform intensities on all images in Dataset 1, we

designed a manual adjustment for both maximum and minimum intensity values by the following mathematic equation:

(1) Post-processed minimum intensity= pre-processed minimum intensity*10

(2) Post-processed minimum intensity= pre-processed maximum intensity/ 2

Post-processing of the 3D images from Dataset 1 using the aforementioned manual mathematical formula resulted in an increase in the pixel intensity of the display images and dampening of background non-specific fluorescent staining.

FARSIGHT automatic cell segmentation

The cell nuclei of 3D images from Dataset 1 was segmented (a computerized contouring method that outlined the edges of cell nuclei) using an existing algorithm from the FARSIGHT toolkit. The FARSIGHT algorithm utilized a multi-step approach for automatic nuclei segmentation (Ram and Rodriguez 2016). This included initial distance transformation by the Fast radial symmetric transform (FRST) method to detect a single nucleus among the densely populated area. It was then followed by H-dome transformation, extended minima transformation, Laplacian of Gaussian (LoG) filtering to refine the point of interest on a radially symmetric object due to intensity threshold. Initial segmentation using the Random walker algorithm resulted in superimposed seeds that correlate to the localization points of the cell-like region within the 3D image stacks. The post-segmentation of the images involved morphological reconstruction using a 3D active contour method. This resulted in a circular outline that mimicked the nuclear edges.

3D convolutional network architecture

The proposed model consisted of two stages: 1) segmentation of the original 3D image and a concatenated image from the segmentation network is fed in as the input, 2) a 3D detection network that detects cell nuclei centers in the image. The proposed network was trained in an end-to-end fashion with stochastic gradient descent on a loss of function comprising two parts. The first part quantified segmentation accuracy, and was computed based on the segmentation network output and the ground truth segmentation manually performed by an expert in 80 set of images from Dataset 1. The second component of the loss of function measured detection accuracy, and was computed based on the ground truth centroid locations of the cell nuclei (manually computed by an expert) and the detection network output.

The proposed network was validated on the remaining 27 set of images from Dataset 1 and 120 set of images from Dataset 2 comparing the proposed model to state-of-the-art cell detection methods using conventional metrics for cell segmentation and detection.

Statistical analyses

The following mathematical equations were used to compute segmentation and detection accuracy. P is precision, R is recall, TP is the number of true positives, FP is the number of false positives, and FN is the number of false negatives:

P= TP/ (TP + FP)

R= TP/ (TP + FN)

F-score: 2PR/ (P +R)

Dice coefficient: $2\frac{[R1 \cap R2|}{|R1|+|R2|}$

Hausdorff distance: max $\{h(R1, R2), h(R2, R1)\}$

Rand error: $\frac{(a+b)}{\binom{n}{2}}$

Graphical generation was done using Graph-Pad (version 5.0, San Diego, CA).

RESULTS

Workflow of the semi-automatic cell counting algorithm

Fast radial symmetry transform (FRST) is a computational process that detects points of interest in radially symmetric objects and has been used for various applications, including iris detection, traffic sign detection, and cell detection in 2D and 3D confocal images (Loy and Zelinsky 2003, Al-Kofahi, Lassoued et al. 2010, Hansen and Ji 2010, Ram and Rodríguez 2013, Ram and Rodríguez 2016). To evaluate whether the FRST algorithm can be used as an automatic cell counting tool in detecting single cell nuclei in 3D confocal images of salispheres derived from mouse parotid glands, we established a workflow to process and segment the images (Figure 3.1). Two hundred and forty-one images were available for analysis, which comprised of a heterogenous population of salispheres that differed in size and number of cell nuclei. An individual 3D image of salispheres was categorized based on size, defined as an equivalent circle diameter: medium-size salispheres (D_S :50-150µm) and large-size salispheres (D_S> 50-150µm). Figure 3.1 shows a flowchart illustrating the main steps of the proposed semi-automatic cell counting method, consisting of four components: 1) intensity thresholding by Fiji ImageJ software to separate the foreground pixels in the nuclear channel from the background pixels, 2) single cell nuclei detection using FRST algorithm, 3) seeds/markers detection of cell nuclei, and 4) segmenting/outlining of cell nuclear boundary by applying the Random walker and watershed (RWW) algorithm. Here, the sum of the pixel volume of the segmented nucleus, which refers to the voxel sum, is the indirect measure of the total number of cell nuclei detected.

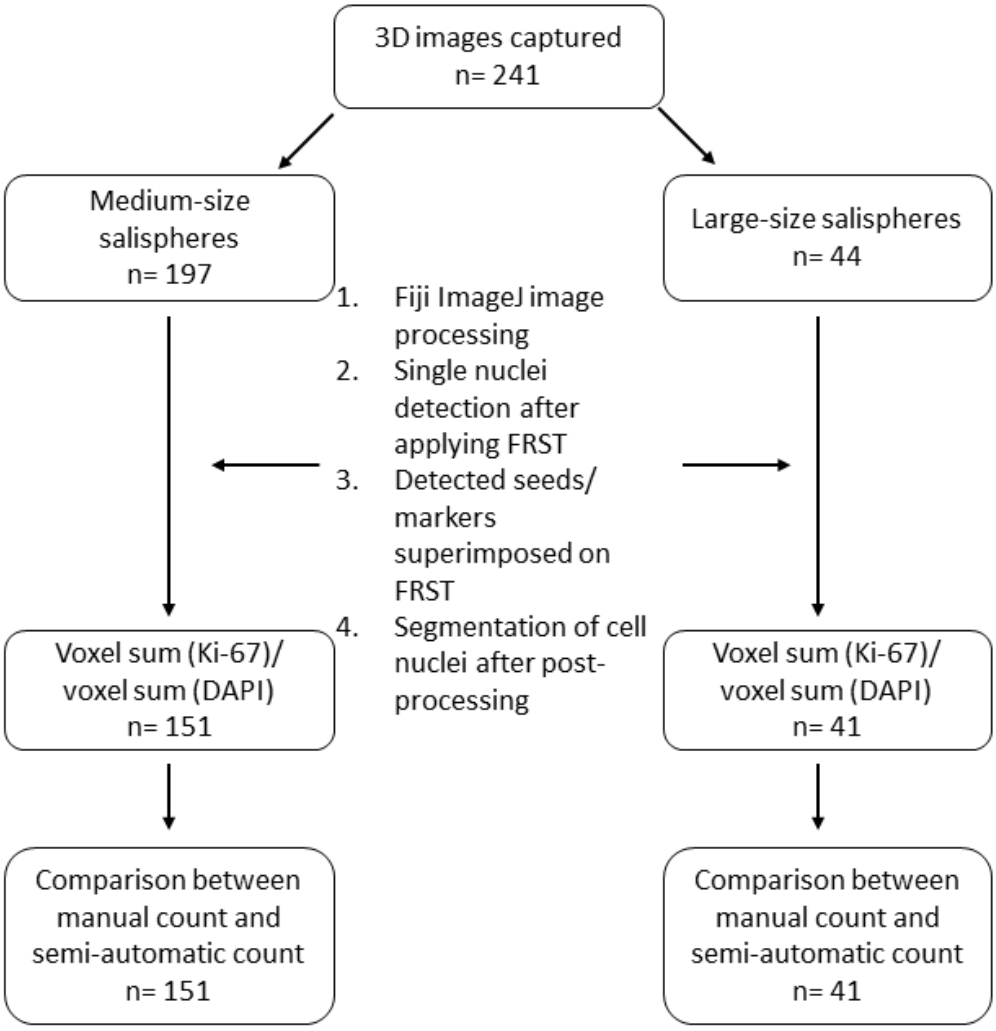

Figure 3.1: Flowchart of semi-automatic image segmentation of 3D confocal images of salispheres. An overview of steps involve in the processing, pre-segmentation, and post-segmentation of 3D confocal images of salispheres using the Fiji ImageJ and FARSIGHT automatic cell segmentation software.

Comparison of manual and automated cell counting methods

Figure 3.2A shows the quality segmentation results of the proposed semi-automatic cell counting method. To assess the performance of the proposed method, we compared it to the manual cell counting method. Here, results from the manual cell counting method is recognized as the ground truth and is the ratio of total number of Ki-67-positive cells to total number of DAPI-positive cells (i.e. proliferation index) manually counted by an expert in a z-stack image of an individual salisphere. Accurate prediction by the proposed method is bound by the condition that the ratio of voxel sum of Ki-67-positive cells to the voxel sum of DAPI-positive cells is within $\pm$10% of the ratio of total number of Ki-67-positive cells to DAPI-positive cells computed by the manual counting method. As shown in Figure 3.2B, the proposed algorithm did a poor task in detecting the predicted cell nuclei and often (~40% of the time) underestimates or overestimates the numbers of cell nuclei presented in the 3D image of medium-size salispheres. The segmentation task became more challenging with the input of large salisphere images, which have a more heterogenous intensity profile due to greater crowding and partial overlapping of cells of varying sizes and shapes (Figure 3.2Av-viii). More than 50% of the time, the proposed algorithm underestimates or overestimates the predicted proliferation index of large-size salispheres. This shows that the proposed semi-automatic cell counting method is not reliable or robust in detecting individual cells in 3D confocal images of salispheres.

A

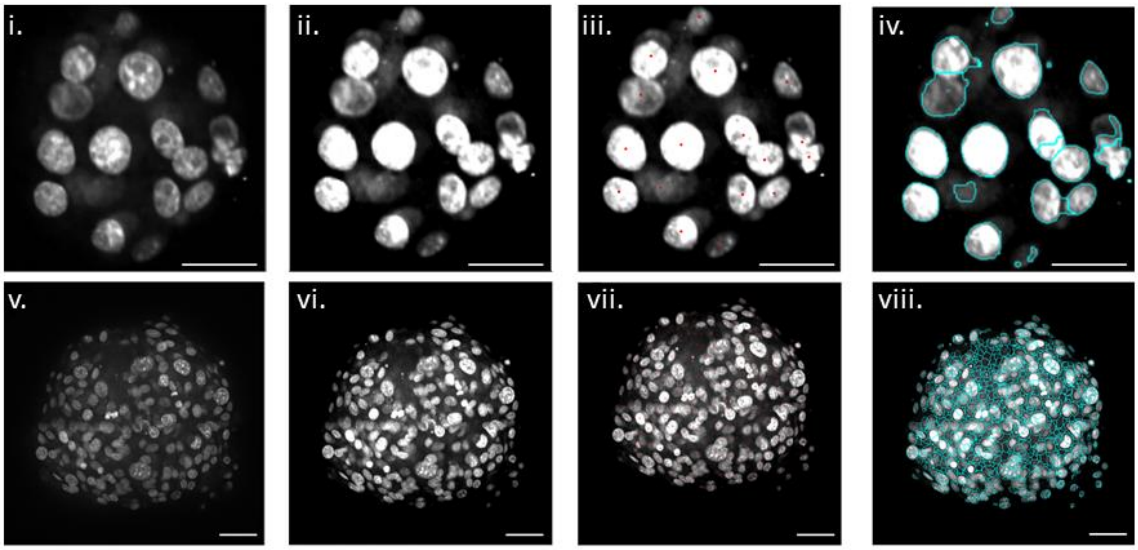

B

	Medium-size salispheres (D_S :50-150µm)	Large-size salispheres (D_S >150µm)
Percentage within range	61%	46%
Percentage under estimation	22%	22%
Percentage overestimation	17%	32%

Figure 3.2: Validation of semi-automatic counting method to manual cell counting method on identifying proliferation cells in 3D confocal images pf salispheres.
Representative slice from the z-stack of medium-size salisphere pre-process (Ai), post-process using ImageJ (Aii), detected seeds after applying Fast radial symmetric transform (FRST) (Aiii), and segmentation by FARSIGHT proposed algorithm (Aiv). Representative slice from the z-stack of large-size salisphere pre-process (Av), post-process using ImageJ (Avi), detected seeds after applying FRST (Avii), and segmentation by FARSIGHT proposed algorithm (Aviii). The proposed semi-automated segmentation algorithm was evaluated with respect to how well it performed in detecting cell nuclei between groups of salispheres when compared to manual counting method (B). Scale bar= 25µm

Proposed 3D convolutional network architecture

To improve the performance of the existing semi-automated cell counting method, we proposed a convolutional network that jointly detects and segments a single nucleus in 3D confocal images. The proposed network consisted of two components: the segmentation network and the detection network. The input of the segmentation network was 3D confocal images of salispheres derived from mouse parotid glands. The output of the segmentation network was a segmentation map, in x-, y-, and z-dimensions, concatenated along the original 3D image. This segmentation map was then fed in as the input to the second module, a detection network that detects cell nuclear centers in the image. Graphical representation of the convolution network architecture is shown in Figure 3.3A.

The proposed convolution network model was trained for both cell segmentation and detection task in an end-to-end fashion with stochastic gradient descent on a loss function. To create ground truth segmentation and detection, single nuclei from eighty sets of 3D images (Dataset 1) were carefully traced for segmentation and manually annotated for detection by an expert. These ground truth segmentation and detection were used to train the network for segmentation and detection accuracy (Figure 3.3B). Dice coefficient was used to quantify segmentation accuracy, and was computed based on the mutual overlap between the segmentation network output and the ground truth segmentation in the training data. For cell detection, the task was to create a density volume map from the input cell images, using the ground truth centroid locations of the cell nuclei in the training data as the output (Figure 3.3A and 3.3B). To evaluate the trained model, besides the 27 sets of images from Dataset 1, the model was independently

validated with 120 images from Broad Bioimage Benchmark Collection (BBBC) dataset set BBBC024 (Dataset 2) (Svoboda, Kozubek et al. 2009). This dataset is a synthetic creation of 3D HL60 cell line (Figure 3.3B).

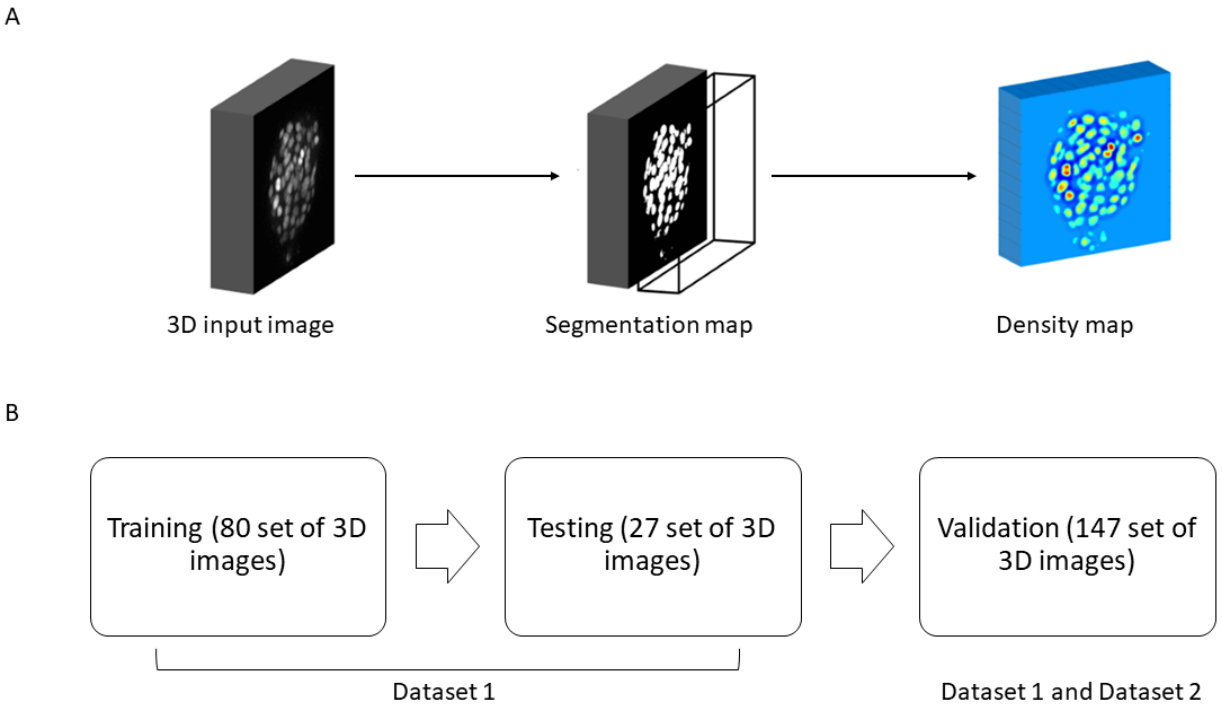

Figure 3.3: Proposed 3D convolutional network architecture.
Graphical representation of the proposed algorithm model, consisting of two components: 3D binary segmentation network whose output was concatenated along with the original 3D image and fed in as the input to a second module, a 3D detection network that detected cell nuclei centers in the image (A). The proposed network was trained in an end-to-end fashion. The model was trained on 80 3D images and tested on 27 3D images from Dataset 1, which are 3D images of salispheres derived from mouse parotid salivary glands. The model was validated against other benchmark cell detection methods using 3D images from Dataset 1 and Dataset 2 (B).

Nucleus segmentation and detection evaluation

To evaluate the performance of the proposed network, referred to as Stem Cell Network (SCeNt), in segmenting and detecting single cell nuclei in 3D confocal images, we compared SCeNt to other state-of-the-art methods, namely the Fast radial symmetry transform (FRST) algorithm, the Random walker and watershed (RWW) algorithm, the Stegmaier et al.'s method (TWANG), the U-net method, and the Dr algorithm using conventional evaluation metrics.

Figure 3.4 shows the qualitative detection results of the compared methods on a sample image from the test data in Dataset 1. For cell detection, we evaluated all the algorithms using a variety of detection evaluation metrics, principally precision P= TP/ (TP + FP), recall R= TP/ (TP + FN), and the measure of an algorithm's accuracy that combines both the mean of precision (P) and recall (R), namely F-score: 2PR/ (P +R). The F-score ranges from 0 (bad detection) to 1 (perfect detection) (Al-Kofahi, Lassoued et al. 2010). Here, each ground truth nucleus is assigned as the predicted nucleus. The assigned predicted nucleus is a true positive, and unassigned predicted nuclei are false positives. Ground truth nuclei with no assigned predicted nuclei are considered false negatives. Table 1 shows the quantitative results on the performance of the compared algorithms for cell detection (Table 1.1). We report that the F-score of the proposed 3D convolutional network is 23.4 percent greater than the FRST algorithm and 5.8 percent greater than the U-net method.

For cell segmentation, we evaluated the performance of the algorithms using the following metrics: mutual overlap (Dice coefficient), the Hausdorff distance (HD), and the Rand error. The Dice coefficient is based on the mutual overlap between the

automated segmentation algorithms (R1) and the manual performed segmentation (R2), and is calculated as follows: $2\frac{[R1 \cap R2]}{|R1|+|R2|}$, where $|R1|$ and $|R2|$ are the number of voxels, which is the three-dimensional equivalent of a pixel. The Dice coefficient range from 0 (no overlap) to 1 (perfect overlap) (Ram, Rodríguez et al. 2012). The Hausdorff distance is the measure of the distance between the boundary of the manually segmented region (R1) and the boundary of the automated segmented region (R2), and is defined as max $\{h(R1, R2), h(R2, R1)\}$. In this regard, a HD of zero suggests there is a perfect overlap; thus, a lower HD signifies better segmentation (Huttenlocher, Klanderman et al. 1993). The Rand error (RE), or index, is a measure of the algorithms' clustering performance and is defined as the frequency in which two segmentations, namely manual (a) and automated (b), agree whether a pair of voxels (n) belong to the same or different objects in a 3D image $\frac{(a+b)}{\binom{n}{2}}$ (Unnikrishnan, Pantofaru et al. 2007). The value of RE is bound between 0 (bad segmentation) and 1 (perfect segmentation). Based on the evaluation metrics previously described, the best performed algorithm for cell segmentation is the one that minimizes the Hausdorff distance and maximizes the Dice coefficient and Rand error. Compared to the current state-of-the art methods for cell segmentation, the proposed network outperforms other methods (i.e. RWW, U-net, and TWANG method), achieving the best mutual overlap measure (DE) and the lowest Rand error and Hausdorff distance (Table 1.2).

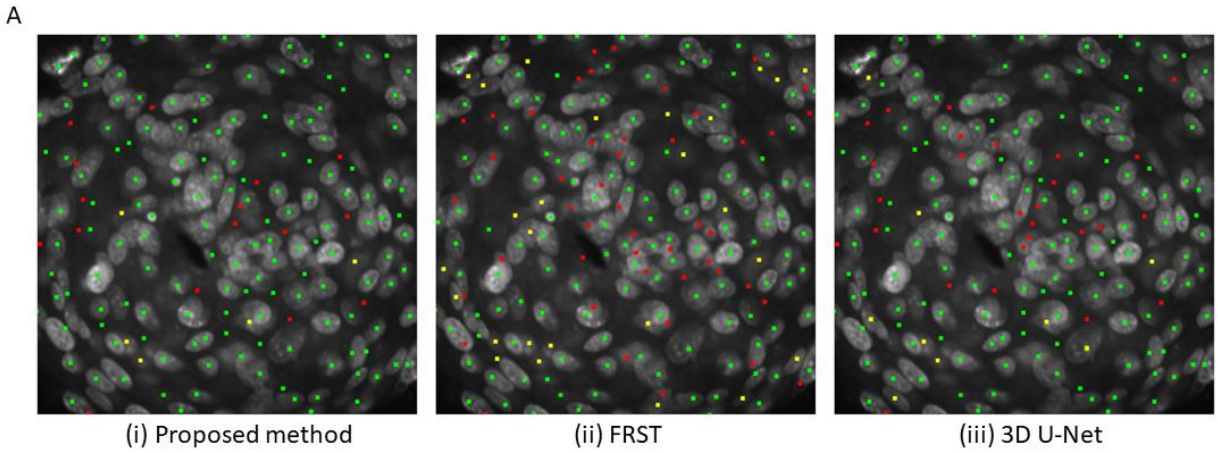

Figure 3.4: Cell detection results using the proposed and other benchmark methods.
Cell detection results on a slice of z-stack from an image in the test dataset of Dataset 1. The true positives (TP), false positives (FP), and false negatives (FN), are shown in green, red, and yellow, respectively.

Data	Method	P	R	F
Data set 1	SCeNt	0.864	0.754	0.805
	FRST	0.621	0.529	0.571
	U-Net	0.796	0.703	0.747
	Dr	0.869	0.769	0.816
Data set 2	SCeNt	0.924	0.901	0.912
	FRST	0.885	0.822	0.852
	U-Net	0.904	0.886	0.895
	Dr	0.931	0.919	0.925

Table 1.1: Quantitative comparison of the performance of the proposed algorithm for cell detection task compared to benchmark methods.
Quantitative results on the test data of 27 3D images from Dataset 1 and 120 3D images from Dataset 2 when compared the precision (P)-, recall (R)-, and coverage measures (F)- scores of the proposed 3D convolutional network (SCeNT) to other state-of-the-art cell detection methods (FRST, U-Net, and Dr).

Data	Method	Dice	HD	RE
Data set 1	SCeNt	0.763	8.72	0.0996
	RWW	0.681	10.32	0.1792
	U-Net	0.717	9.63	0.1047
	Dr	0.781	8.69	0.0849
Data set 2	SCeNt	0.934	4.91	0.0287
	RWW	0.892	6.78	0.0663
	U-Net	0.919	5.02	0.0322
	TWANG	---	6.62	0.0618
	Dr	0.939	4.82	0.0239

Table 1.2: Quantitative comparison of the performance of the proposed algorithm for cell segmentation task compared to benchmark methods.
Qualitative results of the cell segmentation applied to the test data of 27 3D images from Dataset 1 and 120 3D images from Dataset 2 when compared mutual overlap measure (Dice Coefficient), the Hausdorff distance (HD), and the Rand error (RE) of the proposed 3D convolutional network (SCeNT) to other state-of-the-art cell detection methods (RWW, U-Net, Dr, and TWANG).

DISCUSSION

Due to the increasing availability of large amounts of data and advanced computational resources, the development of a reliable and robust automated cell counting method would be greatly beneficial to the health sciences field. For example, the current analysis of tumor proliferation, a prognostic biomarker for invasive breast cancer, is performed in a manual cell counting fashion by a trained pathologist in localized regions of tissue images (Shah, Wang et al. 2017). This method has low reproducibility, labor intensive, and time consuming, which as a result can delay the diagnosis and treatment plan. To date, reliable and robust 3D cell detection and segmentation algorithms are still lacking (Xing and Yang 2016). Existing algorithms face many challenges when it comes to delivering accurate cell detection and segmentation results. The key drawback of these algorithms is that the training image dataset that is used to develop the algorithm is not reflective of the characteristic of microcopy images observed in higher organisms (i.e. mouse and human) in terms of intensity profile, signal-to-noise ratio (SNR), wide spectrum of variation in cell morphology, size, and shape (Al-Kofahi, Lassoued et al. 2010, Ram, Rodríguez et al. 2012, Ram and Rodríguez 2013, Nandy, Chellappa et al. 2016). Using 3D confocal images of salispheres from mouse salivary glands, the current study proposes a 3D convolutional neural network to simultaneously segment and detect individual cell nuclei and demonstrates that the proposed method provides markedly improved detection and segmentation accuracy when compared to other state-of-the-art algorithms.

While the Fast radial symmetry transform (FRST) algorithm provides robust cell detection and segmentation results in 2D histopathological images of human breast tissue

and 3D confocal images of ovary germline from *Drosophila melanogaster* (Al-Kofahi, Lassoued et al. 2010, Ram and Rodríguez 2013), the algorithm performed poorly when processing 3D images from salispheres. The segmentation and detection tasks become more difficult with the input of large-size salisphere images. Careful examination of the segmentation of the cell nucleus in salisphere images by FRST shows that the algorithm often detects both false positives and false negatives. The poor performance of the algorithm may be due to the complexities of the salisphere images. Cell nuclei within the 3D salisphere structure have heterogenous intensity profiles, vary in cell morphology, and often overlap with neighboring cells of varying sizes and shapes. Thus, this observation suggests that detection and segmentation of these highly complex salisphere confocal images require the development of an algorithm that does not rely on a set of assumptions with regards to cell size, shape, and intensity profile.

Conventional manual cell counting relies on a set of subjective and objective parameters established by the user to aid in the decision-making process during cell detection (Choudhry 2016). To mimic the cell segmentation and detection parameters of a manual cell counting method and apply it to an automated algorithm, we utilized the machine learning approaches and used the 3D confocal images of salispheres as the training dataset and proposed a convolution network that jointly segment and detect cell nuclei. The proposed method is robust and reliable in delivering improved segmentation and detection accuracy not only in the dataset in which the algorithm was trained from, but also in another image dataset when compared to other benchmark methods. This indicates the generalizability of the proposed method and future application of it to other 3D microscopy image datasets for cell segmentation and detection.

In summary, our work demonstrates that application of machine learning approaches addresses the drawbacks of existing 3D cell segmentation and detection algorithms and provides markedly improve segmentation and detection accuracy.

CONCLUSION

In the United States, more than 50,000 patients are diagnosed with head and neck cancers (HNC) annually (Siegel, Miller et al. 2017). The current standard of care for HNC involves a combination of therapies, usually surgical resection followed by adjuvant radiation with or without chemotherapy (Belcher, Hayes et al. 2014, Lo Nigro, Denaro et al. 2017). One of the drawbacks of radiation treatment (RT) of head and neck cancer is that surrounding non-malignant tissues, such as the salivary glands, are injured and this can lead to long lasting side effects (Vissink, Jansma et al. 2003, Grundmann, Mitchell et al. 2009). The major complaints by HNC patients who underwent radiotherapy is xerostomia, a sensation of severe dry mouth. Radiation-induced damage to the salivary glands alters the volume, consistency, and pH of the secreted saliva, leading to changes in the oral environment. As a result, HNC patients are at an increased risk for dental caries and oral infections, leading to oral discomfort (Trotti 2000, Brosky 2007, Pinna, Campus et al. 2015). Despite being potentially cured from their cancer, the quality of life of HNC patients is reduced due to the malnutrition and psychosocial problems associated with salivary gland dysfunction (Jabbari, Kim et al. 2005, Braam, Roesink et al. 2007).

Current preventive and palliative care for the management of RT-related xerostomia are limited and largely ineffective (Lopez-Jornet, Camacho-Alonso et al. 2012, Furness, Bryan et al. 2013, Fox, Xiao et al. 2015). Thus, it is of great public health interest that preventative and regenerative therapies are developed to preserve or restore saliva production in HNC patients undergoing radiation treatment. Stem cell-based therapies have been proposed as a regenerative treatment for radiation-induced salivary

gland dysfunction. Preclinical studies have shown that administration of growth factors (i.e. Keratinocyte growth factor (KGF) and Glial cell line-derived neurotrophic factor (GDNF)) at an early critical time point (1-4 days) following radiation treatment stimulated the remaining stem-like populations and led to partial restoration of salivary gland function (Lombaert, Brunsting et al. 2008, Xiao, Lin et al. 2014). Chibly et al. have demonstrated that label-retaining cells, a subpopulation of salivary cells that exhibited stem-like features both *in vivo* and *in vitro*, is maintained 30 days post-radiation, a time point that continues to exhibit a significant loss of salivary function (Chibly, Querin et al. 2014). This suggests that it may be the intracellular effect of radiation damage on the endogenous salivary stem/progenitor cell populations that contributes to radiation-induced glandular dysfunction.

To test this hypothesis, we utilized an *ex vivo*, 3D suspension culture system to assess the self-renewal capacity of cells derived from parotid glands 30 days post-radiation (Chapter I). Our data demonstrate that radiation treatment results in a significant reduction in the number of salispheres formed in culture from parotid glands. Importantly, the decrease in salisphere-forming efficiency, an indirect readout of cell self-renewal capacity, does not appear to be due to a loss in cell viability. Moreover, we show that the addition of FBS, which contains a cocktail of growth factors, to the culture promotes the expansion of salispheres from irradiated parotid glands. These findings shed new light on our current knowledge regarding the self-renewal capacity of the irradiated salivary stem/progenitor populations.

Utilizing the same suspension culture system, we further investigated how radiation therapy affects the self-renewal capacity of salivary stem/progenitor cells. We

observed that not only radiation results in a significant reduction in the number of salispheres formed in culture (Chapter I), but of the number of salispheres formed, the proportion of acini formed is also less (ChapterII). Other epithelial cell systems have shown that acini formation required expression and appropriate localization of proteins that are involved in the establishment of polarity and induction of cellular differentiation program (Furuta, Jiang et al. 2005, Whyte, Thornton et al. 2010, Fessart, Begueret et al. 2013, Gao, Yang et al. 2017). Therefore, we evaluated the levels of polarity and differentiation markers (i.e. ZO-1, β-catenin, and NKCC1) in acini and spheres isolated from parotid glands of untreated or irradiated mice. Our data show that acini have higher levels of polarity and differentiation proteins when compared to spheres. This suggests that radiation cause an intrinsic loss of polarity in a subset of population of salivary cells.

Recent published work from our lab has shown that inactivation of the polarity regulator aPKCζ correlated with salivary gland dysfunction following radiation. Thus, to further investigate role of aPKCζ in salivary cell polarization, we assessed the acini formation capacity of salivary cells in the presence of a myristoylated PKCζ pseudosubtrate inhibitor. We observed that inhibition of PKCζ activity does not alter the number of salisphere formed, but the percentage of acini formed in the presence of PKCζ inhibitor is significantly reduced, which parallels the efficiency rate of acini formation in irradiated cells.

In our study, we demonstrate that the 3D suspension cell culture assay is an effective system to evaluate the potential of a heterogeneous population of cells to behave as stem cells when removed from its *in vivo* environment (Pastrana, Silva-Vargas et al. 2011). Outputs of this assay, which include cell self-renewal (i.e. proliferation index) and

cellular morphogenesis (i.e. acini formation), provide important information to understand the biological processes and signaling events underlying the intracellular effect radiation has on the endogenous salivary stem/progenitor populations. Thus far, analysis of salivary cells' self-renewal and acini formation capacity has been achieved via the manual cell counting method. This method is time consuming, labor intensive, and is subjected to user's bias (Maruhashi, Murakami et al. 1994, Louis and Siegel 2011). To circumvent the reliance on manual cell counting method, we developed an algorithm using machine learning approaches to automatically segment and detect cell nuclei in 3D confocal images of salispheres (Chapter III). We validated the performance task of the proposed algorithm and show that it is efficient compared to the manual cell counting method and outperformed other benchmark methods using conventional cell segmentation and detection evaluations metrics.

In summary, we show that cells derived from irradiated parotid glands have a defect in cell self-renewal (Chapter I) and differentiation capacity (Chapter II). Inhibition of PKCζ kinase activity disrupts acini formation of salivary cells, a similar phenotype that is exhibited in irradiated glands. We propose that utilization of a suspension cell culture assay (Chapter III) to elucidate the upstream and downstream effectors of aPKCζ would provide mechanistic insights that govern the non-responsive phenotype in the salivary stem/progenitor populations following radiation injury.

REFERENCES

Al-Kofahi, Y., W. Lassoued, W. Lee and B. Roysam (2010). "Improved Automatic Detection and Segmentation of Cell Nuclei in Histopathology Images." IEEE Transactions on Biomedical Engineering **57**(4): 841-852.

Ambudkar, I. S. (2012). "Polarization of calcium signaling and fluid secretion in salivary gland cells." Curr Med Chem **19**(34): 5774-5781.

Arany, S., M. A. Catalan, E. Roztocil and C. E. Ovitt (2011). "Ascl3 knockout and cell ablation models reveal complexity of salivary gland maintenance and regeneration." Dev Biol **353**(2): 186-193.

Assy, Z. and H. S. Brand (2018). "A systematic review of the effects of acupuncture on xerostomia and hyposalivation." BMC Complement Altern Med **18**(1): 57.

Aure, M. H., S. Arany and C. E. Ovitt (2015). "Salivary Glands: Stem Cells, Self-duplication, or Both?" J Dent Res **94**(11): 1502-1507.

Aure, M. H., S. F. Konieczny and C. E. Ovitt (2015). "Salivary gland homeostasis is maintained through acinar cell self-duplication." Dev Cell **33**(2): 231-237.

Avila, J. L., O. Grundmann, R. Burd and K. H. Limesand (2009). "Radiation-induced salivary gland dysfunction results from p53-dependent apoptosis." Int J Radiat Oncol Biol Phys **73**(2): 523-529.

Azzam, E. I., J. P. Jay-Gerin and D. Pain (2012). "Ionizing radiation-induced metabolic oxidative stress and prolonged cell injury." Cancer Lett **327**(1-2): 48-60.

Bakarman, E. O. and A. V. Keenan (2014). "Limited evidence for non-pharmacological interventions for the relief of dry mouth." Evid Based Dent **15**(1): 25-26.

Basavaraju, S. R. and C. E. Easterly (2002). "Pathophysiological effects of radiation on atherosclerosis development and progression, and the incidence of cardiovascular complications." Med Phys **29**(10): 2391-2403.

Baum, B. J., I. Alevizos, C. Zheng, A. P. Cotrim, S. Liu, L. McCullagh, C. M. Goldsmith, P. D. Burbelo, D. E. Citrin, J. B. Mitchell, L. K. Nottingham, S. F. Rudy, C. Van Waes, M. A. Whatley, J. S. Brahim, J. A. Chiorini, S. Danielides, R. J. Turner, N. J. Patronas, C. C. Chen, N. P. Nikolov and G. G. Illei (2012). "Early responses to adenoviral-mediated transfer of the aquaporin-1 cDNA for radiation-induced salivary hypofunction." Proc Natl Acad Sci U S A **109**(47): 19403-19407.

Bauman, J. E., E. Cohen, R. L. Ferris, D. J. Adelstein, D. M. Brizel, J. A. Ridge, B. O'Sullivan, B. A. Burtness, L. H. Butterfield, W. E. Carson, M. L. Disis, B. A. Fox, T. F. Gajewski, M. L. Gillison, J. W. Hodge, Q. T. Le, D. Raben, S. E. Strome, J. Lynn and S. Malik (2017). "Immunotherapy of head and neck cancer: Emerging clinical trials from a National Cancer Institute Head and Neck Cancer Steering Committee Planning Meeting." Cancer **123**(7): 1259-1271.

Belcher, R., K. Hayes, S. Fedewa and A. Y. Chen (2014). "Current treatment of head and neck squamous cell cancer." J Surg Oncol **110**(5): 551-574.

Biteau, B., C. E. Hochmuth and H. Jasper (2011). "Maintaining tissue homeostasis: dynamic control of somatic stem cell activity." Cell Stem Cell **9**(5): 402-411.

Blom, M. and T. Lundeberg (2000). "Long-term follow-up of patients treated with acupuncture for xerostomia and the influence of additional treatment." Oral Dis **6**(1): 15-24.

Braam, P. M., J. M. Roesink, C. P. Raaijmakers, W. B. Busschers and C. H. Terhaard (2007). "Quality of life and salivary output in patients with head-and-neck cancer five years after radiotherapy." Radiat Oncol **2**: 3.

Branzei, D. and M. Foiani (2008). "Regulation of DNA repair throughout the cell cycle." Nat Rev Mol Cell Biol **9**(4): 297-308.

Brizel, D. M., T. H. Wasserman, M. Henke, V. Strnad, V. Rudat, A. Monnier, F. Eschwege, J. Zhang, L. Russell, W. Oster and R. Sauer (2000). "Phase III randomized trial of amifostine as a radioprotector in head and neck cancer." J Clin Oncol **18**(19): 3339-3345.

Brosky, M. E. (2007). "The role of saliva in oral health: strategies for prevention and management of xerostomia." J Support Oncol **5**(5): 215-225.

Buczacki, S. J., H. I. Zecchini, A. M. Nicholson, R. Russell, L. Vermeulen, R. Kemp and D. J. Winton (2013). "Intestinal label-retaining cells are secretory precursors expressing Lgr5." Nature **495**(7439): 65-69.

Bullard, T., L. Koek, E. Roztocil, P. D. Kingsley, L. Mirels and C. E. Ovitt (2008). "Ascl3 expression marks a progenitor population of both acinar and ductal cells in mouse salivary glands." Dev Biol **320**(1): 72-78.

Burlage, F. R., H. Faber, H. H. Kampinga, J. A. Langendijk, A. Vissink and R. P. Coppes (2009). "Enhanced proliferation of acinar and progenitor cells by prophylactic pilocarpine treatment underlies the observed amelioration of radiation injury to parotid glands." Radiother Oncol **90**(2): 253-256.

Burlage, F. R., J. M. Roesink, H. H. Kampinga, R. P. Coppes, C. Terhaard, J. A. Langendijk, P. van Luijk, M. A. Stokman and A. Vissink (2008). "Protection of salivary

function by concomitant pilocarpine during radiotherapy: a double-blind, randomized, placebo-controlled study." Int J Radiat Oncol Biol Phys **70**(1): 14-22.

Cadena-Herrera, D., J. E. Esparza-De Lara, N. D. Ramirez-Ibanez, C. A. Lopez-Morales, N. O. Perez, L. F. Flores-Ortiz and E. Medina-Rivero (2015). "Validation of three viable-cell counting methods: Manual, semi-automated, and automated." Biotechnol Rep (Amst) **7**: 9-16.

Cankar, K., Z. Finderle and J. Jan (2011). "The effect of hyperbaric oxygenation on postradiation xerostomia and saliva in patients with head and neck tumours." Caries Res **45**(2): 136-141.

Charron, A. J., S. Nakamura, R. Bacallao and A. Wandinger-Ness (2000). "Compromised cytoarchitecture and polarized trafficking in autosomal dominant polycystic kidney disease cells." J Cell Biol **149**(1): 111-124.

Chibly, A. M., T. Nguyen and K. H. Limesand (2014). "Palliative Care for Salivary Gland Dysfunction Highlights the Need for Regenerative Therapies: A Review on Radiation and Salivary Gland Stem Cells." J Palliat Care Med **4**(4).

Chibly, A. M., L. Querin, Z. Harris and K. H. Limesand (2014). "Label-retaining cells in the adult murine salivary glands possess characteristics of adult progenitor cells." PLoS One **9**(9): e107893.

Chibly, A. M., W. Y. Wong, M. Pier, H. Cheng, Y. Mu, J. Chen, S. Ghosh and K. H. Limesand (2018). "aPKCzeta-dependent Repression of Yap is Necessary for Functional Restoration of Irradiated Salivary Glands with IGF-1." Sci Rep **8**(1): 6347.

Choudhry, P. (2016). "High-Throughput Method for Automated Colony and Cell Counting by Digital Image Analysis Based on Edge Detection." PLoS One **11**(2): e0148469.

Cmelak, A. J. (2012). "Current issues in combined modality therapy in locally advanced head and neck cancer." Crit Rev Oncol Hematol **84**(2): 261-273.

Cognetti, D. M., R. S. Weber and S. Y. Lai (2008). "Head and neck cancer: an evolving treatment paradigm." Cancer **113**(7 Suppl): 1911-1932.

Collan, J., M. Kapanen, A. Makitie, H. Nyman, H. Joensuu, M. Tenhunen and K. Saarilahti (2012). "Submandibular gland-sparing intensity modulated radiotherapy in the treatment of head and neck cancer: sites of locoregional relapse and survival." Acta Oncol **51**(6): 735-742.

Coppes, R. P., A. Meter, S. P. Latumalea, A. F. Roffel and H. H. Kampinga (2005). "Defects in muscarinic receptor-coupled signal transduction in isolated parotid gland cells after in vivo irradiation: evidence for a non-DNA target of radiation." Br J Cancer **92**(3): 539-546.

Coppes, R. P., A. F. Roffel, L. J. Zeilstra, A. Vissink and A. W. Konings (2000). "Early radiation effects on muscarinic receptor-induced secretory responsiveness of the parotid gland in the freely moving rat." Radiat Res **153**(3): 339-346.

Coppes, R. P. and M. A. Stokman (2011). "Stem cells and the repair of radiation-induced salivary gland damage." Oral Dis **17**(2): 143-153.

Cotrim, A. P., A. Sowers, J. B. Mitchell and B. J. Baum (2007). "Prevention of irradiation-induced salivary hypofunction by microvessel protection in mouse salivary glands." Mol Ther **15**(12): 2101-2106.

Deasy, J. O., V. Moiseenko, L. Marks, K. S. Chao, J. Nam and A. Eisbruch (2010). "Radiotherapy dose-volume effects on salivary gland function." Int J Radiat Oncol Biol Phys **76**(3 Suppl): S58-63.

Debnath, J., S. K. Muthuswamy and J. S. Brugge (2003). "Morphogenesis and oncogenesis of MCF-10A mammary epithelial acini grown in three-dimensional basement membrane cultures." Methods **30**(3): 256-268.

Delporte, C., B. C. O'Connell, X. He, H. E. Lancaster, A. C. O'Connell, P. Agre and B. J. Baum (1997). "Increased fluid secretion after adenoviral-mediated transfer of the aquaporin-1 cDNA to irradiated rat salivary glands." Proc Natl Acad Sci U S A **94**(7): 3268-3273.

Delporte, C. and S. Steinfeld (2006). "Distribution and roles of aquaporins in salivary glands." Biochim Biophys Acta **1758**(8): 1061-1070.

Denaro, N., M. C. Merlano and E. G. Russi (2016). "Follow-up in Head and Neck Cancer: Do More Does It Mean Do Better? A Systematic Review and Our Proposal Based on Our Experience." Clin Exp Otorhinolaryngol **9**(4): 287-297.

Devi, S. and N. Singh (2014). "Dental care during and after radiotherapy in head and neck cancer." Natl J Maxillofac Surg **5**(2): 117-125.

Dirix, P., S. Nuyts and W. Van den Bogaert (2006). "Radiation-induced xerostomia in patients with head and neck cancer: a literature review." Cancer **107**(11): 2525-2534.

Dolan, C. P., L. A. Dawson and K. Muneoka (2018). "Digit Tip Regeneration: Merging Regeneration Biology with Regenerative Medicine." Stem Cells Transl Med **7**(3): 262-270.

Eisbruch, A., J. A. Ship, L. A. Dawson, H. M. Kim, C. R. Bradford, J. E. Terrell, D. B. Chepeha, T. N. Teknos, N. D. Hogikyan, Y. Anzai, L. H. Marsh, R. K. Ten Haken and G. T. Wolf (2003). "Salivary gland sparing and improved target irradiation by conformal and intensity modulated irradiation of head and neck cancer." World J Surg **27**(7): 832-837.

Emmerson, E., A. J. May, L. Berthoin, N. Cruz-Pacheco, S. Nathan, A. J. Mattingly, J. L. Chang, W. R. Ryan, A. D. Tward and S. M. Knox (2018). "Salivary glands regenerate after radiation injury through SOX2-mediated secretory cell replacement." EMBO Mol Med.

Fei, P. and W. S. El-Deiry (2003). "P53 and radiation responses." Oncogene **22**(37): 5774-5783.

Fessart, D., H. Begueret and F. Delom (2013). "Three-dimensional culture model to distinguish normal from malignant human bronchial epithelial cells." Eur Respir J **42**(5): 1345-1356.

Fischbach, M. A., J. A. Bluestone and W. A. Lim (2013). "Cell-based therapeutics: the next pillar of medicine." Sci Transl Med **5**(179): 179ps177.

Fox, N. F., C. Xiao, A. J. Sood, T. L. Lovelace, S. A. Nguyen, A. Sharma and T. A. Day (2015). "Hyperbaric oxygen therapy for the treatment of radiation-induced xerostomia: a systematic review." Oral Surg Oral Med Oral Pathol Oral Radiol **120**(1): 22-28.

Furness, S., G. Bryan, R. McMillan, S. Birchenough and H. V. Worthington (2013). "Interventions for the management of dry mouth: non-pharmacological interventions." Cochrane Database Syst Rev(9): CD009603.

Furuta, S., X. Jiang, B. Gu, E. Cheng, P. L. Chen and W. H. Lee (2005). "Depletion of BRCA1 impairs differentiation but enhances proliferation of mammary epithelial cells." Proc Natl Acad Sci U S A **102**(26): 9176-9181.

Gao, L., Z. Yang, C. Hiremath, S. E. Zimmerman, B. Long, P. R. Brakeman, K. E. Mostov, D. M. Bryant, K. Luby-Phelps and D. K. Marciano (2017). "Afadin orients cell division to position the tubule lumen in developing renal tubules." Development **144**(19): 3511-3520.

Grundmann, O., J. L. Fillinger, K. R. Victory, R. Burd and K. H. Limesand (2010). "Restoration of radiation therapy-induced salivary gland dysfunction in mice by post therapy IGF-1 administration." BMC Cancer **10**: 417.

Grundmann, O., G. C. Mitchell and K. H. Limesand (2009). "Sensitivity of salivary glands to radiation: from animal models to therapies." J Dent Res **88**(10): 894-903.

Guggenheimer, J. and P. A. Moore (2003). "Xerostomia: etiology, recognition and treatment." J Am Dent Assoc **134**(1): 61-69; quiz 118-119.

Han, L., L. Wang, F. Zhang, K. J. Liu and B. Xiang (2015). "Effect of Phenylephrine Pretreatment on the Expressions of Aquaporin 5 and c-Jun N-Terminal Kinase in Irradiated Submandibular Gland." Radiat Res **183**(6): 693-700.

Hansen, D. W. and Q. Ji (2010). "In the eye of the beholder: a survey of models for eyes and gaze." IEEE Trans Pattern Anal Mach Intell **32**(3): 478-500.

Helton, E. S. and X. Chen (2007). "p53 modulation of the DNA damage response." J Cell Biochem **100**(4): 883-896.

Hensley, M. L., K. L. Hagerty, T. Kewalramani, D. M. Green, N. J. Meropol, T. H. Wasserman, G. I. Cohen, B. Emami, W. J. Gradishar, R. B. Mitchell, J. T. Thigpen, A.

Trotti, 3rd, D. von Hoff and L. M. Schuchter (2009). "American Society of Clinical Oncology 2008 clinical practice guideline update: use of chemotherapy and radiation therapy protectants." J Clin Oncol **27**(1): 127-145.

Hill, G., D. Headon, Z. I. Harris, K. Huttner and K. H. Limesand (2014). "Pharmacological activation of the EDA/EDAR signaling pathway restores salivary gland function following radiation-induced damage." PLoS One **9**(11): e112840.

Holmberg, K. V. and M. P. Hoffman (2014). "Anatomy, biogenesis and regeneration of salivary glands." Monogr Oral Sci **24**: 1-13.

Hsu, H. J. and D. Drummond-Barbosa (2011). "Insulin signals control the competence of the Drosophila female germline stem cell niche to respond to Notch ligands." Dev Biol **350**(2): 290-300.

Huttenlocher, D. P., G. A. Klanderman and W. J. Rucklidge (1993). "Comparing images using the Hausdorff distance." IEEE Transactions on Pattern Analysis and Machine Intelligence **15**(9): 850-863.

Inohara, H., Y. Takenaka, T. Yoshii, S. Nakahara, Y. Yamamoto, Y. Tomiyama, Y. Seo, F. Isohashi, O. Suzuki, Y. Yoshioka, I. Sumida and K. Ogawa (2015). "Phase 2 study of docetaxel, cisplatin, and concurrent radiation for technically resectable stage III-IV squamous cell carcinoma of the head and neck." Int J Radiat Oncol Biol Phys **91**(5): 934-941.

Jabbari, S., H. M. Kim, M. Feng, A. Lin, C. Tsien, M. Elshaikh, J. E. Terrel, C. Murdoch-Kinch and A. Eisbruch (2005). "Matched case-control study of quality of life and xerostomia after intensity-modulated radiotherapy or standard radiotherapy for head-and-neck cancer: initial report." Int J Radiat Oncol Biol Phys **63**(3): 725-731.

Jellema, A. P., B. J. Slotman, M. J. Muller, C. R. Leemans, L. E. Smeele, K. Hoekman, N. K. Aaronson and J. A. Langendijk (2006). "Radiotherapy alone, versus radiotherapy with amifostine 3 times weekly, versus radiotherapy with amifostine 5 times weekly: A prospective randomized study in squamous cell head and neck cancer." Cancer **107**(3): 544-553.

Johns, M. E. (1977). "The salivary glands: anatomy and embryology." Otolaryngol Clin North Am **10**(2): 261-271.

Johnson, J. T., G. A. Ferretti, W. J. Nethery, I. H. Valdez, P. C. Fox, D. Ng, C. C. Muscoplat and S. C. Gallagher (1993). "Oral pilocarpine for post-irradiation xerostomia in patients with head and neck cancer." N Engl J Med **329**(6): 390-395.

Jones, D. L. and A. J. Wagers (2008). "No place like home: anatomy and function of the stem cell niche." Nat Rev Mol Cell Biol **9**(1): 11-21.

Knox, S. M., I. M. Lombaert, C. L. Haddox, S. R. Abrams, A. Cotrim, A. J. Wilson and M. P. Hoffman (2013). "Parasympathetic stimulation improves epithelial organ regeneration." Nat Commun **4**: 1494.

Knox, S. M., I. M. Lombaert, X. Reed, L. Vitale-Cross, J. S. Gutkind and M. P. Hoffman (2010). "Parasympathetic innervation maintains epithelial progenitor cells during salivary organogenesis." Science **329**(5999): 1645-1647.

Konings, A. W., R. P. Coppes and A. Vissink (2005). "On the mechanism of salivary gland radiosensitivity." Int J Radiat Oncol Biol Phys **62**(4): 1187-1194.

Kopp, J. L., M. Grompe and M. Sander (2016). "Stem cells versus plasticity in liver and pancreas regeneration." Nat Cell Biol **18**(3): 238-245.

Kostakopoulou, K., N. Vargesson, J. D. Clarke, P. M. Brickell and C. Tickle (1997). "Local origin of cells in FGF-4 - induced outgrowth of amputated chick wing bud stumps." Int J Dev Biol **41**(5): 747-750.

Koukourakis, M. I. (2003). "Amifostine: is there evidence of tumor protection?" Semin Oncol **30**(6 Suppl 18): 18-30.

Kwak, M. and S. Ghazizadeh (2015). "Analysis of histone H2BGFP retention in mouse submandibular gland reveals actively dividing stem cell populations." Stem Cells Dev **24**(5): 565-574.

Kwon, O., G. Corrigan, B. D. Myers, R. Sibley, J. D. Scandling, D. Dafoe, E. Alfrey and W. J. Nelson (1999). "Sodium reabsorption and distribution of Na+/K+-ATPase during postischemic injury to the renal allograft." Kidney Int **55**(3): 963-975.

Laheij, A. M., C. N. Rasch, B. W. Brandt, J. J. de Soet, R. G. Schipper, A. Loof, E. Silletti and C. van Loveren (2015). "Proteins and peptides in parotid saliva of irradiated patients compared to that of healthy controls using SELDI-TOF-MS." BMC Res Notes **8**: 639.

Latif, C., S. H. Harvey and M. J. O'Connell (2001). "Ensuring the stability of the genome: DNA damage checkpoints." ScientificWorldJournal **1**: 684-702.

Lee, N., H. Schoder, B. Beattie, R. Lanning, N. Riaz, S. McBride, N. Katabi, D. Li, B. Yarusi, S. Chan, L. Mitrani, Z. Zhang, D. G. Pfister, E. Sherman, S. Baxi, J. Boyle, L. G. Morris, I. Ganly, R. Wong and J. Humm (2016). "Strategy of Using Intratreatment Hypoxia Imaging to Selectively and Safely Guide Radiation Dose De-escalation Concurrent With Chemotherapy for Locoregionally Advanced Human Papillomavirus-Related Oropharyngeal Carcinoma." Int J Radiat Oncol Biol Phys **96**(1): 9-17.

Lee, S. W., K. W. Kang and H. G. Wu (2016). "Prospective investigation and literature review of tolerance dose on salivary glands using quantitative salivary gland scintigraphy in the intensity-modulated radiotherapy era." Head Neck **38 Suppl 1**: E1746-1755.

LeVeque, F. G., M. Montgomery, D. Potter, M. B. Zimmer, J. W. Rieke, B. W. Steiger, S. C. Gallagher and C. C. Muscoplat (1993). "A multicenter, randomized, double-blind, placebo-controlled, dose-titration study of oral pilocarpine for treatment of radiation-induced xerostomia in head and neck cancer patients." J Clin Oncol **11**(6): 1124-1131.

Li, J., Z. Shan, G. Ou, X. Liu, C. Zhang, B. J. Baum and S. Wang (2005). "Structural and functional characteristics of irradiation damage to parotid glands in the miniature pig." Int J Radiat Oncol Biol Phys **62**(5): 1510-1516.

Limesand, K. H., S. Said and S. M. Anderson (2009). "Suppression of radiation-induced salivary gland dysfunction by IGF-1." PLoS One **4**(3): e4663.

Limesand, K. H., K. L. Schwertfeger and S. M. Anderson (2006). "MDM2 is required for suppression of apoptosis by activated Akt1 in salivary acinar cells." Mol Cell Biol **26**(23): 8840-8856.

Lin, A., H. M. Kim, J. E. Terrell, L. A. Dawson, J. A. Ship and A. Eisbruch (2003). "Quality of life after parotid-sparing IMRT for head-and-neck cancer: a prospective longitudinal study." Int J Radiat Oncol Biol Phys **57**(1): 61-70.

Lin, A. L., D. A. Johnson, Y. Wu, G. Wong, J. L. Ebersole and C. K. Yeh (2001). "Measuring short-term gamma-irradiation effects on mouse salivary gland function using a new saliva collection device." Arch Oral Biol **46**(11): 1085-1089.

Liu, X., A. Cotrim, L. Teos, C. Zheng, W. Swaim, J. Mitchell, Y. Mori and I. Ambudkar (2013). "Loss of TRPM2 function protects against irradiation-induced salivary gland dysfunction." Nat Commun **4**: 1515.

Llado, V., Y. Nakanishi, A. Duran, M. Reina-Campos, P. M. Shelton, J. F. Linares, T. Yajima, A. Campos, P. Aza-Blanc, M. Leitges, M. T. Diaz-Meco and J. Moscat (2015). "Repression of Intestinal Stem Cell Function and Tumorigenesis through Direct Phosphorylation of beta-Catenin and Yap by PKCzeta." Cell Rep.

Lo Nigro, C., N. Denaro, A. Merlotti and M. Merlano (2017). "Head and neck cancer: improving outcomes with a multidisciplinary approach." Cancer Manag Res **9**: 363-371.

Lomax, M. E., L. K. Folkes and P. O'Neill (2013). "Biological consequences of radiation-induced DNA damage: relevance to radiotherapy." Clin Oncol (R Coll Radiol) **25**(10): 578-585.

Lombaert, I., M. M. Movahednia, C. Adine and J. N. Ferreira (2017). "Concise Review: Salivary Gland Regeneration: Therapeutic Approaches from Stem Cells to Tissue Organoids." Stem Cells **35**(1): 97-105.

Lombaert, I. M., S. R. Abrams, L. Li, V. P. Eswarakumar, A. J. Sethi, R. L. Witt and M. P. Hoffman (2013). "Combined KIT and FGFR2b signaling regulates epithelial progenitor expansion during organogenesis." Stem Cell Reports **1**(6): 604-619.

Lombaert, I. M., J. F. Brunsting, P. K. Wierenga, H. Faber, M. A. Stokman, T. Kok, W. H. Visser, H. H. Kampinga, G. de Haan and R. P. Coppes (2008). "Rescue of salivary gland function after stem cell transplantation in irradiated glands." PLoS One **3**(4): e2063.

Lombaert, I. M., J. F. Brunsting, P. K. Wierenga, H. H. Kampinga, G. de Haan and R. P. Coppes (2008). "Keratinocyte growth factor prevents radiation damage to salivary glands by expansion of the stem/progenitor pool." Stem Cells **26**(10): 2595-2601.

Lopez-Jornet, P., F. Camacho-Alonso and C. Rodriguez-Aguado (2012). "Evaluation of the clinical efficacy of a betaine-containing mouthwash and an intraoral device for the treatment of dry mouth." J Oral Pathol Med **41**(3): 201-206.

Louis, K. S. and A. C. Siegel (2011). "Cell viability analysis using trypan blue: manual and automated methods." Methods Mol Biol **740**: 7-12.

Loy, G. and A. Zelinsky (2003). "Fast radial symmetry for detecting points of interest." IEEE Transactions on Pattern Analysis and Machine Intelligence **25**(8): 959-973.

Maimets, M., R. Bron, G. de Haan, R. van Os and R. P. Coppes (2015). "Similar ex vivo expansion and post-irradiation regenerative potential of juvenile and aged salivary gland stem cells." Radiother Oncol **116**(3): 443-448.

Makkonen, T. A., J. Tenovuo, P. Vilja and A. Heimdahl (1986). "Changes in the protein composition of whole saliva during radiotherapy in patients with oral or pharyngeal cancer." Oral Surg Oral Med Oral Pathol **62**(3): 270-275.

Mandal, P. K., C. Blanpain and D. J. Rossi (2011). "DNA damage response in adult stem cells: pathways and consequences." Nat Rev Mol Cell Biol **12**(3): 198-202.

Manuel Iglesias, J., I. Beloqui, F. Garcia-Garcia, O. Leis, A. Vazquez-Martin, A. Eguiara, S. Cufi, A. Pavon, J. A. Menendez, J. Dopazo and A. G. Martin (2013). "Mammosphere formation in breast carcinoma cell lines depends upon expression of E-cadherin." PLoS One **8**(10): e77281.

Maria, O. M., A. Zeitouni, O. Gologan and S. D. Tran (2011). "Matrigel improves functional properties of primary human salivary gland cells." Tissue Eng Part A **17**(9-10): 1229-1238.

Marmary, Y., R. Adar, S. Gaska, A. Wygoda, A. Maly, J. Cohen, R. Eliashar, L. Mizrachi, C. Orfaig-Geva, B. J. Baum, S. Rose-John, E. Galun and J. H. Axelrod (2016). "Radiation-Induced Loss of Salivary Gland Function Is Driven by Cellular Senescence and Prevented by IL6 Modulation." Cancer Res **76**(5): 1170-1180.

Martin, K. L., G. A. Hill, R. R. Klein, D. G. Arnett, R. Burd and K. H. Limesand (2012). "Prevention of radiation-induced salivary gland dysfunction utilizing a CDK inhibitor in a mouse model." PLoS One **7**(12): e51363.

Maruhashi, F., S. Murakami and K. Baba (1994). "Automated monitoring of cell concentration and viability using an image analysis system." Cytotechnology **15**(1-3): 281-289.

Mascre, G., S. Dekoninck, B. Drogat, K. K. Youssef, S. Brohee, P. A. Sotiropoulou, B. D. Simons and C. Blanpain (2012). "Distinct contribution of stem and progenitor cells to epidermal maintenance." Nature **489**(7415): 257-262.

Mendelson, A. and P. S. Frenette (2014). "Hematopoietic stem cell niche maintenance during homeostasis and regeneration." Nat Med **20**(8): 833-846.

Miyajima, A., M. Tanaka and T. Itoh (2014). "Stem/progenitor cells in liver development, homeostasis, regeneration, and reprogramming." Cell Stem Cell **14**(5): 561-574.

Mizrachi, A., A. P. Cotrim, N. Katabi, J. B. Mitchell, M. Verheij and A. Haimovitz-Friedman (2016). "Radiation-Induced Microvascular Injury as a Mechanism of Salivary

Gland Hypofunction and Potential Target for Radioprotectors." Radiat Res **186**(2): 189-195.

Mohrin, M., E. Bourke, D. Alexander, M. R. Warr, K. Barry-Holson, M. M. Le Beau, C. G. Morrison and E. Passegue (2010). "Hematopoietic stem cell quiescence promotes error-prone DNA repair and mutagenesis." Cell Stem Cell **7**(2): 174-185.

Molitoris, B. A. and W. J. Nelson (1990). "Alterations in the establishment and maintenance of epithelial cell polarity as a basis for disease processes." J Clin Invest **85**(1): 3-9.

Momot, D., C. Zheng, H. Yin, R. H. Elbekai, M. Vallant and J. A. Chiorini (2014). "Toxicity and biodistribution of the serotype 2 recombinant adeno-associated viral vector, encoding Aquaporin-1, after retroductal delivery to a single mouse parotid gland." PLoS One **9**(3): e92832.

Mountzios, G. (2015). "Optimal management of the elderly patient with head and neck cancer: Issues regarding surgery, irradiation and chemotherapy." World J Clin Oncol **6**(1): 7-15.

Nagasawa, T., S. Hirota, K. Tachibana, N. Takakura, S. Nishikawa, Y. Kitamura, N. Yoshida, H. Kikutani and T. Kishimoto (1996). "Defects of B-cell lymphopoiesis and bone-marrow myelopoiesis in mice lacking the CXC chemokine PBSF/SDF-1." Nature **382**(6592): 635-638.

Nagle, P. W., N. A. Hosper, E. M. Ploeg, M. J. van Goethem, S. Brandenburg, J. A. Langendijk, R. K. Chiu and R. P. Coppes (2016). "The In Vitro Response of Tissue Stem Cells to Irradiation With Different Linear Energy Transfers." Int J Radiat Oncol Biol Phys **95**(1): 103-111.

Nanduri, L. S., M. Maimets, S. A. Pringle, M. van der Zwaag, R. P. van Os and R. P. Coppes (2011). "Regeneration of irradiated salivary glands with stem cell marker expressing cells." Radiother Oncol **99**(3): 367-372.

Nandy, K., R. Chellappa, A. Kumar and S. J. Lockett (2016). "Segmentation of Nuclei From 3D Microscopy Images of Tissue via Graphcut Optimization." IEEE Journal of Selected Topics in Signal Processing **10**(1): 140-150.

Nguyen, V. T., P. Dawson, Q. Zhang, Z. Harris and K. H. Limesand (2018). "Administration of growth factors promotes salisphere formation from irradiated parotid salivary glands." PLoS One **13**(3): e0193942.

Okumura, K., K. Nakamura, Y. Hisatomi, K. Nagano, Y. Tanaka, K. Terada, T. Sugiyama, K. Umeyama, K. Matsumoto, T. Yamamoto and F. Endo (2003). "Salivary gland progenitor cells induced by duct ligation differentiate into hepatic and pancreatic lineages." Hepatology **38**(1): 104-113.

Oronsky, B., S. Goyal, M. M. Kim, P. Cabrales, M. Lybeck, S. Caroen, N. Oronsky, E. Burbano, C. Carter and A. Oronsky (2018). "A Review of Clinical Radioprotection and Chemoprotection for Oral Mucositis." Transl Oncol **11**(3): 771-778.

Parkin, D. M., F. Bray, J. Ferlay and P. Pisani (2005). "Global cancer statistics, 2002." CA Cancer J Clin **55**(2): 74-108.

Pastrana, E., V. Silva-Vargas and F. Doetsch (2011). "Eyes wide open: a critical review of sphere-formation as an assay for stem cells." Cell Stem Cell **8**(5): 486-498.

Patterson, J., L. C. Lloyd and D. A. Titchen (1975). "Secretory and structural changes in the parotid salivary gland of sheep and lambs after parasympathetic denervation." Q J Exp Physiol Cogn Med Sci **60**(3): 223-232.

Pedersen, A. M., A. Bardow, S. B. Jensen and B. Nauntofte (2002). "Saliva and gastrointestinal functions of taste, mastication, swallowing and digestion." Oral Dis **8**(3): 117-129.

Peters, S. B., N. Naim, D. A. Nelson, A. P. Mosier, N. C. Cady and M. Larsen (2014). "Biocompatible tissue scaffold compliance promotes salivary gland morphogenesis and differentiation." Tissue Eng Part A **20**(11-12): 1632-1642.

Pinna, R., G. Campus, E. Cumbo, I. Mura and E. Milia (2015). "Xerostomia induced by radiotherapy: an overview of the physiopathology, clinical evidence, and management of the oral damage." Ther Clin Risk Manag **11**: 171-188.

Plemons, J. M., I. Al-Hashimi, C. L. Marek and A. American Dental Association Council on Scientific (2014). "Managing xerostomia and salivary gland hypofunction: executive summary of a report from the American Dental Association Council on Scientific Affairs." J Am Dent Assoc **145**(8): 867-873.

Poss, K. D. (2010). "Advances in understanding tissue regenerative capacity and mechanisms in animals." Nat Rev Genet **11**(10): 710-722.

Pradhan-Bhatt, S., D. A. Harrington, R. L. Duncan, X. Jia, R. L. Witt and M. C. Farach-Carson (2013). "Implantable three-dimensional salivary spheroid assemblies demonstrate fluid and protein secretory responses to neurotransmitters." Tissue Eng Part A **19**(13-14): 1610-1620.

Pradhan, S. and M. C. Farach-Carson (2010). "Mining the extracellular matrix for tissue engineering applications." Regen Med **5**(6): 961-970.

Pradhan, S., C. Liu, C. Zhang, X. Jia, M. C. Farach-Carson and R. L. Witt (2010). "Lumen formation in three-dimensional cultures of salivary acinar cells." Otolaryngol Head Neck Surg **142**(2): 191-195.

Pringle, S., M. Maimets, M. van der Zwaag, M. A. Stokman, D. van Gosliga, E. Zwart, M. J. Witjes, G. de Haan, R. van Os and R. P. Coppes (2016). "Human Salivary Gland Stem Cells Functionally Restore Radiation Damaged Salivary Glands." Stem Cells **34**(3): 640-652.

Proctor, G. B. and G. H. Carpenter (2007). "Regulation of salivary gland function by autonomic nerves." Auton Neurosci **133**(1): 3-18.

Proctor, G. B. and G. H. Carpenter (2014). "Salivary secretion: mechanism and neural regulation." Monogr Oral Sci **24**: 14-29.

Ram, S. and J. J. Rodriguez (2016). "Size-Invariant Detection of Cell Nuclei in Microscopy Images." IEEE Trans Med Imaging **35**(7): 1753-1764.

Ram, S. and J. J. Rodríguez (2013). Symmetry-based detection of nuclei in microscopy images. 2013 IEEE International Conference on Acoustics, Speech and Signal Processing.

Ram, S. and J. J. Rodríguez (2016). "Size-Invariant Detection of Cell Nuclei in Microscopy Images." IEEE Transactions on Medical Imaging **35**(7): 1753-1764.

Ram, S., J. J. Rodríguez and G. Bosco (2012). Size-invariant cell nucleus segmentation in 3-D microscopy. 2012 IEEE Southwest Symposium on Image Analysis and Interpretation.

Regelink, G., A. Vissink, H. Reintsema and J. M. Nauta (1998). "Efficacy of a synthetic polymer saliva substitute in reducing oral complaints of patients suffering from irradiation-induced xerostomia." Quintessence Int **29**(6): 383-388.

Riley, P., A. M. Glenny, F. Hua and H. V. Worthington (2017). "Pharmacological interventions for preventing dry mouth and salivary gland dysfunction following radiotherapy." Cochrane Database Syst Rev **7**: CD012744.

Roitbak, T., C. J. Ward, P. C. Harris, R. Bacallao, S. A. Ness and A. Wandinger-Ness (2004). "A polycystin-1 multiprotein complex is disrupted in polycystic kidney disease cells." Mol Biol Cell **15**(3): 1334-1346.

Romagnani, P., L. Lasagni, B. Mazzinghi, E. Lazzeri and S. Romagnani (2007). "Pharmacological modulation of stem cell function." Curr Med Chem **14**(10): 1129-1139.

Rugel-Stahl, A., M. E. Elliott and C. E. Ovitt (2012). "Ascl3 marks adult progenitor cells of the mouse salivary gland." Stem Cell Res **8**(3): 379-387.

Sato, T., J. H. van Es, H. J. Snippert, D. E. Stange, R. G. Vries, M. van den Born, N. Barker, N. F. Shroyer, M. van de Wetering and H. Clevers (2011). "Paneth cells constitute the niche for Lgr5 stem cells in intestinal crypts." Nature **469**(7330): 415-418.

Schmitt, C. A. (2011). "Radiotherapy: IMRT reduces incidence of xerostomia in patients with head and neck cancer." Nat Rev Clin Oncol **8**(4): 194.

Schuler, P. J., S. Laban, J. Doescher, L. Bullinger and T. K. Hoffmann (2017). "Novel Treatment Options in Head and Neck Cancer." Oncol Res Treat **40**(6): 342-346.

Scott, J., P. Liu and P. M. Smith (1999). "Morphological and functional characteristics of acinar atrophy and recovery in the duct-ligated parotid gland of the rat." J Dent Res **78**(11): 1711-1719.

Shah, M., D. Wang, C. Rubadue, D. Suster and A. Beck (2017). Deep learning assessment of tumor proliferation in breast cancer histological images. 2017 IEEE International Conference on Bioinformatics and Biomedicine (BIBM).

Shan, Z., J. Li, C. Zheng, X. Liu, Z. Fan, C. Zhang, C. M. Goldsmith, R. B. Wellner, B. J. Baum and S. Wang (2005). "Increased fluid secretion after adenoviral-mediated transfer of the human aquaporin-1 cDNA to irradiated miniature pig parotid glands." Mol Ther **11**(3): 444-451.

Shubin, A. D., T. J. Felong, B. E. Schutrum, D. S. L. Joe, C. E. Ovitt and D. S. W. Benoit (2017). "Encapsulation of primary salivary gland cells in enzymatically degradable poly(ethylene glycol) hydrogels promotes acinar cell characteristics." Acta Biomater **50**: 437-449.

Siegel, R. L., K. D. Miller and A. Jemal (2017). "Cancer Statistics, 2017." CA Cancer J Clin **67**(1): 7-30.

Snippert, H. J., A. Haegebarth, M. Kasper, V. Jaks, J. H. van Es, N. Barker, M. van de Wetering, M. van den Born, H. Begthel, R. G. Vries, D. E. Stange, R. Toftgard and H. Clevers (2010). "Lgr6 marks stem cells in the hair follicle that generate all cell lineages of the skin." Science **327**(5971): 1385-1389.

Specenier, P. and J. B. Vermorken (2013). "Cetuximab: its unique place in head and neck cancer treatment." Biologics **7**: 77-90.

Spielman, A., H. Ben-Aryeh, D. Gutman, R. Szargel and E. Deutsch (1981). "Xerostomia--diagnosis and treatment." Oral Surg Oral Med Oral Pathol **51**(2): 144-147.

Stephens, L. C., G. K. King, L. J. Peters, K. K. Ang, T. E. Schultheiss and J. H. Jardine (1986). "Acute and late radiation injury in rhesus monkey parotid glands. Evidence of interphase cell death." Am J Pathol **124**(3): 469-478.

Sugiyama, T., H. Kohara, M. Noda and T. Nagasawa (2006). "Maintenance of the hematopoietic stem cell pool by CXCL12-CXCR4 chemokine signaling in bone marrow stromal cell niches." Immunity **25**(6): 977-988.

Svoboda, D., M. Kozubek and S. Stejskal (2009). "Generation of digital phantoms of cell nuclei and simulation of image formation in 3D image cytometry." Cytometry A **75**(6): 494-509.

Takahashi, S., E. Schoch and N. I. Walker (1998). "Origin of acinar cell regeneration after atrophy of the rat parotid induced by duct obstruction." Int J Exp Pathol **79**(5): 293-301.

Takakura, K., S. Takaki, I. Takeda, N. Hanaue, Y. Kizu, M. Tonogi and G. Y. Yamane (2007). "Effect of cevimeline on radiation-induced salivary gland dysfunction and AQP5 in submandibular gland in mice." Bull Tokyo Dent Coll **48**(2): 47-56.

Tamarin, A. (1971). "Submaxillary gland recovery from obstruction. I. Overall changes and electron microscopic alterations of granular duct cells." J Ultrastruct Res **34**(3): 276-287.

Tatsuishi, Y., M. Hirota, T. Kishi, M. Adachi, T. Fukui, K. Mitsudo, S. Aoki, Y. Matsui, S. Omura, H. Taniguchi and I. Tohnai (2009). "Human salivary gland stem/progenitor cells remain dormant even after irradiation." Int J Mol Med **24**(3): 361-366.

Taylor, G. P., R. Anderson, A. D. Reginelli and K. Muneoka (1994). "FGF-2 induces regeneration of the chick limb bud." Dev Biol **163**(1): 282-284.

Thorel, F., V. Nepote, I. Avril, K. Kohno, R. Desgraz, S. Chera and P. L. Herrera (2010). "Conversion of adult pancreatic alpha-cells to beta-cells after extreme beta-cell loss." Nature **464**(7292): 1149-1154.

Tian, H., B. Biehs, S. Warming, K. G. Leong, L. Rangell, O. D. Klein and F. J. de Sauvage (2011). "A reserve stem cell population in small intestine renders Lgr5-positive cells dispensable." Nature **478**(7368): 255-259.

Trotti, A. (2000). "Toxicity in head and neck cancer: a review of trends and issues." Int J Radiat Oncol Biol Phys **47**(1): 1-12.

Unnikrishnan, R., C. Pantofaru and M. Hebert (2007). "Toward Objective Evaluation of Image Segmentation Algorithms." IEEE Transactions on Pattern Analysis and Machine Intelligence **29**(6): 929-944.

van Luijk, P., S. Pringle, J. O. Deasy, V. V. Moiseenko, H. Faber, A. Hovan, M. Baanstra, H. P. van der Laan, R. G. Kierkels, A. van der Schaaf, M. J. Witjes, J. M. Schippers, S. Brandenburg, J. A. Langendijk, J. Wu and R. P. Coppes (2015). "Sparing the region of the salivary gland containing stem cells preserves saliva production after radiotherapy for head and neck cancer." Sci Transl Med **7**(305): 305ra147.

Vasavada, R. C., L. Wang, Y. Fujinaka, K. K. Takane, T. C. Rosa, J. M. Mellado-Gil, P. A. Friedman and A. Garcia-Ocana (2007). "Protein kinase C-zeta activation markedly enhances beta-cell proliferation: an essential role in growth factor mediated beta-cell mitogenesis." Diabetes **56**(11): 2732-2743.

Vigneswaran, N. and M. D. Williams (2014). "Epidemiologic trends in head and neck cancer and aids in diagnosis." Oral Maxillofac Surg Clin North Am **26**(2): 123-141.

Vissink, A., J. Jansma, F. K. Spijkervet, F. R. Burlage and R. P. Coppes (2003). "Oral sequelae of head and neck radiotherapy." Crit Rev Oral Biol Med **14**(3): 199-212.

Vissink, A., J. B. Mitchell, B. J. Baum, K. H. Limesand, S. B. Jensen, P. C. Fox, L. S. Elting, J. A. Langendijk, R. P. Coppes and M. E. Reyland (2010). "Clinical management of salivary gland hypofunction and xerostomia in head-and-neck cancer patients: successes and barriers." Int J Radiat Oncol Biol Phys **78**(4): 983-991.

Vissink, A., E. J. s-Gravenmade, E. E. Ligeon and W. T. Konings (1990). "A functional and chemical study of radiation effects on rat parotid and submandibular/sublingual glands." Radiat Res **124**(3): 259-265.

Vivino, F. B., I. Al-Hashimi, Z. Khan, F. G. LeVeque, P. L. Salisbury, 3rd, T. K. Tran-Johnson, C. C. Muscoplat, M. Trivedi, B. Goldlust and S. C. Gallagher (1999). "Pilocarpine tablets for the treatment of dry mouth and dry eye symptoms in patients with Sjogren syndrome: a randomized, placebo-controlled, fixed-dose, multicenter trial. P92-01 Study Group." Arch Intern Med **159**(2): 174-181.

Walker, N. I. and G. C. Gobe (1987). "Cell death and cell proliferation during atrophy of the rat parotid gland induced by duct obstruction." J Pathol **153**(4): 333-344.

Wang, L. D. and A. J. Wagers (2011). "Dynamic niches in the origination and differentiation of haematopoietic stem cells." Nat Rev Mol Cell Biol **12**(10): 643-655.

Wasserman, T. H., D. M. Brizel, M. Henke, A. Monnier, F. Eschwege, R. Sauer and V. Strnad (2005). "Influence of intravenous amifostine on xerostomia, tumor control, and survival after radiotherapy for head-and- neck cancer: 2-year follow-up of a prospective, randomized, phase III trial." Int J Radiat Oncol Biol Phys **63**(4): 985-990.

Weintraub, N. L., W. K. Jones and D. Manka (2010). "Understanding radiation-induced vascular disease." J Am Coll Cardiol **55**(12): 1237-1239.

Whyte, J., L. Thornton, S. McNally, S. McCarthy, F. Lanigan, W. M. Gallagher, T. Stein and F. Martin (2010). "PKCzeta regulates cell polarisation and proliferation restriction during mammary acinus formation." J Cell Sci **123**(Pt 19): 3316-3328.

Wilson, A., E. Laurenti, G. Oser, R. C. van der Wath, W. Blanco-Bose, M. Jaworski, S. Offner, C. F. Dunant, L. Eshkind, E. Bockamp, P. Lio, H. R. Macdonald and A. Trumpp (2008). "Hematopoietic stem cells reversibly switch from dormancy to self-renewal during homeostasis and repair." Cell **135**(6): 1118-1129.

Wong, W. Y., M. Pier and K. H. Limesand (2018). "Persistent disruption of lateral junctional complexes and actin cytoskeleton in parotid salivary glands following radiation treatment." Am J Physiol Regul Integr Comp Physiol.

Xiao, N., Y. Lin, H. Cao, D. Sirjani, A. J. Giaccia, A. C. Koong, C. S. Kong, M. Diehn and Q. T. Le (2014). "Neurotrophic factor GDNF promotes survival of salivary stem cells." J Clin Invest **124**(8): 3364-3377.

Xing, F. and L. Yang (2016). "Robust Nucleus/Cell Detection and Segmentation in Digital Pathology and Microscopy Images: A Comprehensive Review." IEEE Reviews in Biomedical Engineering **9**: 234-263.

Xiong, F., H. Gao, Y. Zhen, X. Chen, W. Lin, J. Shen, Y. Yan, X. Wang, M. Liu and Y. Gao (2011). "Optimal time for passaging neurospheres based on primary neural stem cell cultures." Cytotechnology **63**(6): 621-631.

Xiong, X., X. Li, Y. A. Wen and T. Gao (2016). "Pleckstrin Homology (PH) Domain Leucine-rich Repeat Protein Phosphatase Controls Cell Polarity by Negatively

Regulating the Activity of Atypical Protein Kinase C." J Biol Chem **291**(48): 25167-25178.

Young, D., C. C. Xiao, B. Murphy, M. Moore, C. Fakhry and T. A. Day (2015). "Increase in head and neck cancer in younger patients due to human papillomavirus (HPV)." Oral Oncol **51**(8): 727-730.